

SECURITY CLASSIFICATION OF THIS PAGE

<b>REPORT DOCUMENTATION PAGE</b>		Form Approved OMB No. 0704-0188	
<b>AD-A218 059</b>		1b. RESTRICTIVE MARKINGS NONE	
		3. DISTRIBUTION / AVAILABILITY OF REPORT APPROVED FOR PUBLIC RELEASE; DISTRIBUTION UNLIMITED. <span style="float: right; border: 1px solid black; border-radius: 50%; padding: 5px;">/</span>	
6a. NAME OF PERFORMING ORGANIZATION AFIT STUDENT AT UNIVERSITY OF DAYTON		6b. OFFICE SYMBOL (if applicable)	
6c. ADDRESS (City, State, and ZIP Code)		7a. NAME OF MONITORING ORGANIZATION AFIT/CIA	
8a. NAME OF FUNDING / SPONSORING ORGANIZATION		8b. OFFICE SYMBOL (if applicable)	
8c. ADDRESS (City, State, and ZIP Code)		7b. ADDRESS (City, State, and ZIP Code) Wright-Patterson AFB OH 45433-6583	
9. PROCUREMENT INSTRUMENT IDENTIFICATION NUMBER		10. SOURCE OF FUNDING NUMBERS	
		PROGRAM ELEMENT NO.	PROJECT NO.
11. TITLE (Include Security Classification) (UNCLASSIFIED) REFLECTOR ANTENNA DESIGNS FOR AIRBORNE RADAR APPLICATIONS		TASK NO.	WORK UNIT ACCESSION NO.
		12. PERSONAL AUTHOR(S) GEORGE MARIO BESENYEI	
13a. TYPE OF REPORT THESIS/DISSERTATION		13b. TIME COVERED FROM _____ TO _____	
14. DATE OF REPORT (Year, Month, Day) 1988		15. PAGE COUNT 131	
16. SUPPLEMENTARY NOTATION APPROVED FOR PUBLIC RELEASE IAW AFR 190-1 ERNEST A. HAYGOOD, 1st Lt, USAF Executive Officer, Civilian Institution Programs			
17. COSATI CODES		18. SUBJECT TERMS (Continue on reverse if necessary and identify by block number)	
FIELD	GROUP		
19. ABSTRACT (Continue on reverse if necessary and identify by block number)			
DTIC ELECTE FEB 15 1990 S                      D D u                      D			
90 02 14 051			
20. DISTRIBUTION / AVAILABILITY OF ABSTRACT <input checked="" type="checkbox"/> UNCLASSIFIED/UNLIMITED <input type="checkbox"/> SAME AS RPT. <input type="checkbox"/> DTIC USERS		21. ABSTRACT SECURITY CLASSIFICATION UNCLASSIFIED	
22a. NAME OF RESPONSIBLE INDIVIDUAL ERNEST A. HAYGOOD, 1st Lt, USAF		22b. TELEPHONE (Include Area Code) (513) 255-2259	
		22c. OFFICE SYMBOL AFIT/CI	

ABSTRACT

REFLECTOR ANTENNA DESIGNS FOR AIRBORNE RADAR APPLICATIONS

Name: Besenyei, George M.  
University of Dayton, 1988

Advisors: Dr. G. A. Thiele, Dr. R. P. Penno, and  
Dr. K. M. Pasala

→ This paper examines simple Cassegrain, Twist-Cassegrain, and Inverse Cassegrain reflector antenna designs for airborne radar applications. The author chooses an optimized Twist-Cassegrain design and examines its performance using the Hughes Vector Diffraction simulation run on an IBM 3038 mainframe at building R-2, Radar Systems Group, Hughes Aircraft Company, Los Angeles, CA. Numerous historical examples of Twist-Cassegrain designs are also presented. *Theses 1/1*

REFLECTOR ANTENNA DESIGNS FOR  
AIRBORNE RADAR APPLICATIONS

Thesis

Submitted to

The School of Engineering of the  
UNIVERSITY OF DAYTON

In Partial Fulfillment of the Requirements for  
The Degree  
Master of Science in Electrical Engineering

by

George Mario Besenyei

UNIVERSITY OF DAYTON

Dayton, Ohio

November, 1988

Accession For	
NTIS CRA&I	<input checked="" type="checkbox"/>
DTIC TAB	<input type="checkbox"/>
Unannounced	<input type="checkbox"/>
Justification	
By _____	
Distribution/	
Availability Codes	
Dist	Avail and/or Special
A-1	



REFLECTOR ANTENNA DESIGNS FOR AIRBORNE RADAR APPLICATIONS

APPROVED BY:

---

Gary A. Thiele, Ph.D.  
Associate Dean/Director  
Graduate Engineering & Research  
School of Engineering  
Committee Chairperson

---

Krishna M. Pasala, Ph.D.  
Associate Professor  
Electrical Engineering  
Committee Member

---

Robert P. Penno, Ph.D.  
Assistant Professor  
Electrical Engineering  
Committee Member

---

Gary A. Thiele, Ph.D.  
Associate Dean/Director  
Graduate Engineering & Research  
School Of Engineering

---

Gordon A. Sargent, Ph.D.  
Dean  
School of Engineering

## Table of Contents

	page
ABSTRACT . . . . .	iii
TABLE OF CONTENTS. . . . .	iv
LIST OF ILLUSTRATIONS. . . . .	vi
LIST OF TABLES . . . . .	ix
LIST OF SYMBOLS. . . . .	x
ACKNOWLEDGEMENTS . . . . .	xi
CHAPTER	
1. INTRODUCTION . . . . .	1
Background	
Purpose Statement	
Method of Investigation	
Literature Search	
Overview	
2. FUNDAMENTAL PRINCIPLES AND THEORY. . . . .	8
Simple Cassegrain Design	
Twist-Cassegrain Design	
Inverse-Cassegrain Design	
Soviet Cassegrain Design	
Propagation Modes	
Horn Feed Design	
Effective Radiated Power	
Method of Scanning	
Antenna Gain and Loss Budgets	
Three DB Beamwidth	
3. OPTIMIZED TWIST-CASSEGRAIN DESIGNS . . . . .	52
English Twist-Cassegrain Designs	
Swedish Twist-Cassegrain Designs	
Optimized Swedish Design	
Basic Parameters of Optimized Design	

4. PERFORMANCE ANALYSIS OF OPTIMIZED DESIGN . . . . 70

Modified Vector Diffraction Program  
Rusch Scattering Equations  
Far Field Pattern Results

5. CONCLUSIONS AND RECOMMENDATIONS. . . . .105

APPENDICES

Appendix A: Proofs of Fundamental Principles  
and Approximations . . . . .108

Appendix B: Suitable Traveling Wave Tubes . . .115

Appendix C: Swedish Antenna Design-Simulated  
Patterns. . . . .116

Appendix D: Vector Diffraction Program Inputs .125

REFERENCES. . . . . 128

## LIST OF ILLUSTRATIONS

	page
1. Cassegrain Telescope . . . . .	9
2. Simple Cassegrain Reflector Antenna. . . . .	9
3. A Double Reflector Antenna With Polarization Shiftability . . . . .	16
4. Early Polarization Changing Antenna Design . . . . .	19
5. Early Twist-Reflector Antenna . . . . .	21
6. Twist-Reflector Design With a Hyperboloid Subreflector . . . . .	22
7. Transmission Line Equivalents For a Twist-Reflector	24
8. Geometry of Inverse Cassegrain Antenna . . . . .	27
9. Measured Gain of Inverse Cassegrain Antenna . . . . .	29
10. Monopulse Feed Excitation . . . . .	33
11. Four Quadrant Monopulse Feed Design . . . . .	34
12. Universal Radiation Pattern of a Horn Flared in the E-Plane . . . . .	38
13. Universal Radiation Pattern of a Horn Flared in the H-Plane . . . . .	40
14. The Pyramidal Horn. . . . .	41
15. Airborne Radar Block Diagram. . . . .	43
16. Five Bar Raster Search Pattern . . . . .	45
17. Edge Illumination Versus Efficiency Factor. . . . .	48

	page
18. The Marconi Twist-Cassegrain Antenna (Aerial) . . .	53
19. GEC Twist-Cassegrain Antenna Installed in a Tornado F MK 2 Aircraft (Front View) . . . . .	55
20. Swedish Twist-Cassegrain Antenna . . . . .	57
21. Multimode Monopulse Feed For Swedish Antenna . . .	58
22. Dual-band Twist Cassegrain Design. . . . .	59
23. Twist-Reflector Cross Section . . . . .	59
24. Optimized Swedish Twist-Cassegrain Antenna With Pyramidal Feed . . . . .	61
25. Geometry of Hughes Simulation. . . . .	71
26. Geometry of Rusch Integrals. . . . .	74
27. Secondary Pattern for E-Plane for Design A . . . .	80
28. Secondary Pattern for H-Plane for Design A . . . .	81
29. Primary Pattern for E-Plane for Design A . . . . .	82
30. Primary Pattern for H-Plane for Design A . . . . .	83
31. Secondary Pattern for E-Plane for Design B . . . .	86
32. Secondary Pattern for H-Plane for Design B . . . .	87
33. Primary Pattern for E-Plane for Design B . . . . .	88
34. Primary Pattern for H-Plane for Design B . . . . .	89
35. Secondary Pattern for E-Plane for Design C . . . .	91
36. Secondary Pattern for H-Plane for Design C . . . .	92
37. Primary Pattern for E-Plane for Design C . . . . .	93
38. Primary Pattern for H-Plane for Design C . . . . .	94
39. Primary Pattern for E-Plane for Design D . . . . .	96

	page
40. Primary Pattern for H-Plane for Design D . . . . .	97
41. Secondary Pattern for E-Plane for Design D . . . . .	98
42. Secondary Pattern for H-Plane for Design D . . . . .	99
43. Secondary Pattern for E-Plane for Design E . . . . .	.101
44. Secondary Pattern for H-Plane for Design E . . . . .	.102
45. Primary Pattern for E-Plane for Design E . . . . .	.103
46. Primary Pattern for H-Plane for Design E . . . . .	.104
47. Geometry of Apperture Blockage . . . . .	.109
48. Geometry for Rectangular Apperture . . . . .	.112
49. Pattern of Uniformly Illuminated Rectangular Apperture. . . . .	.114
50. Secondary Pattern for E-Plane for Swedish Design at 9.2 GHz . . . . .	.117
51. Secondary Pattern for H-Plane for Swedish Design at 9.2 GHz . . . . .	.118
52. Primary Pattern for E-Plane for Swedish Design at 9.2 GHz . . . . .	.119
53. Primary Pattern for H-Plane for Swedish Design at 9.2 GHz . . . . .	.120
54. Secondary Pattern for E-Plane for Swedish Design at 9.3 GHz . . . . .	.121
55. Secondary Pattern for H-Plane for Swedish Design at 9.3 GHz . . . . .	.122
56. Primary Pattern for E-Plane for Swedish Design at 9.3 GHz . . . . .	.123
57. Primary Pattern for H-Plane for Swedish Design at 9.3 GHz . . . . .	.124

## LIST OF TABLES

	page
1. Calculation of Area Gain . . . . .	.12
2. Antenna Loss Budget . . . . .	.13
3. Four Quadrant Monopulse Feed Design . . . . .	.35
4. Loss Budget for a Twist-Cassegrain Reflector Antenna . . . . .	.47
5. Parameters of Optimized Design A . . . . .	.64
6. Basic Parameters of Design B . . . . .	.65
7. Basic Parameters of Design C . . . . .	.66
8. Basic Parameters of Design D . . . . .	.67
9. Basic Parameters of Design E . . . . .	.68

## LIST OF SYMBOLS

<u>Symbol</u>	<u>Definition</u>
a	distance between grid and ground plane
$b_g$	equivalent susceptance of wire grid
B	blockage ratio = $d/D$
$\psi_0$	angle from focal pt. to subreflector edge
D	paraboloid diameter
d	hyperboloid diameter
F	focal length of paraboloid
f	focal length of hyperboloid
$\lambda_0$	hyperboloid half angle

## ACKNOWLEDGMENTS

This paper is dedicated to my wife Paula, without whose constant encouragement this paper could never have been completed. In addition, this paper is also dedicated to the late Frederick Williams, Chief Scientist, Hughes Aircraft Company, for his technical expertise in air-to-air radar systems design imparted to me during 1984 and 1985, while serving as a consultant to the Air Force.

The author would especially like to thank Arthur F. Seaton, Senior Scientist, Hughes Aircraft Company, for his overwhelming support in the simulation activity, as well as, for his ability to answer difficult antenna design questions. Furthermore, the author is grateful for the Independent Research and Development funding of the simulation activity provided by the Hughes Aircraft Company, through William Kessler, Radar Systems Group.

In addition, the author would like to thank Robert Dahlin, Arkady Associates, for his source material on Soviet reflector antenna design. This material was quite unique and otherwise totally nonexistent in U.S. and European literature.

Finally, this author would like to thank Dr. Gary A. Thiele, Dr. K. M. Pasala, and Dr. Robert Penno, all of the University of Dayton, for their technical assistance and review of this paper. Also, this author would like to thank all the personnel of AFIT/CI who have assisted this project through the funding of two trips to Los Angeles, CA.

Chapter 1  
INTRODUCTION

BACKGROUND

Reflector antennas derived from geometric optics have been used extensively for radio telescope and ground search radars over the years. However, only within the last 20 years have airborne radar applications even been proposed, prototyped, and developed. Much of the critical development of these reflector antenna designs have been accomplished by the United Kingdom (Marconi), Israel (IAI Elta Electronics), Sweden, and the Soviet Union. American efforts were accomplished by the Wheeler Labs (now part of Hazeltine Corp.), and Westinghouse Defense Electronics. Westinghouse abandoned their design due to tracking problems. Hughes purchased a Swedish design for testing, but never incorporated it into any production airborne radar. Currently no US military aircraft use reflector antenna designs such as the simple Cassegrain, Twist Cassegrain, or Inverse Cassegrain. This is due to the US insistence upon using only state-of-the art technology.

## PURPOSE STATEMENT

It is the purpose of this paper to show the feasibility of using reflector antennas derived from geometric optics for airborne radar applications in low cost jet fighter aircraft of the future. Feasibility will be shown by: adequate antenna gain for a 85 dBW Effective Radiated Power specification, low first sidelobes (less than -20 Db down from main beam), adequate scan pattern, and low system losses. In addition, this antenna should be able to radiate anywhere in the I-band regime (8-10 GHZ). This antenna will be used strictly with low Pulse-Repetition Frequency (PRF) signals only (1000 pulses per second or less). While these specifications on sidelobe level are higher than what could be achieved with array antennas, they are lower than the standard 13 dB criteria to detect targets.

## METHOD OF INVESTIGATION

The writer will examine the following reflector antenna designs for suitability in meeting the feasibility requirements established in the purpose statement: simple Cassegrain, Twist-Cassegrain, and Inverse Cassegrain (also referred to as mirror antennas in most foreign literature). Real data will be furnished whenever possible. Finally the writer will choose an optimum antenna design and show the optimum theoretical performance achievable in the form of primary and secondary reflector patterns. This will be accomplished using the Hughes Aircraft Vector Diffraction simulation, which integrates the Rusch integrals. A brief description of this simulation is given in Chapter 4 of this paper.

## LITERATURE SEARCH

The subject of reflector antenna designs using geometric optics approaches has been widely researched primarily in the 1960's and 1970's in this country. Very little attention is being given to these designs in the US today. No airborne radar in this country presently uses or is being designed which is built around any geometric optics type antenna (simple Cassegrain, Twist-Cassegrain, or Inverse Cassegrain). Foreign sources have overwhelmingly dominated the research and development in this area since the mid-1970's. Nevertheless, the concept of these antenna structures for airborne radar applications has been well proven in many foreign radar systems. The documentation on these systems is however quite limited. Detailed design information is often left out in many journals in which these foreign radars appear.

The US documentation on reflector antennas designed using geometric optics seem to begin with the work done by Peter Hannon, Harold Wheeler, and others from the Wheeler Laboratories (Hannon 1955 and 1961). Other work, in the area of simulation for Cassegrain antennas has been accomplished by W.V.T Rusch and P.D. Potter for NASA.

The analysis techniques used by Rusch and Potter are published in the textbook: Analysis of Reflector Antennas (Rusch and Potter, 1970). Much of this work is based on two studies done by Rusch (July, 1963 and May, 1963). Furthermore, the Hughes Vector Diffraction Simulation, on which most of the analysis of this paper is based upon, was derived originally from a NASA Jet Propulsion Laboratory simulation developed by Rusch, Potter, and Jungmeyer.

About the same time period Paul Jensen, Hughes Aircraft Company conducted research into simple Cassegrain type antennas for ground based tracking purposes (Jensen, 1961). He later made a significant contribution to The Handbook of Antenna Design (1984) with detailed design procedures for a simple Cassegrain reflector.

Twist-Cassegrain designs using double wire grid twist-reflectors were first reported in Sweden (Josefsson, 1973) which essentially provided 100% bandwidth capability, a great improvement over the single wire grid twist-reflectors which provided a 30% bandwidth capability. Later, L.G. Josefsson would write his doctoral dissertation on "Wire Polarizers for Microwave Antennas" (1978), which essentially developed wire grid polarizers suitable for Twist-Cassegrain antennas. In Los Angeles, at RADAR 86, Josefsson presented a dual band Twist-Cassegrain antenna.

Furthermore, a low sidelobe Twist-cassegrain antenna was presented at the 1973 Internal Radar conference (Dahlsjo, 1973). This is the design referred to in this paper as the "Swedish Twist-Cassegrain Design".

In England, GEC Avionics developed their own Twist-Cassegrain antenna (aerial) for use in the Tornado F Mk2 interceptor for the Royal Air Force (Spooner and Sage, 1985). This antenna is part of the Foxhunter AI radar which is designed to operate fully coherently. In addition, Marconi Avionics Ltd. developed a Twist-Cassegrain antenna which is described in this paper (Mahony, 1981).

In the USSR, several books and papers refer to off-axis capability in Cassegrain type (two mirror) antennas (Galimov, 1969 and Bakhrakh and Galimov, 1981). The translation into English is not fully adequate at times to preserve the original meaning of ideas and concepts being presented. In addition, these documents tend to be terse.

Finally, in Israel, Elta Electronics developed an Inverse Cassegrain design based on US Naval Research Laboratory principles and designs (Orleansky, Samson, and Havkin, 1987; Lewis and Shelton, 1980).

## OVERVIEW

This paper will develop the fundamental principles and theory of cassegrain type (those derived from geometric optics) reflector antennas in Chapter 2. In Chapter 3, the author will develop an optimized Swedish design that would be desirable to the US Air Force. Other designs will be examined. Chapter 4 will contain the performance analysis of the optimized design by way of far-field patterns obtained by simulation using the Hughes Vector Diffraction Program on an IBM 3038 computer. Finally, conclusions and recommendations will be presented in Chapter 5.

CHAPTER 2  
FUNDAMENTAL PRINCIPLES AND THEORY

SIMPLE CASSEGRAIN DESIGN

Simple Cassegrain reflectors are those derived from a Cassegrain telescope. A Cassegrain telescope consists of two mirrors and an observing optical instrument, as shown in Figure 1, reference Ingalls, 1953. Simple Cassegrain reflector antennas are described in detail in Hannon, 1961. They are composed primarily of a paraboloidal main reflector and a hyperboloidal subreflector. The feed (generally four horn monopulse or single pyramidal horn) is located at the vertex of the paraboloid. This is quite a desirable position since its rear location and forward direction of the feed eliminate long transmission lines and provide more flexibility in feed design than front-fed paraboloids. A diagram of a simple Cassegrain antenna is depicted in Figure 2.

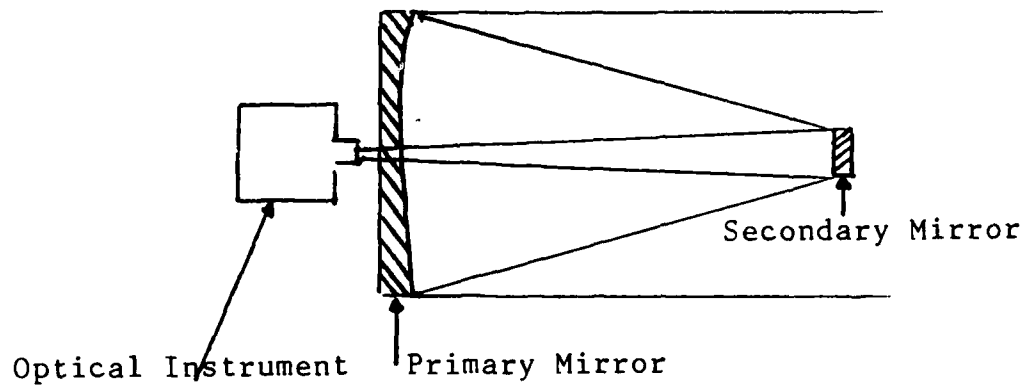


Figure 1. Cassegrain telescope

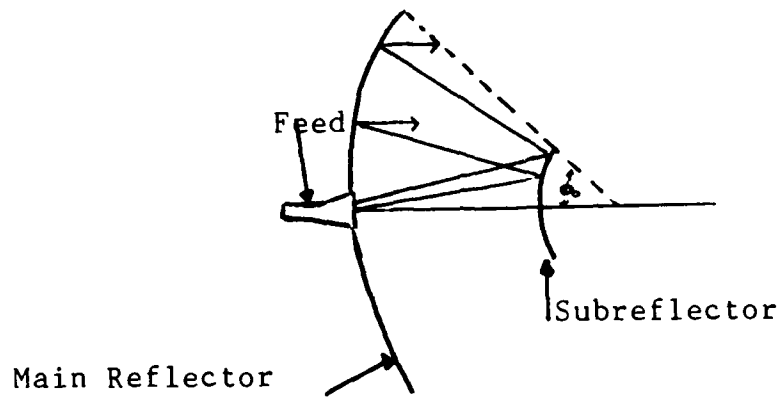


Figure 2. Simple Cassegrain reflector antenna

### Basic Design Parameters and Calculations

The diameter of the paraboloid main reflector is fixed in order to fit within the radome of the aircraft. The author assumes the limitation is 30 inches for the maximum possible diameter. Simulation cases will be run at both 27 and 30 inches diameters. The results are presented in Chapter 4 of this paper. The paraboloid diameter principally governs the total system gain and the antenna efficiency achievable.

The focal length (of the paraboloid) / diameter (of the paraboloid) ratio of 0.6 will be used. This will be referred to as the F/D ratio. For the 27 inch case of the paraboloid main reflector, simulations with  $F/D = 0.5$  and  $F/D = 0.7$  will also be run, with the results presented in Chapter 4 as well. The F/D ratio is chiefly governed by mechanical considerations. To minimize spillover, past the paraboloid edges, according to Hansen (1959), a deep dish with a small F/D is desirable. This is however, not practical in an airborne radar design, with limited available space. Furthermore, Carter (1955) found that in low noise design, the far out side lobes caused by the longitudinal and cross-polarized currents on a highly curved reflector dictate the choice of a shallower dish (a larger F/D).

According to Jensen (1962), the typical values of F/D chosen range between 0.25 and 0.42 for simple Cassegrain ground based reflectors. The author will work strictly in the range of F/D between 0.5 and 0.7 for his airborne radar application.

Next, the diameter,  $d$ , of the subreflector will be minimized to avoid blockage using the minimum blockage condition presented in Hannon (1961). Specifically, we have  $d = (2 \lambda F/k)^{1/2}$ , where  $k$  is ordinarily slightly less than one. The proof of this equation appears in Appendix A of this paper. Furthermore, two of the assumptions upon which this proof is based upon (the beamwidth between nulls and  $E_0$  relationship) are also proven in Appendix A.

The blockage ratio can be defined as  $B = d/D$ . It is usually chosen to meet the minimum blockage condition above for a simple Cassegrain design. However, the author will show in a case presented in Chapter 4 that for an airborne radar application, this configuration is extremely degraded by edge diffraction effects, resulting in an undesirable antenna pattern (see pattern in Chapter 4).

Jensen (1962) developed an expression for the loss in antenna gain due to blockage by the subreflector,  $G_L$ , as:  $G_L = 20 \log (1 - 2B^2)$ . For our considerations, at minimum blockage and 9.3 GHz operation,  $G_L$  is about 0.3 dB.

Calculation of antenna gain, G, without losses (also referred to as the area gain in the literature) can be approximated by  $(D^2 / \lambda^2)$  (Culter, 1947). Table 1 below shows the calculation of area gain for various frequencies of interest between 8 to 10 GHz for D = 27 inches.

Table 1  
Calculation of Area Gain

Frequency (GHz)	Wavelength (meters)	Area Gain (dB)
8.5	0.0353	35.7
9.0	0.0344	35.9
9.3	0.0333	36.2
9.4	0.0319	36.6
9.6	0.3125	36.8

We can now develop an antenna loss budget such as the one depicted below in Table 2 for the case of frequency equal to 9.3 GHz, ignoring the losses due to the radome.

Table 2  
Antenna Loss Budget

Antenna gain without losses	36.20 dB
Loss due to subreflector blockage	- 0.26 dB
Taper and spillover loss	- 1.20 dB
Monopulse sum & differ. network	- 0.40 dB
Random Error	- 0.25 dB
<u>Mismatch</u>	<u>- 0.30 dB</u>
Effective antenna gain	33.79 dB

The result is an effective antenna gain quite suitable for airborne radar applications. However, there are a number of penalties associated with this design. The most severe penalty is a limit in the usable 3-dB beamwidth for a simple Cassegrain antenna.

### Problems With Simple Cassegrain Designs

According to Hannon (1961), a one-degree beamwidth might be considered as a rough boundary above which the simple Cassegrain design, even though optimized, would be unattractive. Hannon developed a formula relating  $(d/D)^2$  to beamwidth, primarily based on experimental evidence. Essentially he states  $(d/D)^2 = (\pi/2k) \times (2\theta_{3dB}) \times (F/D)$ . It is apparent from this relationship that an antenna with a narrow beamwidth can have less relative aperture blocking than one with a wide beamwidth. In airborne radars 2 to 3 degree beamwidths are quite commonly used. Therefore the simple cassegrain design is simply not suitable for the narrow beamwidths it imposes upon the radar system.

In addition, subreflectors less than  $10 \lambda$  exhibit huge amounts of edge diffraction and simply do not make sense to build according to A. F. Seaton, Senior Scientist, Radar Systems Group, Hughes Aircraft Company, Los Angeles, CA. In Chapter 4 of this paper, a simulation is run with a  $5 \lambda$  subreflector resulting in an unacceptable antenna pattern. Similarly, Dijk, Jeuken, and Manders state that blocking and diffraction by the subreflector decrease the overall efficiency by about 8% (Dijk, Jeuken, and Manders, 1968). The simple Cassegrain design will be abandoned in lieu of a Twist-Cassegrain design described next.

## TWIST-CASSEGRAIN REFLECTOR ANTENNAS

### The Principle of Polarization Twisting

A polarization twisting double-reflector antenna is shown in Figure 3. Essentially it is composed of three major elements. They are the reflector, the polarization changer, and the transreflector. In addition, a feed and some means for focusing are required to complete the antenna.

An incoming plane wave having a certain polarization, say  $P_A$ , is portrayed by ray 1 (at the right). This wave passes through the first surface, called the transreflector, because the surface is designed to be transparent to polarization,  $\vec{P}_A$ . The wave next encounters a surface, called the polarization changer, which changes the polarization of the wave in a particular manner as it passes through. Next, the wave is incident on a surface called the reflector, which is designed to completely reflect any wave. Finally, the wave again passes through the polarization changer, with a new polarization,  $\vec{P}_B$ . This new polarization is such that the transreflector may be designed to completely reflect it, while still remaining transparent to polarization,  $\vec{P}_A$ .

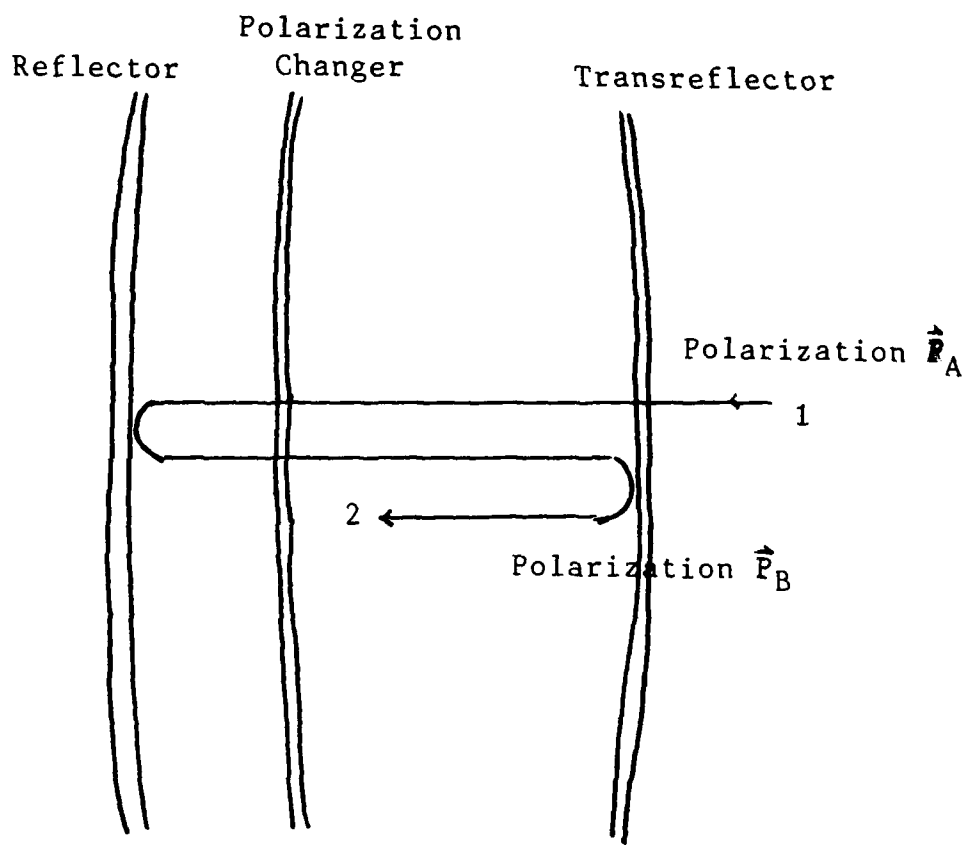


Figure 3. A double reflector antenna with polarization shiftability

Thus the wave is now reflected at the transreflector. In Figure 3, the polarization changer is shown as a distinct component between the two reflecting surfaces. In some designs however, the polarization changer may be incorporated as part of either the reflector or the transreflector.

In an antenna, the wave is focused into a feed. The focusing may be accomplished by the two reflecting surfaces, an additional focusing element, or both. The feed may be located on either side of the polarization changer. The polarization of the feed should be that of the focused wave it is receiving.

### Early Twist Cassegrain Designs

The design in Figure 4 employs a quarter-wave plate as the polarization changer. An incoming vertically polarized wave (VP) passes through the transreflector unchanged. The wave then goes through the plate, which changes the polarization to right-hand circular polarization (RCP). Upon reflection from the reflector, the wave is changed to left-hand circular polarization (LCP). Then, after traveling across the plate again, the wave becomes polarized horizontally (HP). The wave is now completely reflected by the transreflector. Upon passing through the quarter-wave plate again, this wave is finally changed to left-hand circular polarization. The feed is designed for left-hand circular polarization, and transmits the wave to the plumbing through a hole in the apex of the reflector.

The design in Figure 4 is shown with a paraboloidal reflector and a flat transreflector. For this antenna, all the focusing action is provided by the paraboloid. The transreflector provides an image of the feed at the focus of the paraboloid. The distance from the paraboloidal apex to the flat transreflector is one-half that to the image of the feed. Thus this antenna is half as long as one using a single reflector of the same focal length.

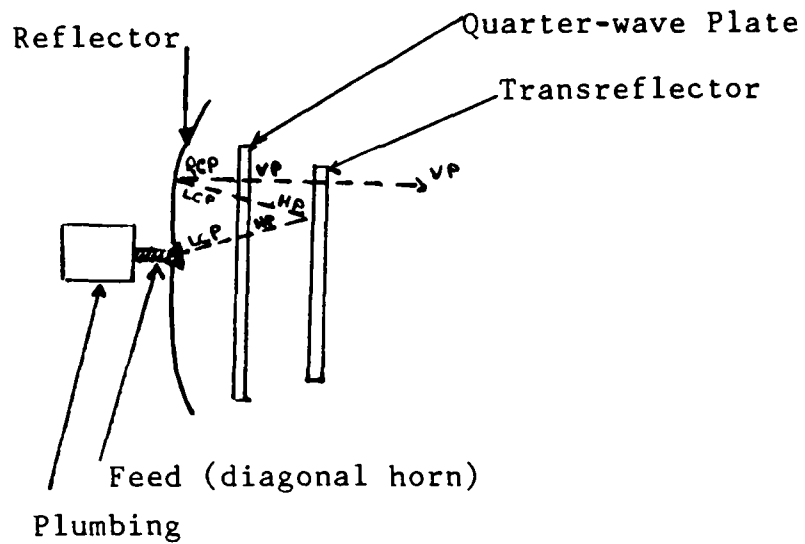


Figure 4. Early polarization changing antenna design

Another advantage is that the feed is not required to be located out in front of the main reflector. Therefore, there is a minimum of blockage and diffraction caused by the feed, and the feed and plumbing are close together. Feed blockage for an ordinary parabolic reflector is typically characterized by a loss of -0.5 dB according to Georgia Institute of Technology's D.G. Bodnar (1984).

In the design shown in Figure 5 is the same as that of Figure 4, except that the polarization changer is now incorporated with the reflector to make a "twistreflector" (ref. Hannon, 1961). Since the polarization changer now has a hole for the feed, the wave incident on the feed is horizontally polarized. Therefore the feed is horizontally polarized.

With this design in mind, the transreflector can now be replaced by a hyperboloid such as that shown in Figure 6. In this design the paraboloid reflector surface "twists" the reflected polarization to vertical, which passes through the subreflector (which is horizontally polarized) essentially unaffected. The subreflector blockage associated with the simple Cassegrain design can now be reduced since the subreflector is transparent to the wave from the paraboloid (Jensen and Rusch, 1984).

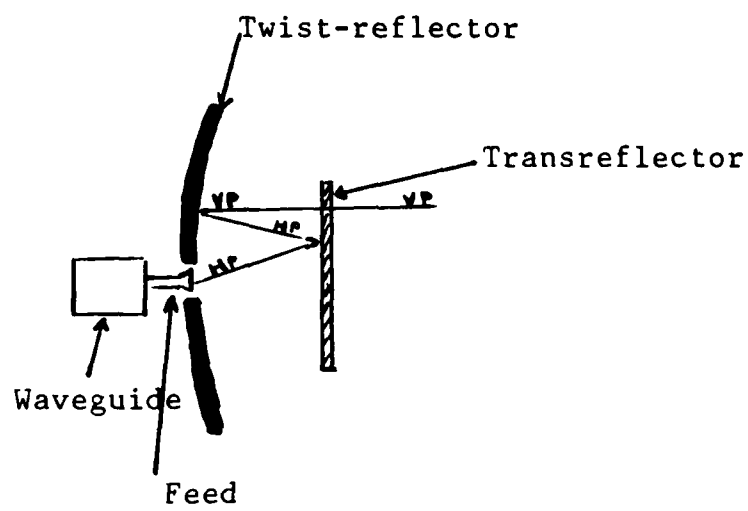


Figure 5. Early twist-reflector antenna

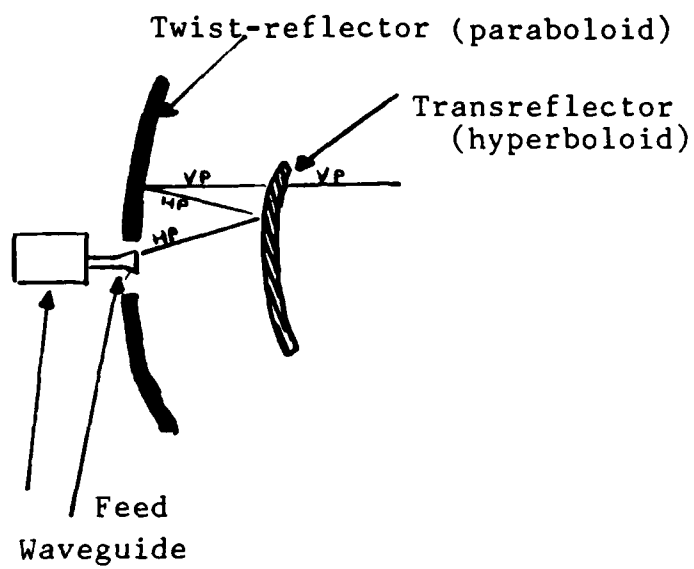


Figure 6. Twist-reflector design with a hyperboloid subreflector

### Detailed Design of a Twist-Reflector

In 1955 Wheeler Labs developed a design for a twist-reflector having wideband and wide angle performance (Hannon, 1955). This twist-reflector was comprised of parallel metal wires in one wire grid in front of a metal sheet. It was designed according to the following equations:

$$b_g = -2.05 (f_0/f) \text{ and,}$$

$$a = 0.358 \lambda_0$$

where  $b_g$  is the equivalent susceptance of the wire grid normalized to the admittance of free space,  $a$  is the distance between the grid and the ground plane, and  $\lambda_0$  is the wavelength at the center frequency  $f_0$  (G.G. MacFarlane, 1946).

To analyze the twist-reflector we must look at the two transmission line equivalents, one for the component of the incident (linearly polarized) electric field which is parallel to the wire grid as shown in Figure 7(a), and the other for the orthogonal component which is perpendicular to the wire grid as shown in Figure 7(b). In order to physically twist the polarization 90 degrees, the preceding components should have the same magnitude or a mismatch loss results (the grid is inclined 45 degrees with respect to the incident polarization).

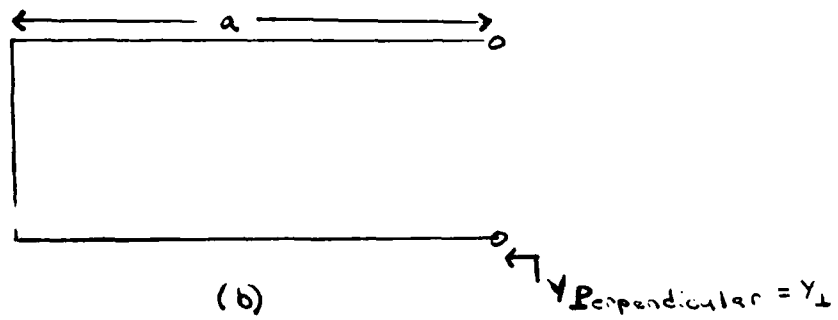
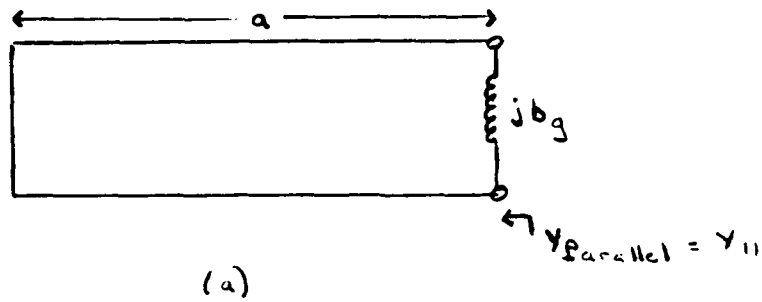


Figure 7. Transmission line equivalents for a twist-reflector  
 (a) parallel, (b) perpendicular polarization

It is shown in Hannon, 1955 that in order to obtain a linearly polarized reflected wave, the input admittances should be reciprocals of each other, that is  $y_{\parallel} = 1/y_{\perp}$ . A departure from this condition implies some degree of elliptical polarization, which may be characterized by a cross polarization attenuation constant,  $P_{cross}$ , such that

$$P_{cross} = 1 + [(b_{\parallel} - b_{\perp}) / (1 + b_{\parallel} b_{\perp})]^2,$$

where  $y_{\parallel} = j b_{\parallel}$  and  $y_{\perp} = j b_{\perp}$ . In addition, wire grid spacing was  $3 \lambda / 8$  from a ground plane (H. Jasik, 1961).

Two wire grids require a general synthesis that is rather complex. The general approach is start from a common single-wire grid twist-reflector, with a center frequency  $f_1$ , and add an additional wire grid such that the wires are parallel to the first grid and in such a position that the admittance of the equivalent line equivalent (for parallel polarization) is infinite in the position of the additional grid. This holds true only for one frequency chosen as  $f_1$ . Further, the insertion of the additional grid has not changed the polarization twisting properties of the reflector at frequency  $f_1$ . Twist-reflectors, with two wire grids can be constructed to give very broad bandwidths in the order of 100 percent, while single grid twist-reflectors have a bandwidth of 30 percent at the most (Josefsson, 1971).

## THE INVERSE CASSEGRAIN ANTENNA

### Background

The Inverse Cassegrain antenna (also referred to as a mirror antenna in the literature) was developed primarily by the Naval Research Laboratories (NRL) and Elta Electronics (Israel). It is a relatively new design and not known to be installed in any jet fighter to date. Its design, however, is unique and is developed below.

### Design Characteristics

The Inverse Cassegrain antenna design is shown in Figure 8 on the next page. Note that the only moving part is a broadband meanderline twistreflector which is scanned. A double-ridged feed and a wire grid paraboloid are stationary in this design. The twistreflector reflects the beam of the paraboloid and at the same time rotates its plane of polarization by 90 degrees. The twisted beam now passes through the wire grid paraboloid reflector. If the beam were not twisted, it would imply have been reflected back to the twistreflector.

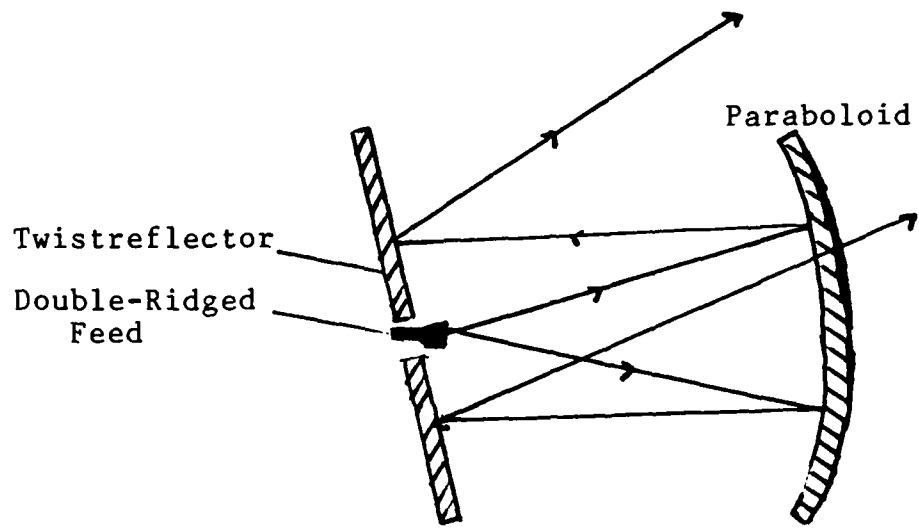


Figure 8. Geometry of Inverse Cassegrain Antenna

Collimation of the beam is accomplished by fixing the wire grid (of the paraboloid) parallel to the plane of polarization of the beam (Orleansky, Samson, and Havkin, 1987). According to Elta Electronics the twistreflector need only be moved through half of the scan angle required. Also rotary joints can be completely eliminated in this configuration.

The advantage of this configuration is that an ultra-wideband twistreflector can be constructed from a meanderline structure. This structure is in turn made up of a meanderline polarizer and a flat reflecting surface (Orlansky, et al., 1987). Meanderline polarizers are described by Young, Robinson, and Hacking in their paper, "Meanderline Polarizer" (Young, et al., 1973). Basically, the polarizer consists of a stack of insulating sheets, each printed with conductive meanderlines and separated by foam spacers. Since the meanderline polarizer can be designed for wideband performance, this twistreflector can operate over more than an octave.

Finally, Figure 9 shows the total measured gain versus normalized frequency for an Inverse Cassegrain antenna. Note the overall gain measured at the compact antenna range at Elta Electronics is erratic, and unpredictable.

The total average gain, which is 29.77 dB, is sufficient for airborne radar applications. The Hughes simulation can not accurately represent this geometry, as it was designed for a twist-Cassegrain geometry. While this antenna is interesting, more data on performance (and losses) is needed to optimize this configuration.

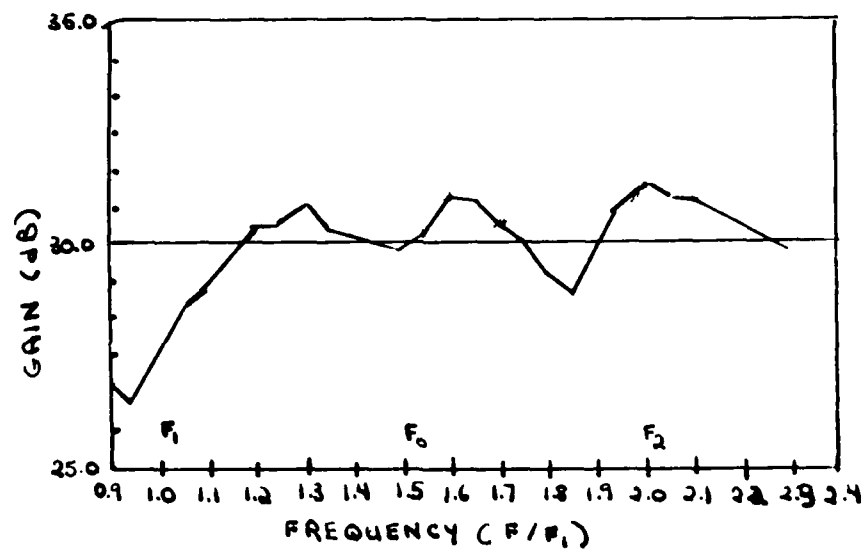


Figure 9. Measured gain of Inverse Cassegrain Antenna

## SOVIET CASSEGRAIN DESIGN

A number of open source Soviet publications on "Mirror" antennas have appeared over the years. They include many works such as Reflector Scanning Antennas (Bakhrakh and Galimov, 1981), as well as, the Design of Optimum Two-Mirror Antennas with the Oscillation of the Radiation Patterns (Galimov, 1969).

According to an evaluation of the above two sources by Arkady (Dahlin, 1982), it appears new designs for reflector antennas have been implemented in the USSR. No equivalent has been found in US antenna design approaches. The Galimov text contains a design of very wide scan angle cassegrain antennas. The objective of the design seems to indicate a desire for achieving a nearly uniform gain over the entire angular coverage. The approach adopted is a technique for generating special reflector shapes for achieving nearly uniform performance over the scanned volume, but at the expense of "On-axis" (boresight) performance (Dahlin, 1982).

The performance and use of such an antenna if applied to a tracking system have an enormous impact. With this design philosophy, the tracking need not be maintained on boresight ("on-axis").

## PROPAGATION MODES

Using the familiar relation developed in microwaves for a hollow rectangular waveguide (Chatterjee, 1986, and Liao, 1985), one can determine the cutoff frequency of standard WR-90 waveguides ( $a = 2.286$  cm,  $b = 1.016$  cm). The cutoff frequency for the  $TE_{10}$  mode occurs at the 6.562 GHz. The  $TE_{20}$  mode occurs at 13.12 GHz. The  $TE_{01}$  mode occurs at 14.76 GHz. The  $TM_{11}$  mode occurs at 16.16 GHz. Thus if we operate below 13 GHz, only the  $TE_{10}$  mode will be present. Thus since we are operating strictly between 8 to 10 GHz, we do not have to design a mode filter to remove all unwanted higher modes of propagation.

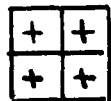
## HORN FEED DESIGN

### Monopulse Feed Design

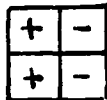
A four horn monopulse feed system (Leonov and Fomichev, 1986) will be utilized in this design in order to provide three different signals. The signals are (a) the sum signal, (b) the azimuth error signal, and (c) an elevation error signal. In order to generate the sum pattern, the feed circuitry drives all four horns in phase. In addition, to produce maximum radiation the horns will give the largest antenna gain when generating the sum pattern. Thus the sum signal is used for range tracking.

Difference signals for azimuth and elevation tracking may be processed on a time shared basis. In order to form the difference patterns, horn pairs are driven in antiphase as shown in Figure 10. This will produce two regions of opposite polarity, which creates the two lobes necessary for tracking both azimuth and elevation.

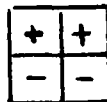
In Figure 11, we show a four quadrant monopulse feed design. For simplicity, the figure shows a circular feed separated by both horizontal and vertical septums. In reality the overall feed can be rectangular in shape, with the same basic results shown in Table 3 on the next page.



Sum signal



Azimuth Difference signal



Elevation Difference signal

Figure 10. Monopulse Feed Excitations

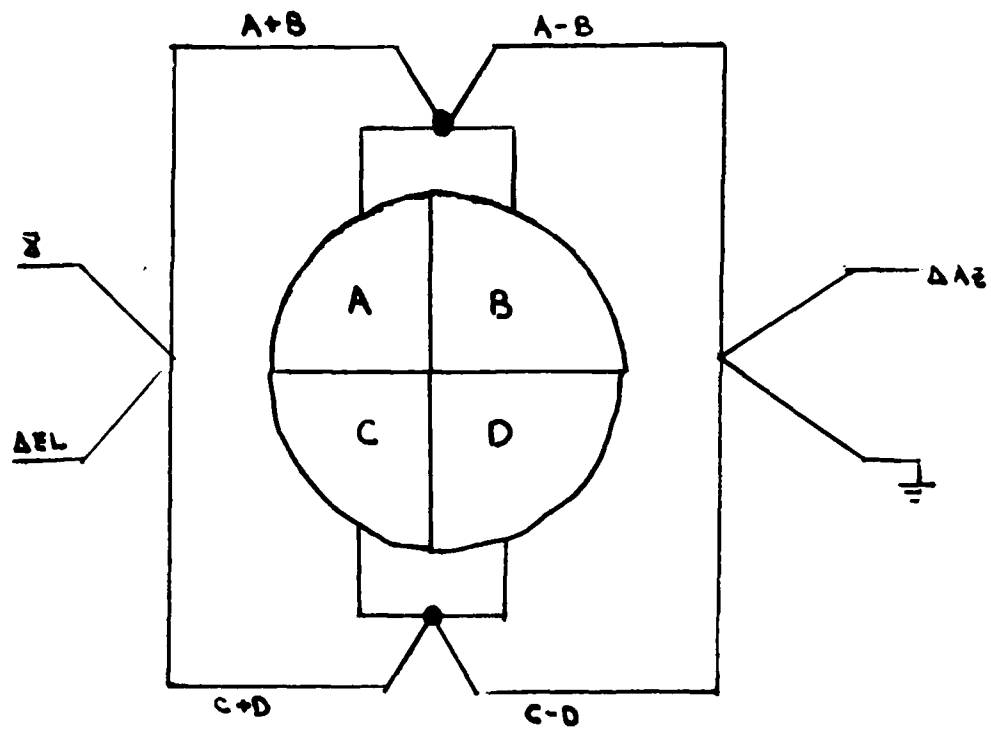


Figure 11. Four Quadrant Monopulse Feed Design

Table 3  
Four Quadrant Monopulse Feed Design

---

Signal      Composition

$$\begin{aligned}\Sigma &= A + B + C + D \\ \Delta EL &= A + B - C - D \\ \Delta AZ &= A - B + C - D\end{aligned}$$

The basic idea of the four quadrant monopulse feed can now be generalized as follows. The sum signal is the sum of all beams. That is:

$$\Sigma = A + B + C + D,$$

where A, B, C, and D are the signals from each beam. This is the signal used to measure and track range, and as a reference for the error signals. The error signals are the difference signals for both azimuth,  $\Delta_{Az}$ , and elevation,  $\Delta_{EL}$ :

$$\Delta_{Az} = A - B + C - D$$

which is the error in the azimuthal plane, and

$$\Delta_{EL} = A + B - C - D$$

which is the error in the elevation plane.

The monopulse horn does demand increased complexity and cost (compared to a rectangular horn) as it requires three receiver channels matched in amplitude and phase. However, a monopulse radar can in theory track a target with a single pulse (Tzannes, 1985). This is not possible with a rectangular horn fed radar system, but it is not essential for our purposes so we will now examine the rectangular feed designs available and show how they can be combined using the superposition principle into a pyramidal horn.

### Rectangular E-Plane Horn Design

We will choose a horn flared in the E-plane to establish the  $TE_{10}$  mode. Using Figure 12 on the next page, we will determine the size of the aperture,  $b$ , required in wavelengths (Johnson and Jasik, 1984). For a 10 dB edge taper, the corresponding relative voltage required is 0.3162 volts without losses. We choose  $\lambda/4$  of phase error as acceptable.

Then,  $b/\lambda \sin \theta_E$  is approximately equal to 1.6 without losses (obtained from Figure 12). Now we must take the path loss taper into account. This has been found experimentally as (ITE Antenna Handbook, 2nd Edition):

$$L \text{ (db)} = 10 \log_{10} (\cos^4 (\theta_E/2))$$

and,

$$\theta_E/2 = \tan^{-1} (.25 / (F/D))$$

Therefore  $L$ (dB), at an  $F/D$  value of 0.6, is equal to approximately -1.39 dB. Thus the actual taper on the E-plane horn is 10 dB -1.39 dB = 8.61 dB.

Now we must find the actual  $b/\lambda$  required, using a taper of 8.61 dB (.3711 volts) and  $\lambda/4$  of phase error. Then  $b/\lambda \sin \theta_E = 0.8$  and  $b = 1.127 \lambda$  at  $\theta_E = 45.235$  degrees. Therefore at a frequency of 9.2 GHz,  $\lambda = 1.283$  inches, and  $b = 1.446$  inches.

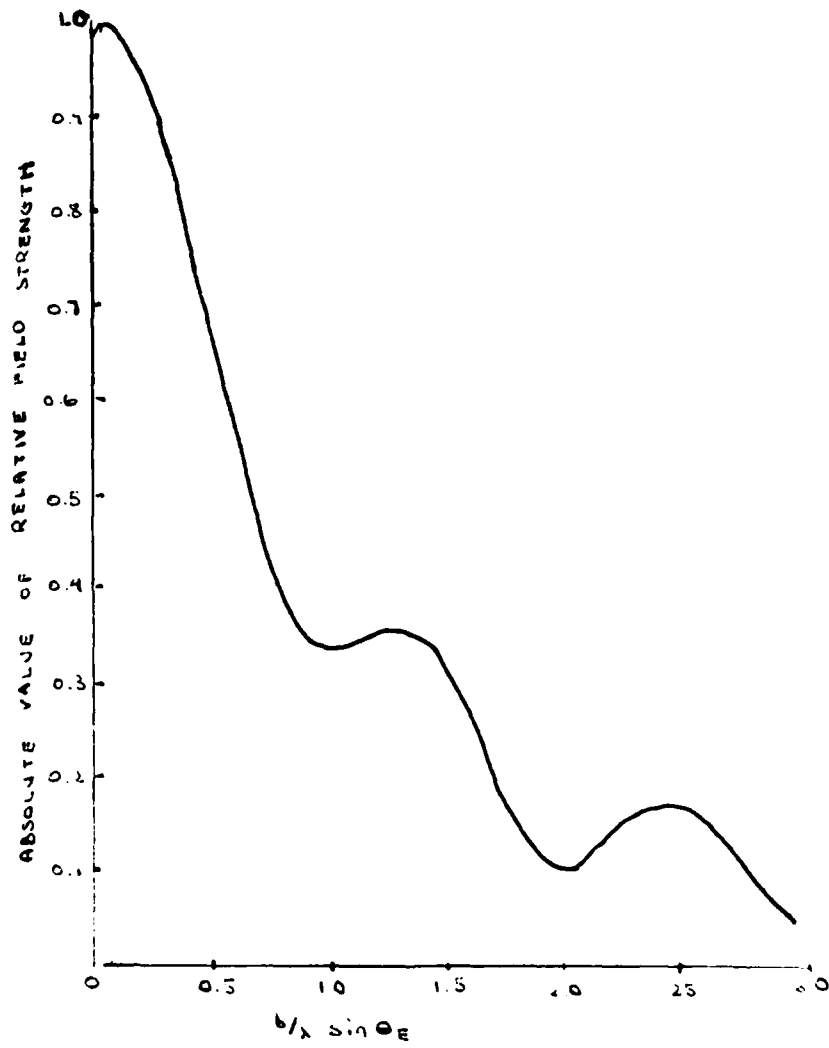


Figure 12. Universal radiation pattern of a horn flared in the E-plane (sectoral or pyramidal)

### Rectangular H-plane Horn Feed Design

The H-plane horn design will be accomplished similarly to that of the E-plane design. Now, we will determine the aperture,  $a$ , required in wavelengths using Figure 13. For a 10 dB edge taper, the corresponding voltage is 0.3162 volts without losses. We again choose  $\lambda/4$  of phase error as acceptable. Then  $a/\lambda \sin \theta_H = 1.2$  (without losses), obtained from Figure 13. Again, we must take the path loss taper into account. Now let  $\theta_E = \theta_H$ , then  $L(\text{dB}) = -1.39$  dB which are the path losses. Again, using 8.61 dB as the actual taper (subtracting out losses), a relative voltage of approximately 0.3711 volts can be obtained. We choose  $\lambda/4$  of phase error as acceptable. Then,

$$a/\lambda \sin \theta_H = 1.1$$

and  $\theta_H = 45.235$  degrees, then  $a = 1.159 \lambda$ .

### The Pyramidal Horn Feed

A pyramidal horn is obtained by flaring both the E-plane and H-plane horns simultaneously as shown in Figure 14. By the superposition principle, the results obtained independently for apertures "a" and "b" are still valid.

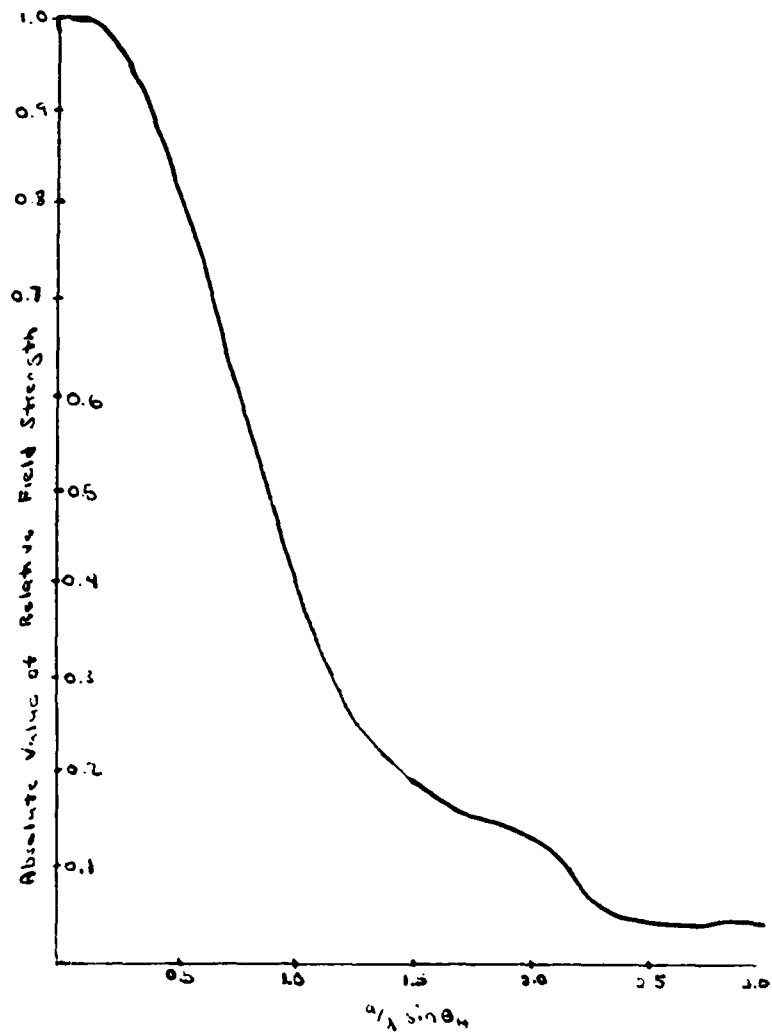


Figure 13 Universal radiation pattern of a horn flared in the H-plane (sectoral or pyramidal)

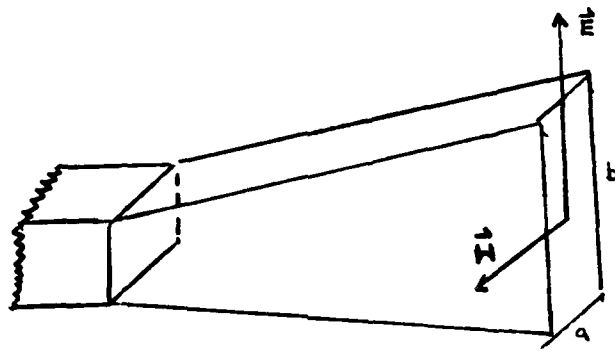


Figure 14. The Pyramidal Horn

## EFFECTIVE RADIATED POWER

The Effective Radiated Power (ERP) for any radar system, whether ground based or airborne can be calculated using the equation given below:

$$\text{ERP(dB)} = G(\text{dB}) + 10 \log (P_T) - L_s(\text{dB})$$

where G is the antenna gain (area gain - antenna losses),  $P_T$  is the power available out of a microwave tube, and  $L_s$  is the total system losses.

Antenna gain calculations can be found for both the simple cassegrain and twist cassegrain reflector antennas in Chapter 2 and 3 respectively. Output power for various commercially available Traveling Wave Tubes (TWT's) is listed in Appendix B of this paper. A TWT was chosen as the microwave power tube due to its high frequency stability and its ability to produce waveforms with pulse to pulse coherency.

System losses are generally taken to be in the order of 3-6 dB by various airborne radar designers. These losses include both waveguide and rotary joint losses for a typical airborne radar depicted in Figure 15.

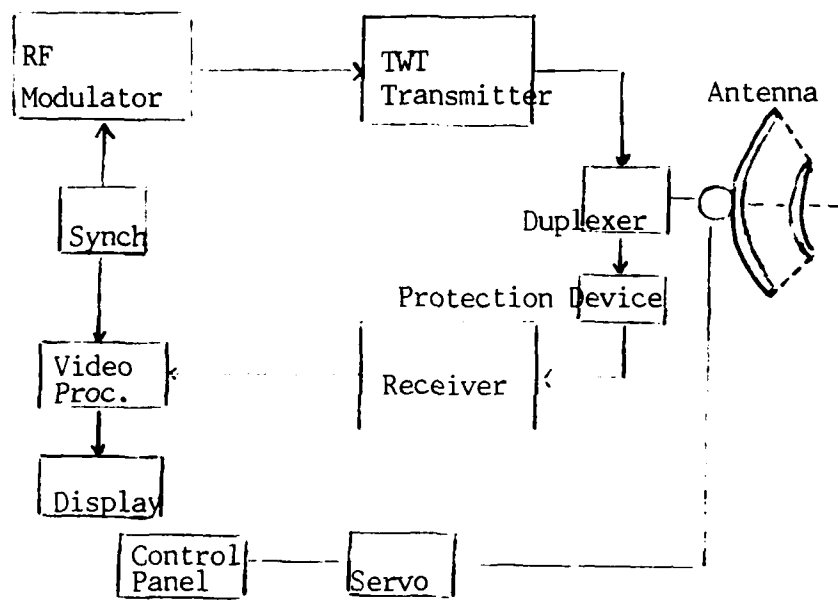


Figure 15. Airborne Radar Block Diagram

## METHOD OF SCANNING

The entire antenna structure for the optimized Swedish design is to be mechanically scanned through a maximum an angle of  $\pm 60$  degrees off boresight. The antenna scan pattern is essentially a five bar raster scan pattern as shown in Figure 16. Four bars are actually used for scanning (search pattern) and one bar will be used as the "flyback bar" to reset the search pattern. In track mode the antenna scan pattern will narrow to  $\pm 25$  degrees off boresight, for a more rapid update rate on hostile threats. The five bar scan pattern is to be used in track mode as well as in search mode to give a track while scan capability of up to ten targets. Beyond ten threats the system will simply track (with a coordinate position memory) of the nearest ten threats. To attempt to track multiple threats in any extremely saturated environment has historically proven quite difficult for most radar designers, with reliance on secondary sensors such as Identify Friend or Foe (IFF) sensors or electro-optic means. A boresight mode will be used for weapons delivery.

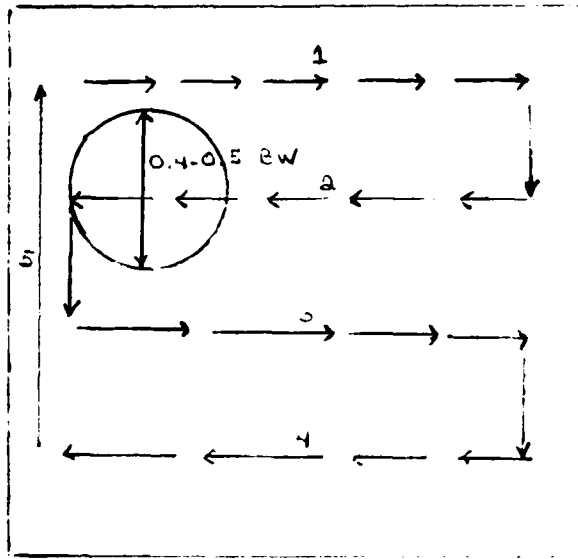


Figure 16. Five Bar Raster Search Pattern

## ANTENNA GAIN AND LOSS BUDGETS

The antenna gain for a paraboloid reflector can be calculated using the relationship  $G = \epsilon_{ap} (\pi D/\lambda)^2$  (Cutler, 1947). The efficiency for a front fed paraboloid is in the order of 55 percent while that of the cassegrain designs is substantially higher, within the range of 70 to 80 percent. The antenna efficiency can be approximated by use of the equation (Stutzman and Thiele, 1981):

$$\epsilon_{ap} = e \epsilon_1 \epsilon_2 \epsilon_3 \epsilon_4 \epsilon_5 \epsilon_6 \epsilon_7 \epsilon_8$$

where  $e$  represents ohmic losses,  $\epsilon_1$  is the spillover efficiency,  $\epsilon_2$  represents random surface error,  $\epsilon_3$  is the aperture blockage efficiency,  $\epsilon_4$  is the spar blockage efficiency,  $\epsilon_5$  is the squint factor,  $\epsilon_6$  is the astigmatism efficiency,  $\epsilon_7$  is the surface leakage efficiency,  $\epsilon_8$  is the depolarization efficiency, etc.

By working with a loss budget in decibels, we can compute (usually within 3dB) the total antenna gain for a particular reflector antenna, which is achievable experimentally. Table 4, on the next page gives typical losses associated with a Twist-Cassegrain reflector antenna that are most significant. Several of the losses (given as efficiencies) can be assumed to be negligible.

Table 4

Loss Budget for a Twist-Cassegrain Reflector Antenna

Gain or loss source	Gain or loss (dB)
Area Gain (27 inch reflector, 9.2 GHz)	36.83
Taper and Spillover efficiency	-1.1
Mismatch (VSWR = 1.7)	-0.3
Leakage thru the subreflector	-0.2
Loss in the polarization rotation device	-0.1
Imperfect rotation of polarization	-0.1
Scattering by wires in the subreflector to the desired polarization	-0.25
Sum and difference network	-0.4
Random errors in the surfaces of the <u>two reflectors</u>	<u>-0.25</u>
Total Antenna Gain	34.13

Note: This loss data is nearly the best physically achievable, in actual practice we can expect greater loss.

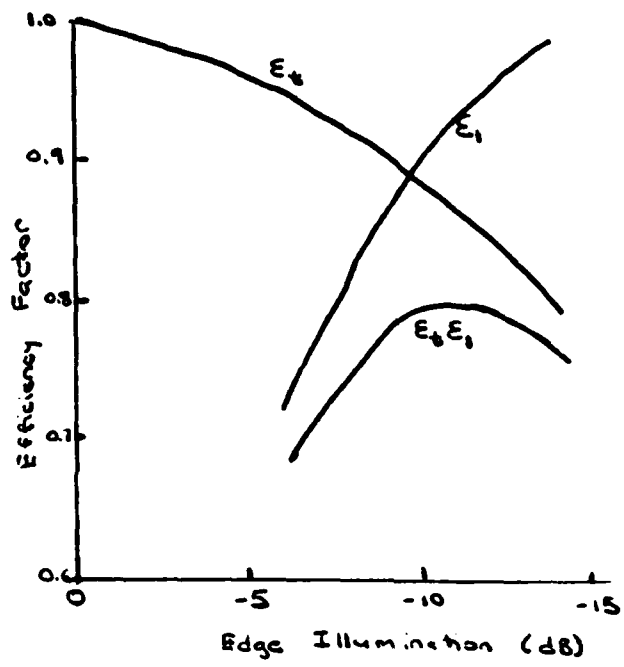


Figure 17. Edge Illumination Versus Efficiency Factor

Spillover efficiency,  $\epsilon_1$ , is defined as that percentage of the total energy radiated from the feed that is intercepted by the subreflector (Jensen, 1986). It can be calculated as follows:

$$\epsilon_1 = \int_0^{2\pi} \int_0^{\psi} f^2(\psi, \phi) \sin\psi d\psi d\phi / \int_0^{2\pi} \int_0^{\pi} f^2(\psi, \phi) \sin\psi d\psi d\phi$$

where  $f(\psi, \phi)$  is the feed pattern.

In our case, the efficiency factor,  $\epsilon_1$ , is approximately equal to 0.774 or -1.11 dB (including the edge taper) for an angle,  $\psi_0$ , from the focal point to the edge of the subreflector equal to 45.24 degrees (see listing EG621310). The Hughes Vector diffraction program computes these losses as a function of  $\psi_0$ , and prints results at one degree intervals. Interpolation is required to get the correct loss figure accuracy to 0.1 dB. A value of -10 dB edge taper is frequently quoted as providing an optimum efficiency factor,  $\epsilon_1$  (Stutzman and Thiele, 1981). Figure 17 shows the general relationship for this efficiency factor (Stutzman and Thiele, 1981, Figure 8-26). The maximum value of this efficiency factor is approximately 0.8, near -11 dB edge tapers.

The efficiency factor for random surface error,  $\epsilon_2$ , is associated with far-field cancellations arising from random phase errors in the aperture field. It is defined as:

$$\epsilon_2 = e^{-(4\pi\sigma/\lambda)^2}$$

Here  $\delta'$  is the rms surface deviation (Stutzman & Thiele). In most cases  $\epsilon_2$  is almost unity. RMS surface tolerances generally depend on the type of surface and range from .04 mm for machined aluminum to 0.64 for spun aluminum. A simple formula for representing surface accuracy as a function of reflector diameter is by Stutzman and Thiele as

$$\delta' = 3 \times 10^{-2} D \text{ mm}$$

where D (reflector diameter) is in meters.

Aperture blockage efficiency,  $\epsilon_3$ , is due to the presence of a subreflector in front of the main reflector. This efficiency ranges from 0.990 (for  $d/D = 0.05$ ) to 0.835 (for  $d/D = 0.20$ ) according to Stutzman and Thiele.

Other efficiency factors  $\epsilon_4$  through  $\epsilon_8$  are also values very near unity and will not be discussed here. For example  $\epsilon_7$ , the surface leakage efficiency = 0.99 for a mesh with several grid wires per wavelength (Stutzman and Thiele).

### THREE DB BEAMWIDTH

The Three DB Beamwidth can be approximated using the formula (Williams, 1984):

$$\theta_{3dB} = K_{BW} (\lambda / D) \text{ degrees}$$

where  $K_{BW}$  is the beamwidth constant which is generally equal to 50 to 80, but is dependent on the aperture distribution used. For example, for a paraboloidal distribution, the beamwidth constant is equal to 72.8 (Jasik, 1961). For an airborne radar a narrow 2 to 3 degree pencil beam is sufficient to track targets, in angle (Williams, 1984).

CHAPTER 3  
OPTIMIZED TWIST-CASSEGRAIN DESIGNS

ENGLISH TWIST-CASSEGRAIN DESIGNS

Marconi has developed a Twist-Cassegrain aerial (antenna) design for use in airborne radars. In this case the feed was a pyramidal horn, the subreflector was composed of a wire grid, and the main reflector was utilized to twist the polarization from horizontal to vertical (Scorer, Graham, and Barnard, 1978).

The twist-reflector was comprised of a solid metal back reflector and a wire grid which are spaced approximately one quarter wavelength apart. The F/D ratio chosen was 0.46, with a value of  $D = 20 \lambda$ . Figure 18 shows the layout of this antenna design.

Another Twist-Cassegrain aerial, shown in Figure 19, is used in the GEC Foxhunter Airborne Radar (Spooner and Sage, 1985). It has a wide RF bandwidth to accommodate both the radar and CW illuminator operating bands. This type of aerial enables the high gain required for long detection ranges necessary for search modes.

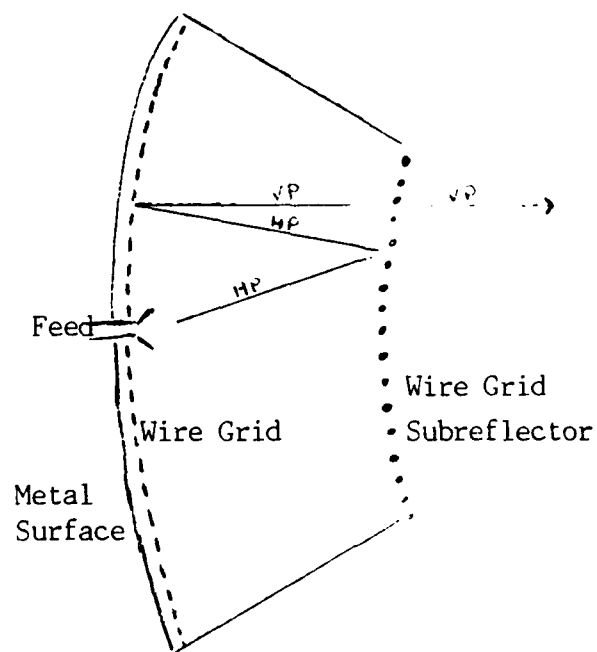


Figure 18. Marconi Twist-Cassegrain Antenna (Aerial)

A two-plane monopulse feed is provided for track modes and separate dipoles are provided at a lower frequency for the transmission and reception of Identify Friend or Foe interrogation signals (Spooner and Sage, 1985). Nomex honeycomb and glass fiber materials are used in the construction of the aerial to produce a rigid, low inertia assembly.

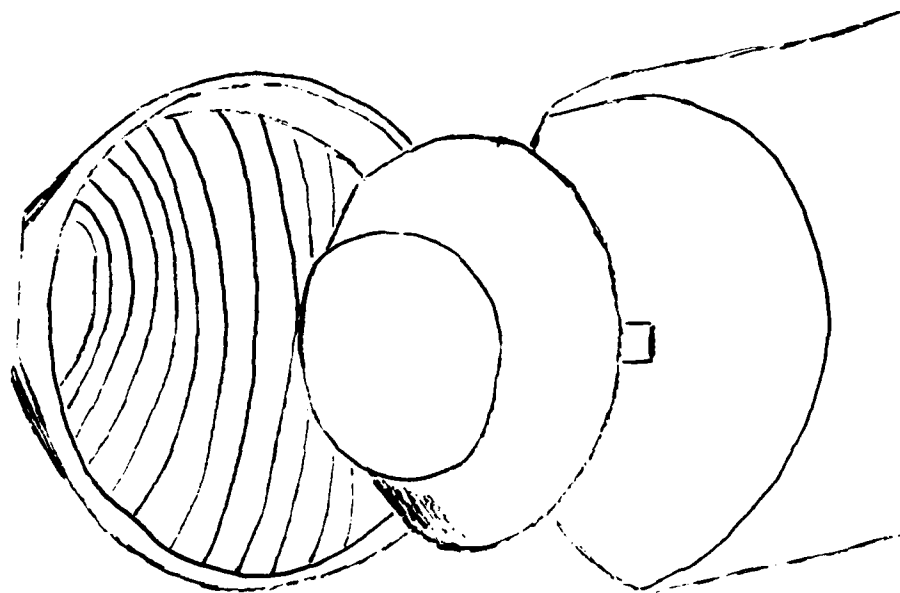


Figure 19. GEC Twist-Cassegrain Antenna Installed in Tornado F  
MK 2 Aircraft (Front View)

## SWEDISH TWIST-CASSEGRAIN DESIGNS

The Swedish design principally consists of a 27.0 inch diameter main reflector and a subreflector approximately 23.91 inches in diameter as shown in Figure 20. In addition, it contains an elaborate three channel, two port, multimode monopulse feed as shown in Figure 21. It is designed to radiate in X-band. Another Swedish design is fully described in a paper entitled "A Low Side Lobe Cassegrain Antenna" (Dahlsjo, 1973). In addition, another Swedish design allows for both X-band and Ka-band capabilities. This design is shown in Figures 22 and 23 (Dahlsjo, Ljungstrom, and Magnusson, 1986).

The general principle of both designs is to have a linearly polarized monopulse feed illuminating a subreflector, which is placed directly in front of the vertex of main reflector. The polarization of the ray reflected off the subreflector is twisted ninety degrees in the main reflector. Now, no aperture blockage is caused by the polarization sensitive subreflector. Finally, a transparent cone supports the subreflector. This cone is lined with polarization sensitive absorbers which are used to reduce the spillover effects of the monopulse feed.

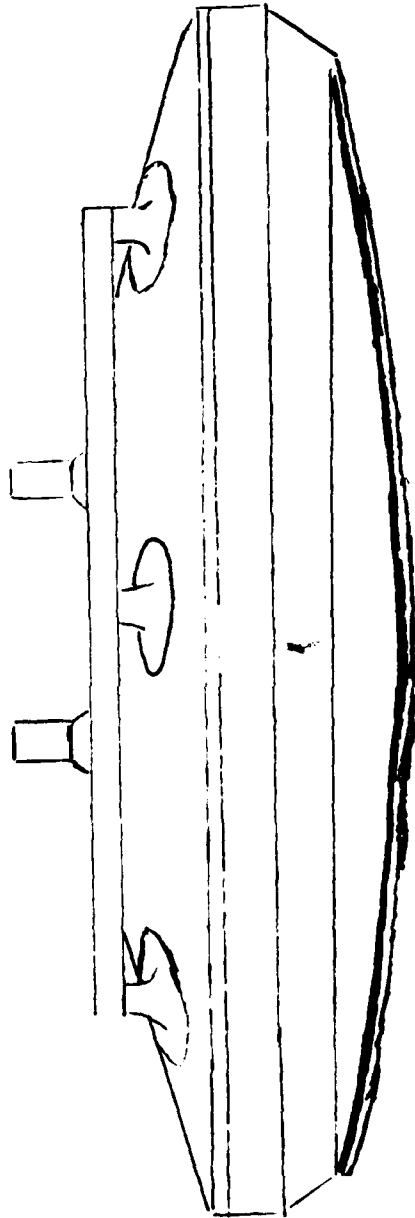


Figure 20. Swedish Twist-Cassegrain Antenna

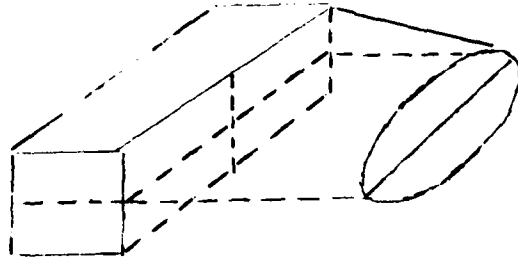


Figure 21. Multimode Swedish Monopulse Feed

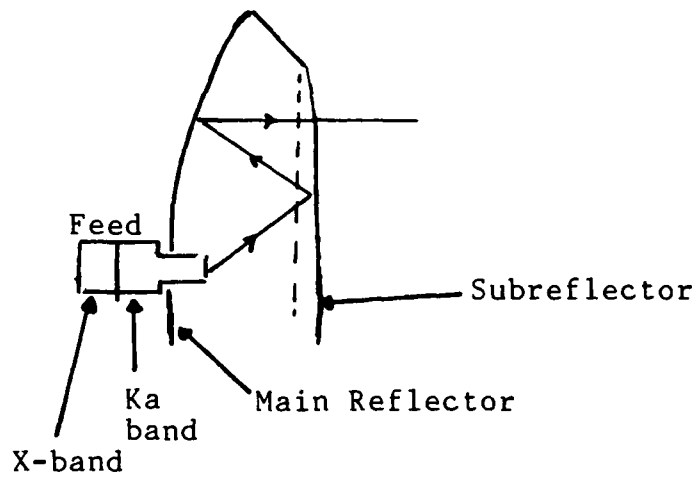


Figure 22 Dual-band Twist Cassegrain Design

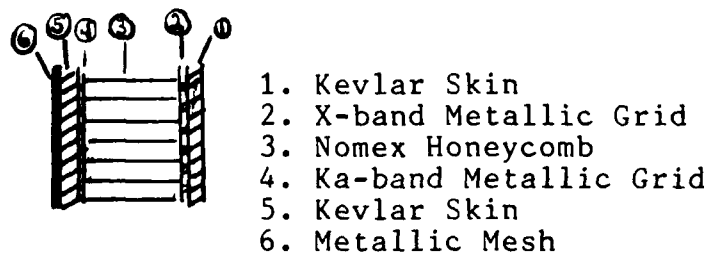


Figure 23. Twist-Reflector Cross Section

## OPTIMIZED SWEDISH DESIGN

The writer will utilize the Swedish design, because of its more compact structure and its ability to be given a broad-band capability by the simple addition of another wire grid structure to the twist-reflector (Josefsson, 1981). Furthermore, this design has been experimentally shown to produce antenna gains in excess of 25 dB and moderate to low sidelobes.

The writer will incorporate a pyramidal horn feed instead of the monopulse feed. The Hughes Vector Diffraction Program described in Chapter 4 will treat this feed as a point source in its simulation. The pyramidal horn feed is chosen for high reliability, low cost, and a desire to maintain a single mode structure radiating the  $TE_{10}$  mode only. Corrugated horns were ruled out due to their multimode structures and the writer's desire not to introduce a mode filter into the design.

Figure 24 on the next page shows the layout of this design with a paraboloid twist-reflector and a hyperboloid subreflector. The design retains the support cones which are equipped with absorber material to attenuate the spillover radiation.

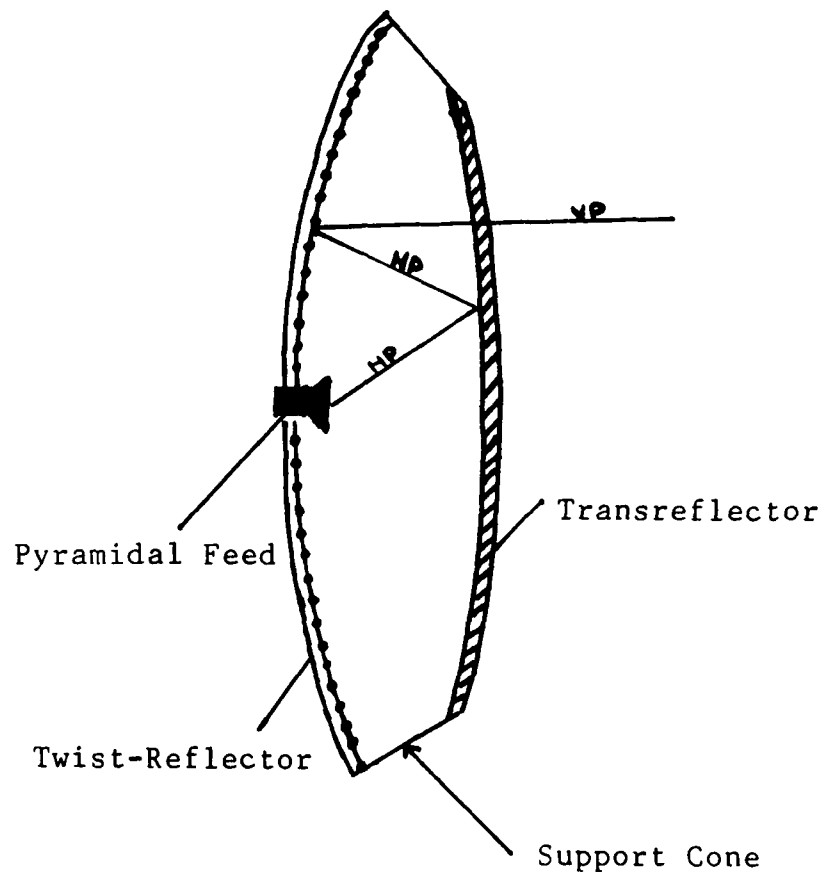


Figure 24. Optimized Swedish Twist-Cassegrain Antenna With Pyramidal Feed

### System Design Description

The twist-Cassegrain antenna has a weight of approximately 10 pounds and has a paraboloid diameter of nearly 28.4 inches (approximately 5 per cent larger than the basic Swedish design for greater antenna gain). Note that a 30.0 inch design was also considered, but discarded in Chapter 4 of this paper, as well as, a 27.0 inch paraboloid with a 6.4 inch subreflector.

The curved subreflector is constructed with a quarter-wave sandwich of two gratings of closely spaced thin wires inbedded between the fiberglass skins and the foam core. This gives us a perfect reflector for horizontal polarization and in addition, good transmission for vertical polarization. The twist reflector grating of wires is oriented at 45 degrees to the incident polarization and placed about  $3/8 \lambda$  from the reflecting surface. This gives a 90 degree twisting of the incident polarization over a broad frequency band (I-band) and over a wide range of incident angles. The reflector surface is a fine structure wire mesh inbedded in the outer fiberglass skin.

## BASIC PARAMETERS OF THE OPTIMIZED DESIGN

The parameters of the candidate designs A through E are listed in the following pages in Tables 5 through 9. The basic 27 inch diameter (of the paraboloid) was not considered due to its inferior antenna gain than that of the 28.4 or 30.0 inch designs, even though it produced respectable first sidelobe levels greater than -25 dB down from the main lobe.

Table 5  
Parameters of Optimized Design A

Diameter of the paraboloid	28.4 inches
Diameter of the subreflector	25.0 inches
Focal length of the paraboloid	17.0 inches
F/D ratio	0.6
Eccentricity	-9.0
Wavelength	1.28 inches
Frequency	9.21 GHz
Angle Alpha 0	61.50 degrees

Table 6  
Basic Parameters of Design B

Diameter of the paraboloid	28.4 inches
Diameter of the subreflector	25.0 inches
Focal length of the paraboloid	14.2 inches
F/D ratio	0.5
Eccentricity	-49.6
Wavelength	1.28 inches
Frequency	9.21 GHz
Angle Alpha 0	61.50 degrees

Table 7

Basic Parameters of Design C

Diameter of the paraboloid	28.4 inches
Diameter of the subreflector	25.0 inches
Focal length of the paraboloid	19.8 inches
F/D ratio	0.7
Eccentricity	-5.4
Wavelength	1.28 inches
Frequency	9.21 GHz
Angle Alpha 0	61.50 degrees

Table 8

Basic Parameters of Design D

Diameter of the paraboloid	30.0 inches
Diameter of the subreflector	26.6 inches
Focal length of the paraboloid	18.0 inches
F/D ratio	0.6
Eccentricity	-9.02
Wavelength	1.28 inches
Frequency	9.21 GHz
Angle Alpha 0	61.50

Table 9  
Basic Parameters of Design E

Diameter of the paraboloid	27.0 inches
Diameter of the hyperboloid	6.4 inches
Focal length of the paraboloid	16.2 inches
F/D ratio	0.6
Eccentricity	1.82
Wavelength	1.28 inches
Frequency	9.21 GHz
Angle Alpha 0	13.87 degrees

Note: This represents a case with approximately a  $5 \lambda$  subreflector. The purpose is to show edge diffraction effects of small subreflectors.

### First Sidelobe Level Estimates

Using the approximations for a circular aperture distribution developed in the Antenna Theory and Design (Stutzman and Thiele, 1984), we choose a cosine on a pedestal distribution (equivalent to a  $\cos^2\theta$ ) since that is the distribution utilized in the Hughes Vector Diffraction Program and is not easily changable. We assume -10 dB edge illumination and therefore expect -22.3 dB first sidelobe levels which is very near those obtained by simulation in Chapter 4.

## CHAPTER 4

### PERFORMANCE ANALYSIS OF OPTIMIZED DESIGN

#### MODIFIED VECTOR DIFFRACTION PROGRAM

The Hughes Aircraft Company's Modified Vector Diffraction Program currently is executable in Building R-2 of the Radar Systems Group facility in El Segundo, California. In 1975, Hughes modified an existing vector diffraction computer program originally written by W.V.T. Rusch for the Jet Propulsion Laboratory. At that time it was modified to be used on an IBM 370 computer. Over the years, it has been upgraded and currently runs on an IBM 3038 computer.

The computer program basically calculates the integrals for scattering from an arbitrary reflector. In its present form, the program is used to compute far field patterns of the hyperbolic subreflectors and parabolic reflectors in a Cassegrain arrangement. Figure 25 shows the geometry of this arrangement (Bargeliotis, 1975). The descriptive variable names of the parameters used in the program are shown in Appendix D.

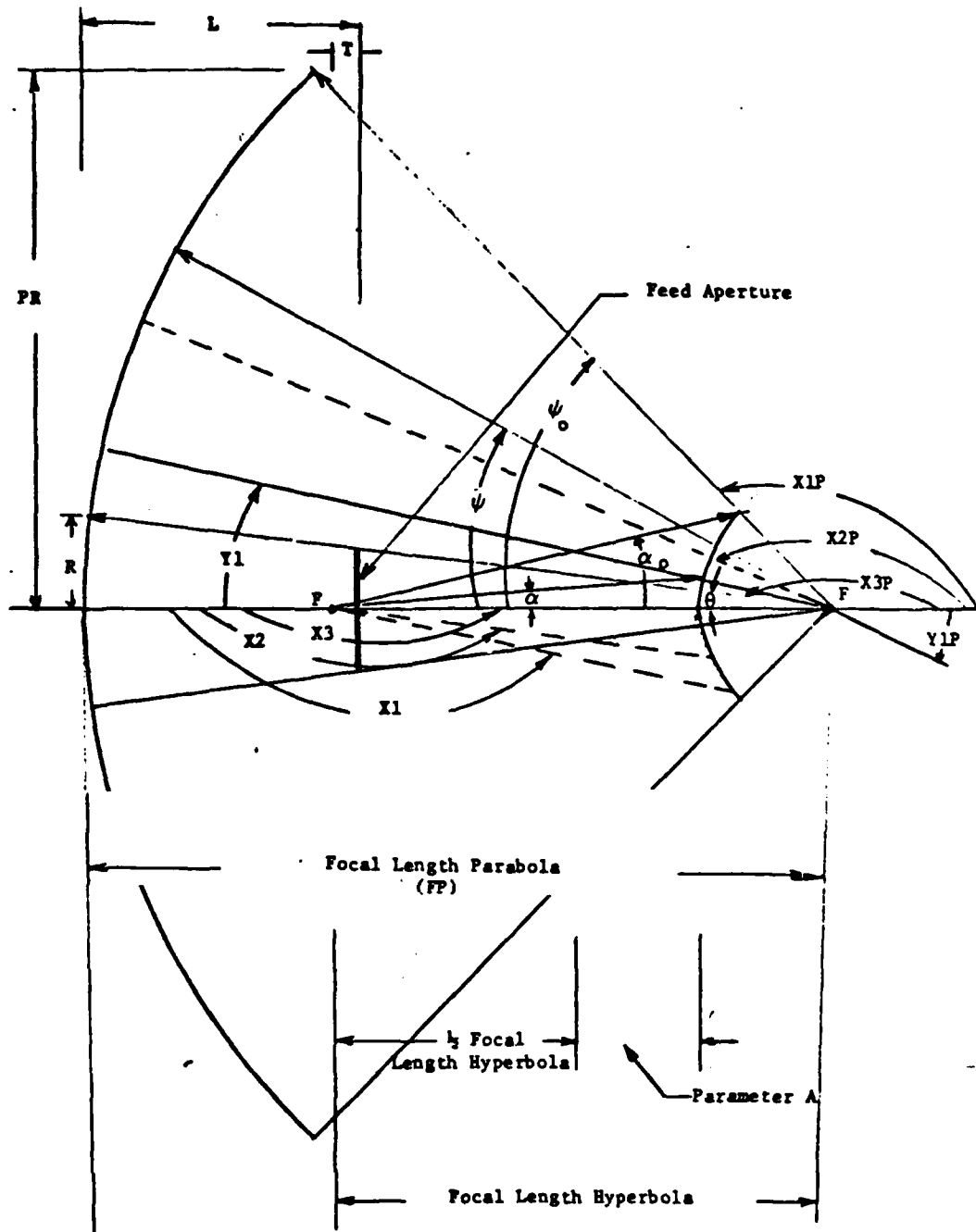


Figure 25. Geometry of Hughes Simulation

The illumination of the hyperbolic subreflector is assumed to be symmetric with respect z-axis. A symmetrical feed pattern of  $\cos^2\theta$  is utilized in the program. The scattering field from the hyperbolic subreflector is then found by a mode expansion and integration process and is added to the incident field to yield the total field of the feed-hyperboloid system. This field is then taken as the incident field to the paraboloid and the process is repeated by computation of the scattering field from the paraboloid by mode expansion and integration and addition to the incident field. Next, far field patterns of the E-plane and the H-plane are computed and plotted by a CALCOMP 1055 plotter for both the primary (hyperboloid) and secondary (paraboloid) reflectors. The program takes into account the aperture blocking by the hyperboloid and also computes the efficiency of the antenna by use of the EFFY subroutine.

## RUSCH SCATTERING EQUATIONS

### Background

Rusch uses the Kirchhoff theory of physical optics (current-distribution method) to calculate the diffraction pattern resulting from a spherical wave incident upon an arbitrary truncated surface of revolution such as a hyperboloid or a paraboloid (Rusch, 1963).

### The Field Integrals

In terms of the geometry shown in Figure 26, the incident electric field,  $E_{inc}$ , of the spherical wave emerging from point O may be described as:

$$E_{inc}(\theta, \phi) = A(\theta) e^{ikR}/R E(\theta, \phi) \quad (4.1)$$

Here the unit vector  $E(\theta, \phi)$  describes the polarization of the incident field, and  $A(\theta)$  is the pattern factor of the incident field assumed to be axially symmetric.

Rusch assumes that the axially symmetric reflecting surface can be described by a polar equation:

$$(k \rho)g(\theta') = -1, \quad \theta_0 \leq \theta' \leq \pi \quad (4.2)$$

where, for a paraboloid of focal length,  $F$ , we have:

$$g(\theta') = (1 - \cos\theta') / (4 \pi F / \lambda). \quad (4.3)$$

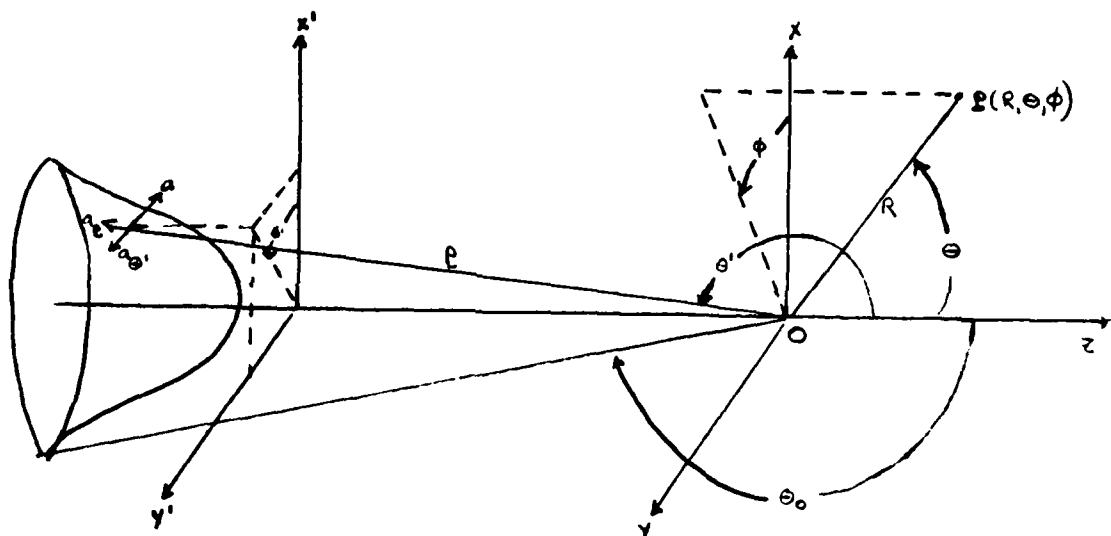


Figure 26. Geometry of Rusch Integrals

Also, for a hyperboloid of eccentricity,  $e$ , we have:

$$g(\theta') = (1 + e\cos\theta')/kep. \quad (4.4)$$

Note that equation 4.2 is sufficiently general to include all axially symmetric surfaces which are single-valued functions of  $\theta$ .

From Equation 4.2 and the geometry of Figure 26 it can be shown that the outward surface normal,  $n$ , from the front of the reflector is:

$$\vec{n} = (g(\theta') \vec{a}_z + g'(\theta') \vec{a}_\theta) / \{ [g(\theta')]^2 + [g'(\theta')]^2 \}^{1/2} \quad (4.5)$$

The differential surface element,  $dS$ , on the reflector is:

$$dS = -e^2 \{ [g(\theta')]^2 + [g'(\theta')]^2 \} / g(\theta') \sin\theta' d\theta' d\phi' \quad (4.6)$$

If the wavelength of the incident field is small compared with the transverse dimensions and the radius of curvature of the reflector, and if the reflector is many wavelengths distant from the source, the current distribution induced on the illuminated front of the surface can be closely approximated by assuming that at every point the incident field is reflected as an infinite plane wave from an infinite plane tangent at the point of incidence. The current in the "shadow" region on the back of the reflector is assumed to make a negligible contribution to the field. By integrating the induced surface current distribution over the front of the reflector, it is possible to compute the scattered field as shown in Silver, 1949 as:

$$\vec{E}_s(\theta, \phi) = (i/\lambda) (e^{ikR}/R) \int_s A(\theta') (e^{ikr(1-\cos\theta')} \vec{a}_r) [\vec{n} \times \vec{h}(\theta', \phi')]_{\text{trans}} dS(\theta', \phi') \quad (4.7)$$

In Equation 4.7,  $\vec{h}(\theta', \phi')$  is defined as  $\vec{a}_\phi \times \vec{e}(\theta', \phi')$  and the only components involved in the integration are the transverse components of  $\vec{n} \times \vec{h}(\theta', \phi)$ . If the primary source is polarized in the x-direction, in which case  $\vec{e}(\theta', \phi) = [-\cos\theta \vec{a}_\theta - \sin\theta \vec{a}_\phi]$ , the  $\phi$ -component of the scattered field is:

$$a_\phi \cdot E_s = (i/k\lambda)(e^{i k R}/R) \int_0^{\theta_2} [A(\theta') e^{i a \sin\theta'}] / [g(\theta')]^2 \\ \{ [(1+\cos\theta')g(\theta') - \sin\theta'g'(\theta')] \\ \cos\phi' \sin(\phi' - \phi) e^{i \xi \cos(\phi' - \phi)} d\phi' + g(\theta') \cdot \\ \sin\phi \int_0^{2\pi} e^{i \xi \cos(\phi' - \phi)} d\phi' \} d\theta' \quad (4.8)$$

where:

$$a(\theta, \theta') = [\cos\theta' \cos\theta - 1] / g(\theta') \quad (4.9)$$

and:

$$\xi(\theta, \theta') = [-\sin\theta \sin\theta'] / g(\theta'). \quad (4.10)$$

In addition, we have:

$$\int_0^{2\pi} \cos\theta' \sin(\phi' - \phi) e^{i \xi \cos(\phi' - \phi)} d\phi' = -\pi \sin\phi \{ J_0(\xi) \\ + J_2(\xi) \} \quad (4.11)$$

and:

$$\int_0^{2\pi} e^{i \xi \cos(\phi' - \phi)} d\phi' = 2\pi J_0(\xi). \quad (4.12)$$

Next, the  $\phi$ -component of the total field is:

$$\vec{E}_\phi = (\vec{E}_{inc} + \vec{E}_s) \cdot \vec{a}_\phi \quad (4.13)$$

or:

$$E_\phi(R, \theta, \phi) = (i/2)(e^{i k R}/R) \sin\phi (R_\phi + iI_\phi). \quad (4.14)$$

$R_\phi$  and  $I_\phi$  in Equation 4.14 are defined as:

$$R_\phi = \int_{\theta_1}^{\theta_2} \left[ \frac{A(\theta') \cos \alpha (\sin \theta')}{[g(\theta')]^2} \{ g(\theta') [J_0(\phi) - J_2(\phi)] + [g'(\theta') \sin \theta' - g(\theta') \cos \theta'] [J_0(\phi) + J_2(\phi)] \} \right] d\theta' \quad (4.15)$$

$$I_\phi = 2A(\theta) + \int_{\theta_1}^{\theta_2} \left[ \frac{A(\theta') \sin \alpha (\sin \theta')}{[g(\theta')]^2} \{ g(\theta') [J_0(\phi) - J_2(\phi)] + [g'(\theta') \sin \theta' - g(\theta') \cos \theta'] [J_0(\phi) - J_2(\phi)] \} \right] d\theta' \quad (4.16)$$

The H-plane pattern is then  $[(R_\phi)^2 + (I_\phi)^2]^{1/2}$

Similarly the  $\theta$ -component of the total field is:

$$E_\theta(R, \theta, \phi) = (i/2)(e^{i k R} / R) \cos \phi [R_\theta + i I_\theta] \quad (4.17)$$

where  $R_\theta$  and  $I_\theta$  are defined as:

$$R_\theta = \int_{\theta_1}^{\theta_2} \left[ \frac{A(\theta') \cos \alpha (\sin \theta')}{[g(\theta')]^2} \{ \cos \theta [1 + \cos \theta'] g(\theta') - \sin \theta' g(\theta') \} \times [J_0(\phi) - J_2(\phi)] - 2 \sin \theta [\sin \theta' g(\theta') + \cos \theta' g'(\theta')] \times J_1(\phi) - 2 \cos \theta g(\theta') J_0(\phi) \right] d\theta' \quad (4.18)$$

$$I_\theta = 2A(\theta) + \int_{\theta_1}^{\theta_2} \left[ \frac{A(\theta') \sin \alpha (\sin \theta')}{[g(\theta')]^2} \{ \cos \theta [(1 + \cos \theta') g(\theta') - \sin \theta' g(\theta')] \times [J_0(\phi) - J_2(\phi)] - 2 \sin \theta [\sin \theta' g(\theta') + \cos \theta' g(\theta')] \times J_1(\phi) - 2 \cos \theta g(\theta') J_0(\phi) \} \right] d\theta' \quad (4.19)$$

The E-plane pattern is then  $[(R_\theta)^2 + (I_\theta)^2]^{1/2}$

## FAR FIELD PATTERN RESULTS

### Design A

The F/D ratio is fixed at 0.6 (approximately the same as the Swedish design). The diameter of the main reflector is 28.346 inches (about 5 percent larger than the basic Swedish design). The purpose of this size increase is to increase directivity and gain, but not increase the volume or weight significantly. The simulation is run over a frequency of 9.2 GHz with the output incremented every degree over 180 degrees.

The far field patterns (secondary pattern off of the main reflector) are shown in Figures 27 and 28 for the E- and H-planes respectively. The data and results for this case can be found in listing EG62131J. The results are too voluminous to be included in this paper in other than graphical form.

In addition, the primary pattern off of the hyperboloid are shown in Figures 29 and 30 respectively. Notice the first sidelobe in the E-plane appears at -21 dB below the main lobe and -22.5 dB below the main lobe for the H-plane.

**TWIST CASSEGRAIN ANTENNA**  
**SECONDARY PATTERN: E-PLANE**

DIA. = 28.348 IN. FREQ = 9.2 GHZ  
F/D = 0.6

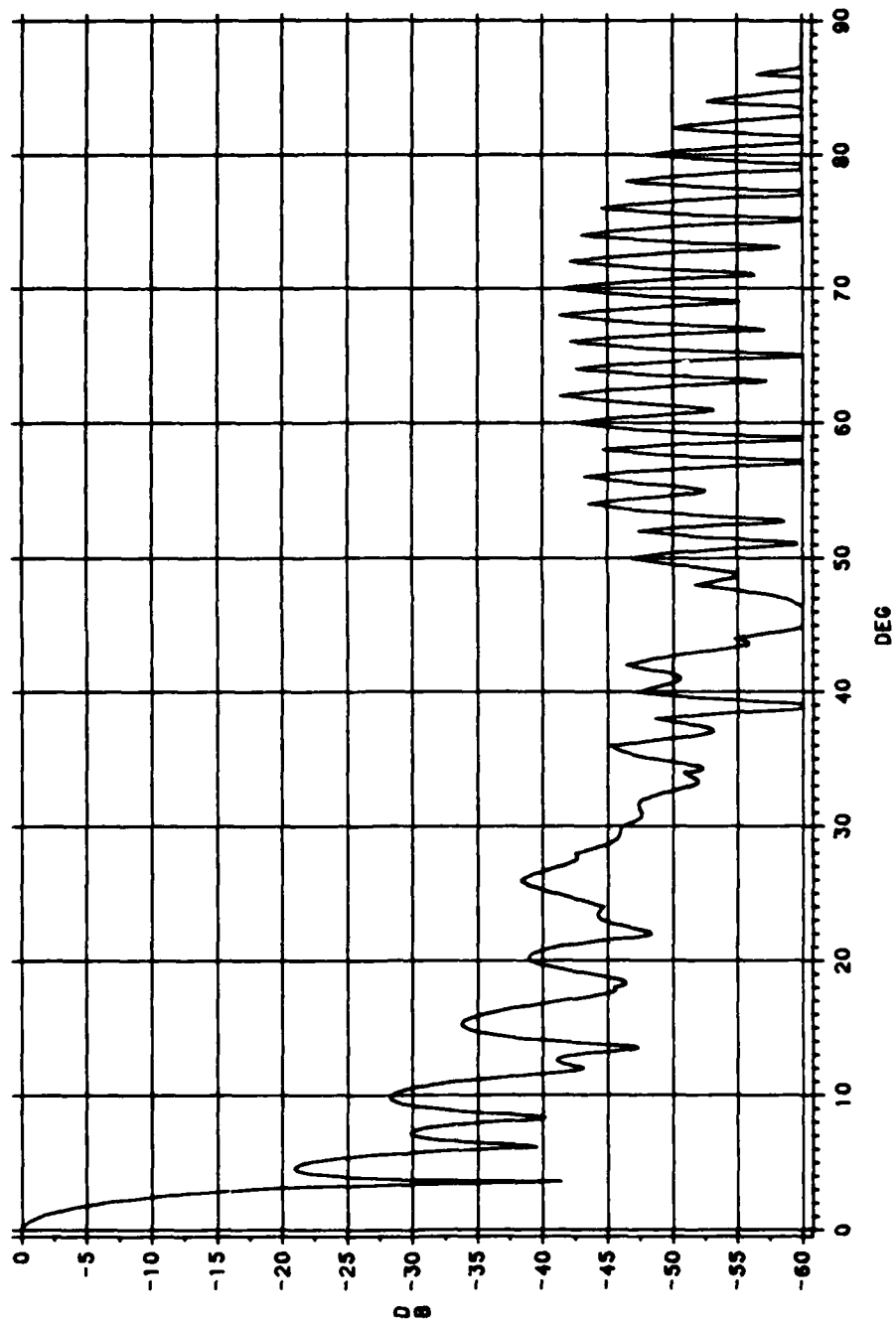


Figure 27. Secondary Pattern for E-Plane for Design A

**TWIST CASSEGRAIN ANTENNA**  
SECONDARY PATTERN, H-PLANE

DIA. = 28.346 IN. FREQ = 9.2 GHZ  
F/D = 0.6

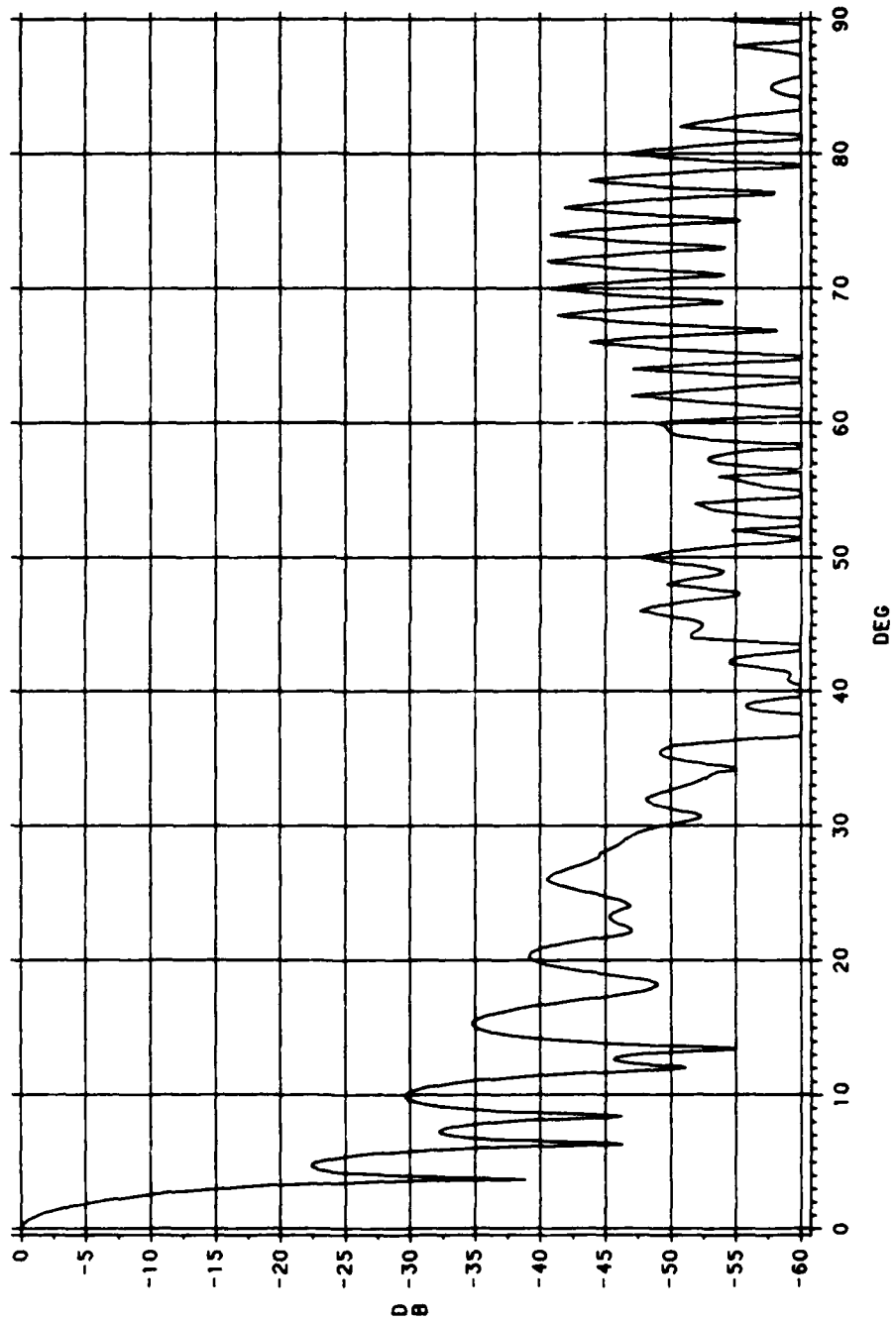
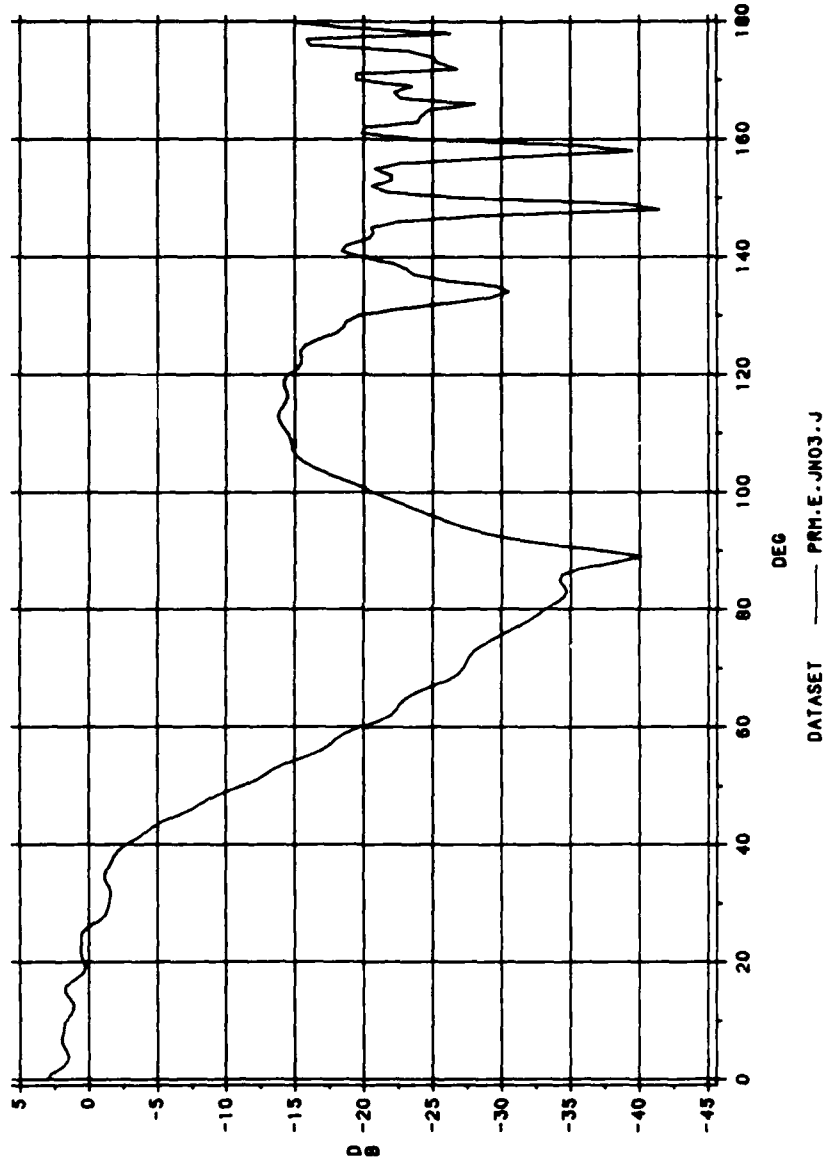


Figure 28. Secondary Pattern for H-Plane for Design A

**TWIST CASSEGRAIN ANTENNA**  
PRIMARY PATTERN - E-PLANE

DIA. = 28.346 IN. FREQ = 9.2 GHz  
F/D = 0.6



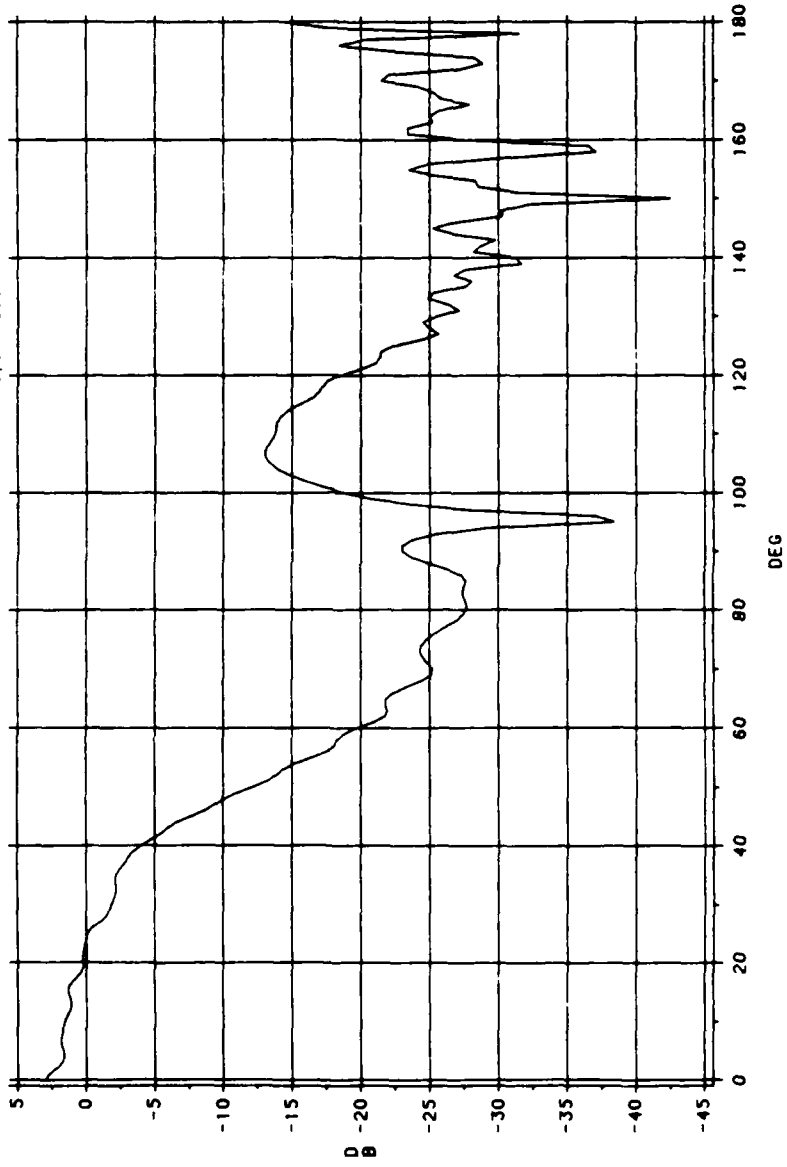
29JUL88 16:21:06

Figure 29. Primary Pattern for E-Plane for Design A

**TWIST CASSEGRAIN ANTENNA**  
PRIMARY PATTERN - H-PLANE

DIA. = 28.346 IN. FREQ = 9.2 GHZ

F/D = 0.6



DATA SET ——— PRM.H.JN03.J

05AUG88, 11:02:38

Figure 30. Primary Pattern for H-Plane for Design A

Since we desired at symmetrical -25 dB first sidelobes for both planes, this design is not chosen as the optimized design. While airborne radars with -13 dB first sidelobe level have been found experimentally to operate over the years primarily in "pulsed systems", they represent poor designs in todays jamming environment. State-of-the art systems today, using array technology can achieve below -35 dB first sidelobe levels (Williams, 1984).

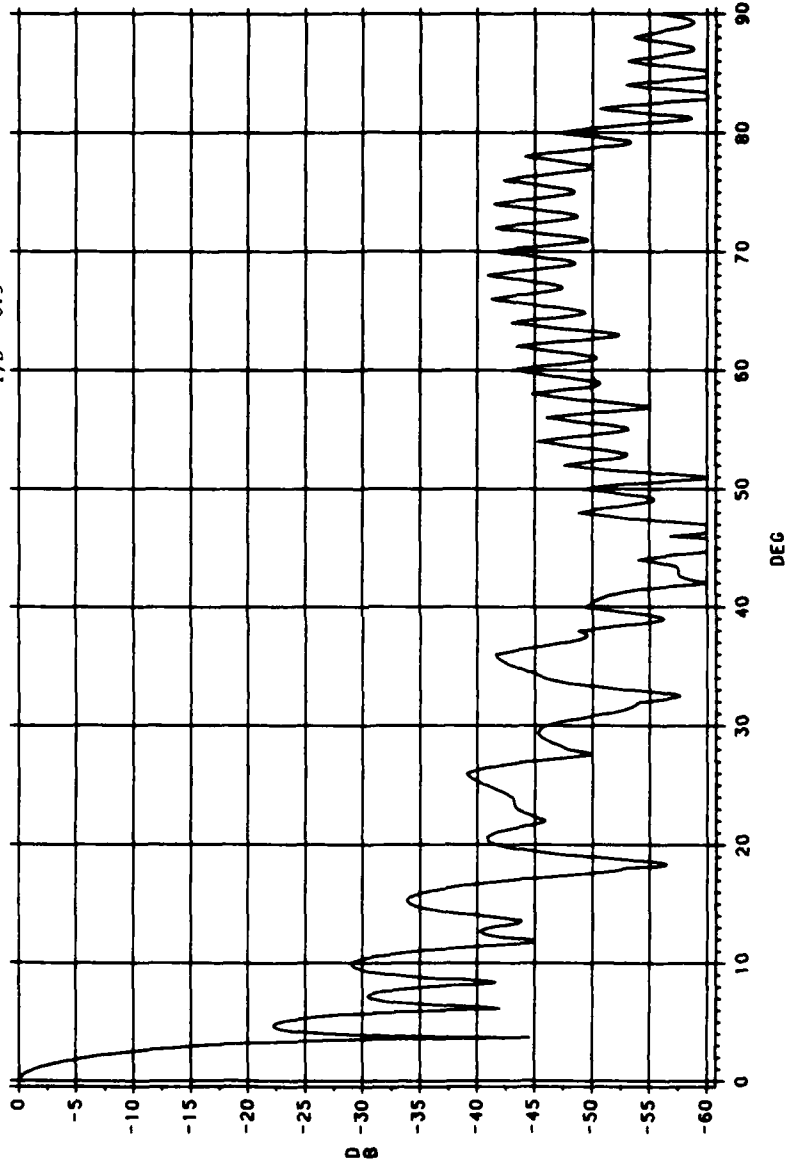
### Design B

In this design we again have a 28.346 inch main reflector, however, now we have changed the F/D ratio to 0.5 for a more compact antenna structure. The frequency was kept at 9.2 GHz for consistency. The results for this case can be found in listing EG62131L. These results are plotted for the far field pattern for the E and H planes in Figures 31 and 32 respectively. The primary patterns for both the E and H planes are plotted in Figures 33 and 34 respectively. The far field pattern for the E-plane shows a first sidelobe level at -22.3 dB, while the H-plane pattern shows a -22.5 dB first sidelobe level. While, both are above the required -25 dB first sidelobe level goal stated in the purpose statement, the patterns show good uniformity overall.

TWIST CASSEGRAIN ANTENNA  
SECONDARY PATTERN, E-PLANE

DIA. = 28.346 IN. FREQ = 9.2 GHz

F/D = 0.5



DATASET SEN.E.JN09.L

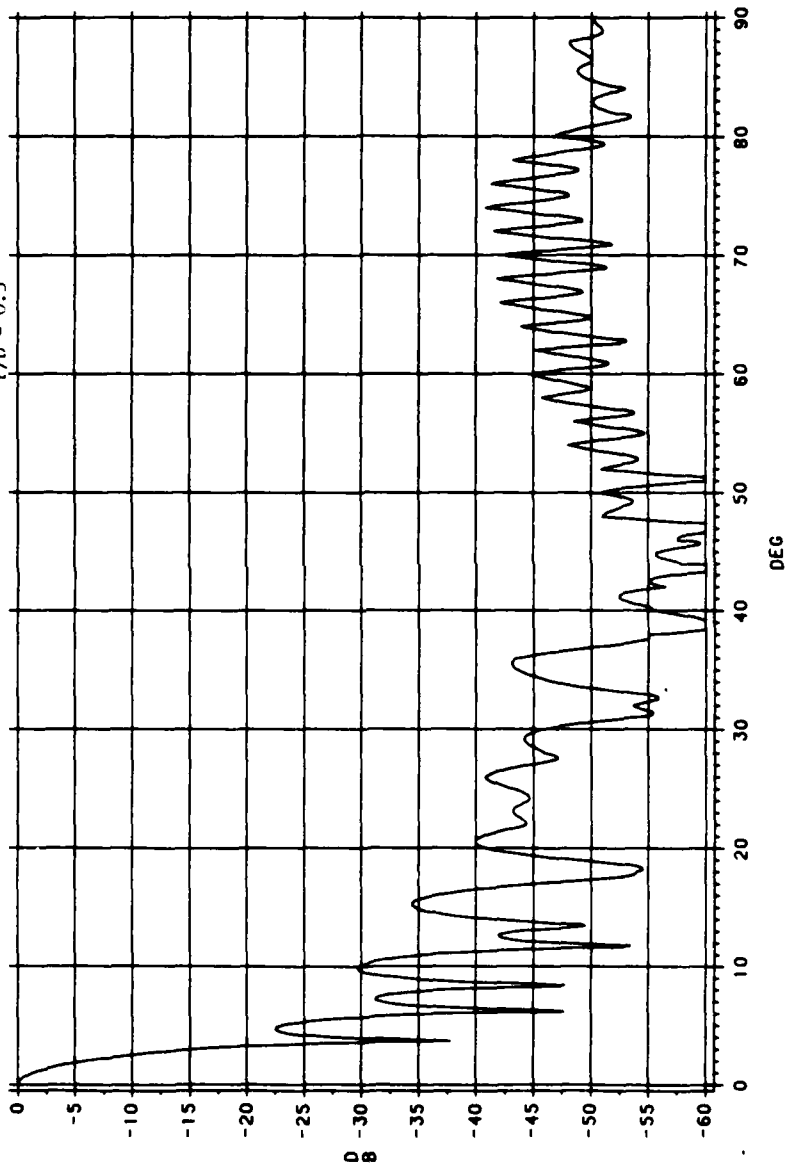
16 JUN 88 15:09:45

Figure 31. Secondary Pattern for E-Plane for Design B

TWIST CASSEGRAIN ANTENNA  
SECONDARY PATTERN: H-PLANE

DIA. = 28.346 IN. FREQ = 9.2 GHZ

F/D = 0.5

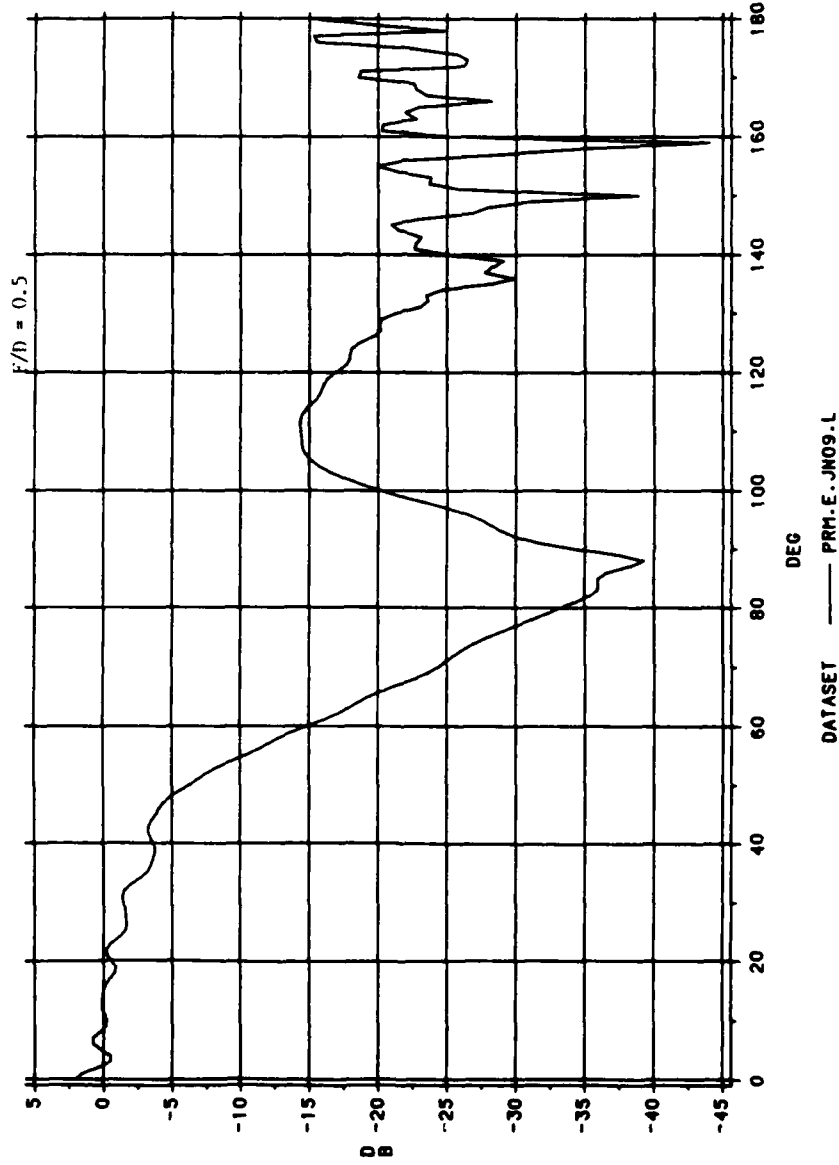


16JUN88:12:09:24

Figure 32. Secondary Pattern for H-Plane for Design B

TWIST CASSEGRAIN ANTENNA  
PRIMARY PATTERN - E-PLANE

DIA. = 28.346 IN. FREQ = 9.2 GHZ

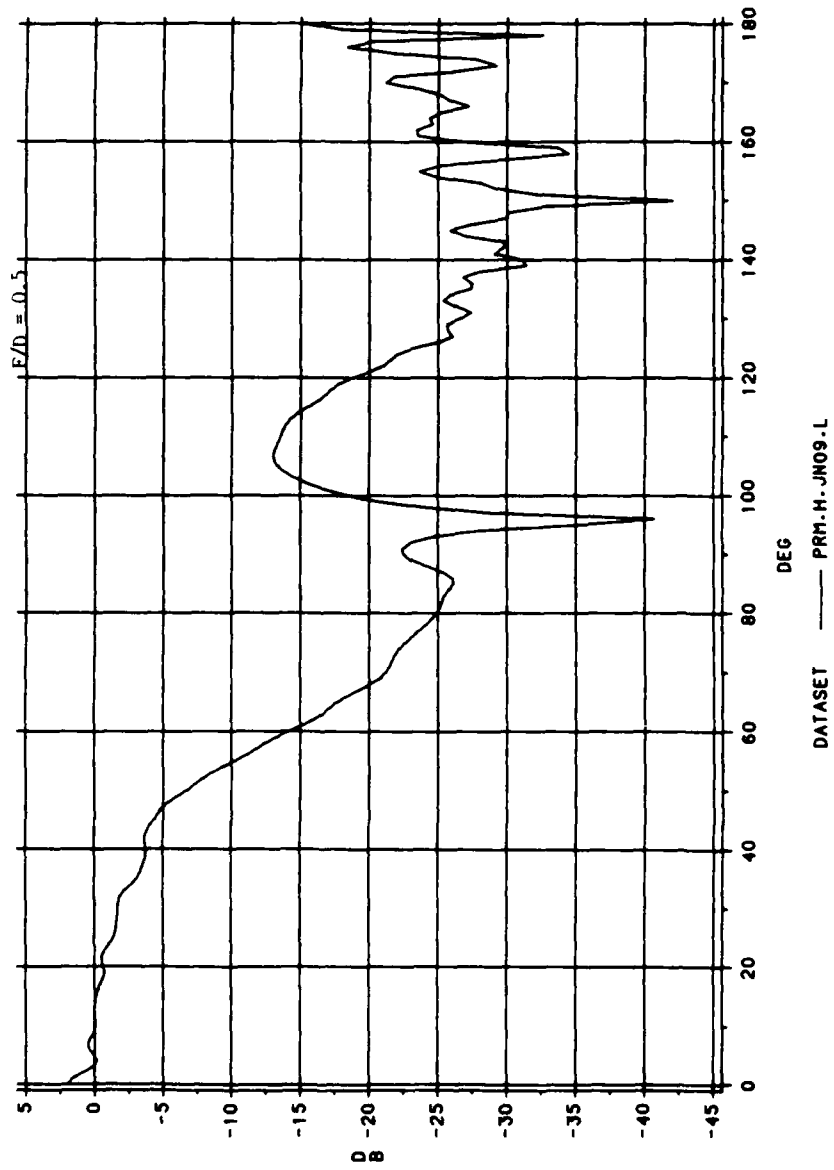


14JUN88 17:39:09

Figure 33. Primary Pattern for E-Plane for Design B

**TWIST CASSEGRAIN ANTENNA**  
 PRIMARY PATTERN, H-PLANE

DIA = 28.346 IN. FREQ = 9.2 GHZ



14 JUN 88 17:47:49

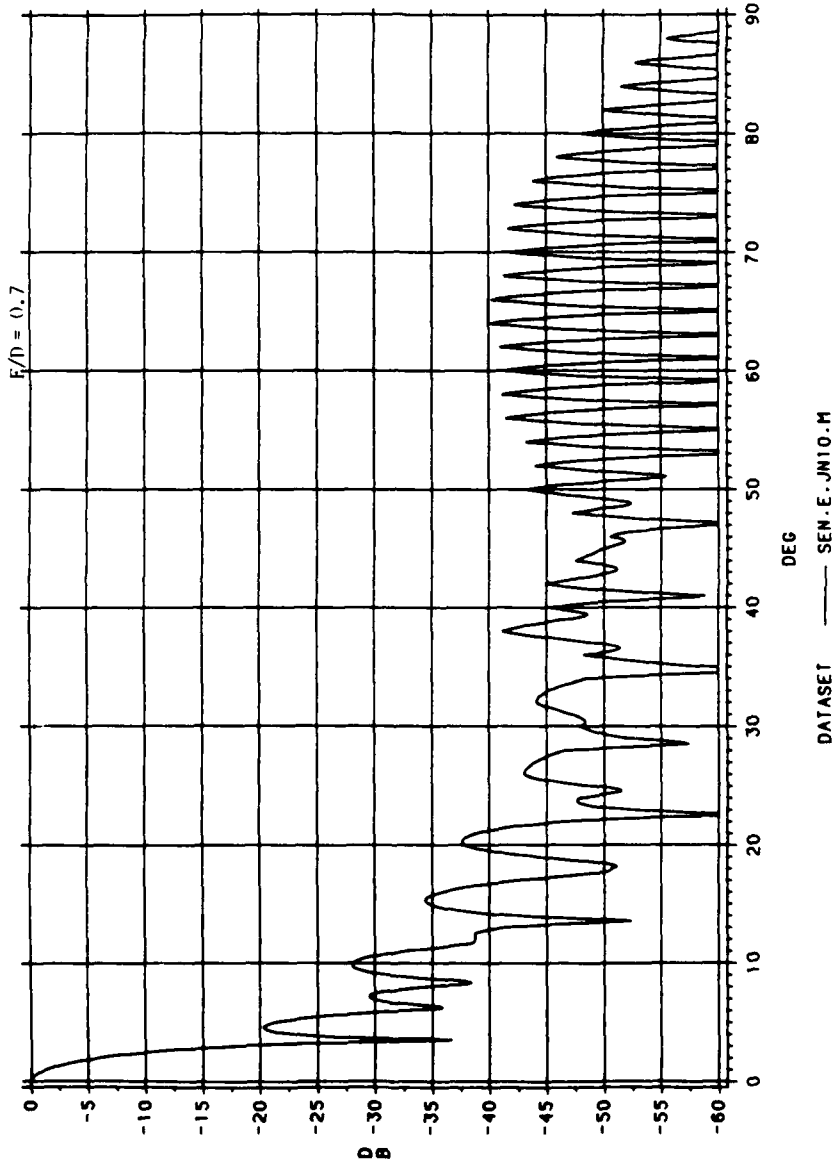
Figure 34. Primary Pattern for H-Plane for Design B

### Design C

In this design we fix the F/D ratio at 0.7, maintain a 28.346 diameter main reflector, and continue to radiate at 9.2 GHz. The results of this simulation appear in listing EG62131M. The far field patterns for the E and H planes respectively appear in Figures 35 and 36. The plots of the primary patterns for the E and H planes appear in Figures 37 and 38. Notice that the first sidelobe level for the far field pattern is at -20.3 dB for the E-plane and -22.3 dB for the H-plane. The E-plane sidelobe level is too low, will the H-plane level is acceptable (even though it is above the -25 dB goal level set in purpose statement). In addition, this design elongates the total length of the antenna structure, which is undesirable for limited space purposes. Thus we must rule out this design as nonacceptable.

TWIST CASSEGRAIN ANTENNA  
SECONDARY PATTERN: E-PLANE

DIA. = 28.346 IN. FREQ = 9.2 GHZ

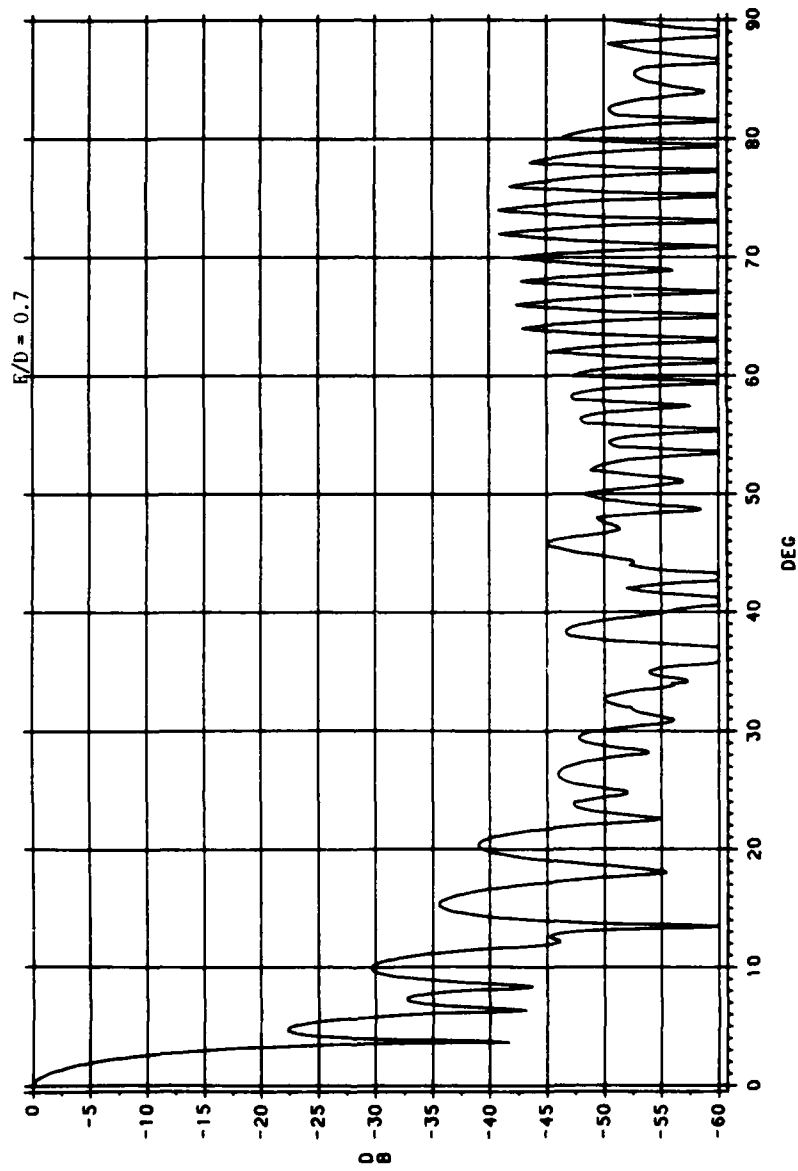


16JUN88 14:27:29

Figure 35. Secondary Pattern for E-Plane for Design C

TWIST CASSEGRAIN ANTENNA  
SECONDARY PATTERN: H-PLANE

DIA. = 28.346 IN. FREQ = 9.2 GHZ



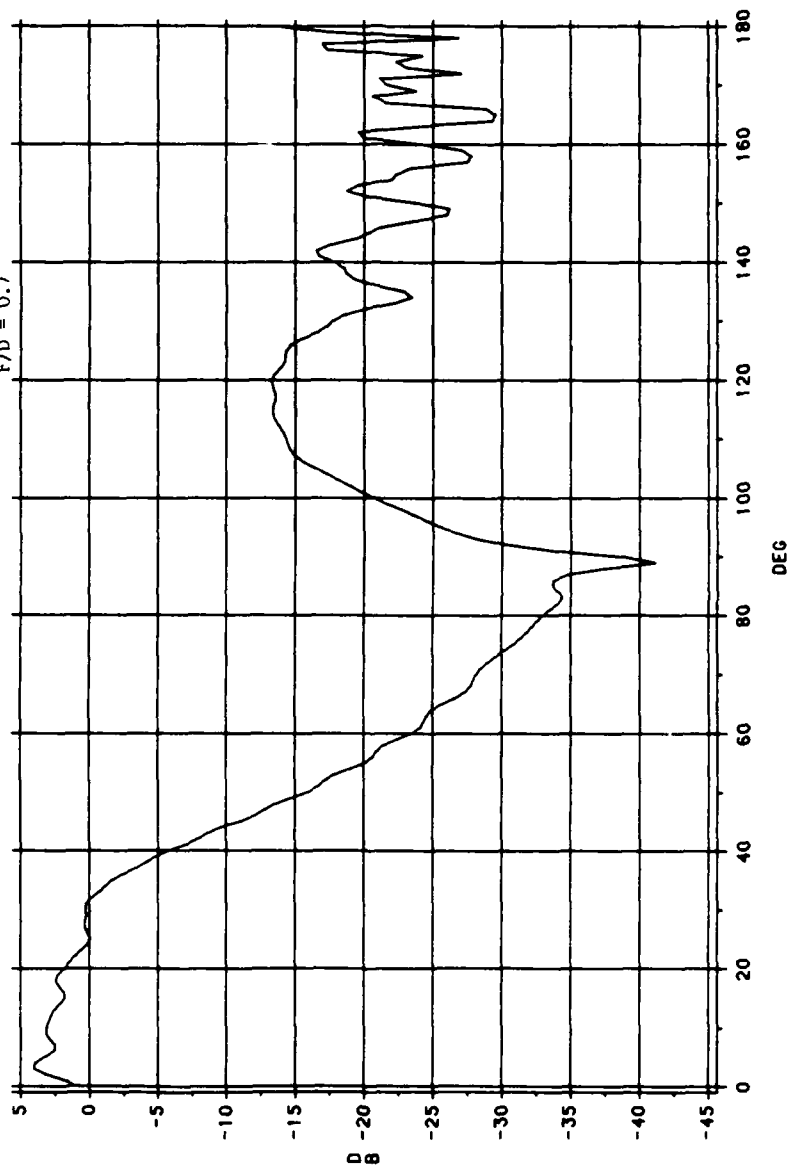
16JUN88 14:01:44

Figure 36. Secondary Pattern for H-Plane for Design C

**TWIST CASSEGRAIN ANTENNA**  
PRIMARY PATTERN, E-PLANE

DIA = 28.346 IN. FREQ = 9.2 GHZ

F/D = 0.7



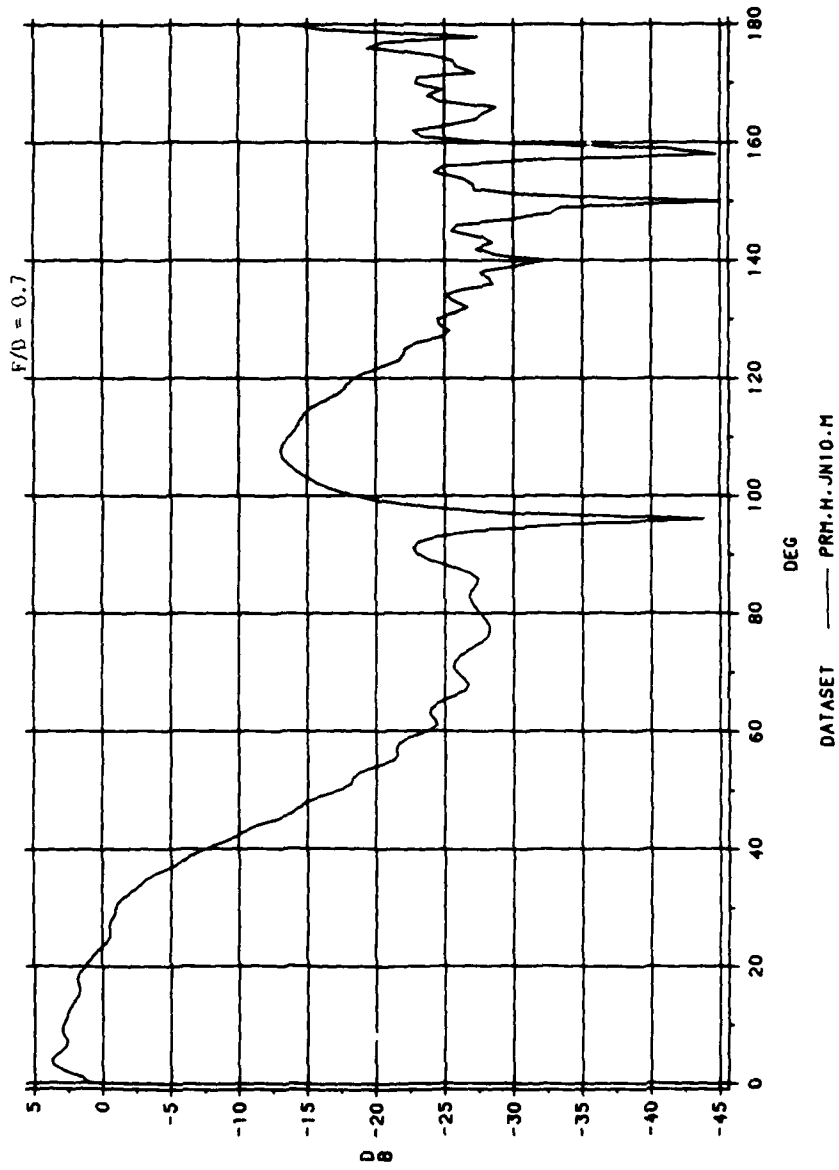
DATASET PRM.E.JN10.M

14 JUN 88 18:07:22

Figure 37. Primary Pattern for E-Plane for Design C

**TWIST CASSEGRAIN ANTENNA**  
PRIMARY PATTERN: H-PLANE

D1A = 28.346 IN. FREQ = 9.2 GHZ



14 JUN 88 18:00:22

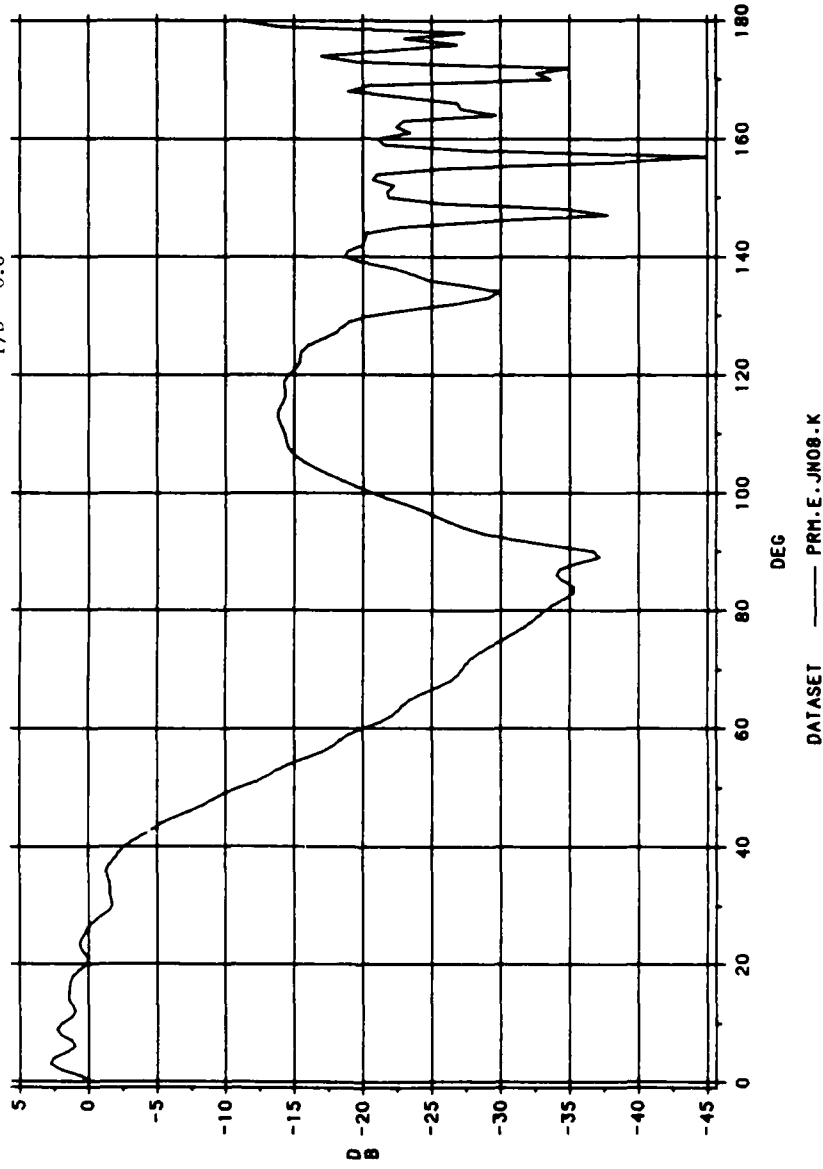
Figure 38. Primary Pattern for H-Plane for Design C

### Design D

This design uses a 30 inch main reflector and an F/D ratio of 0.6, radiating at 9.2 GHz. The subreflector size has been increased to maintain the same proportion as in the basic Swedish design. The results for this simulation are in listing EG62131k. The Far-Field Patterns are shown in Figures 41 and 42 for the E-Plane and H-Plane respectively. The primary patterns are shown in Figures 39 and 40 for the E-Plane and H-Plane respectively. The E-Plane far field pattern for Design D has a first sidelobe level at approximately -21 dB. The H-Plane pattern has a first sidelobe level of -23 dB. While the H-Plane pattern is superior to that of Design B, the E-Plane pattern is not. We thus rule out this design.

**TWIST CASSEGRAIN ANTENNA**  
PRIMARY PATTERN - E-PLANE

DIA. = 30.0 IN. FREQ = 9.2 GHZ  
F/D = 0.6



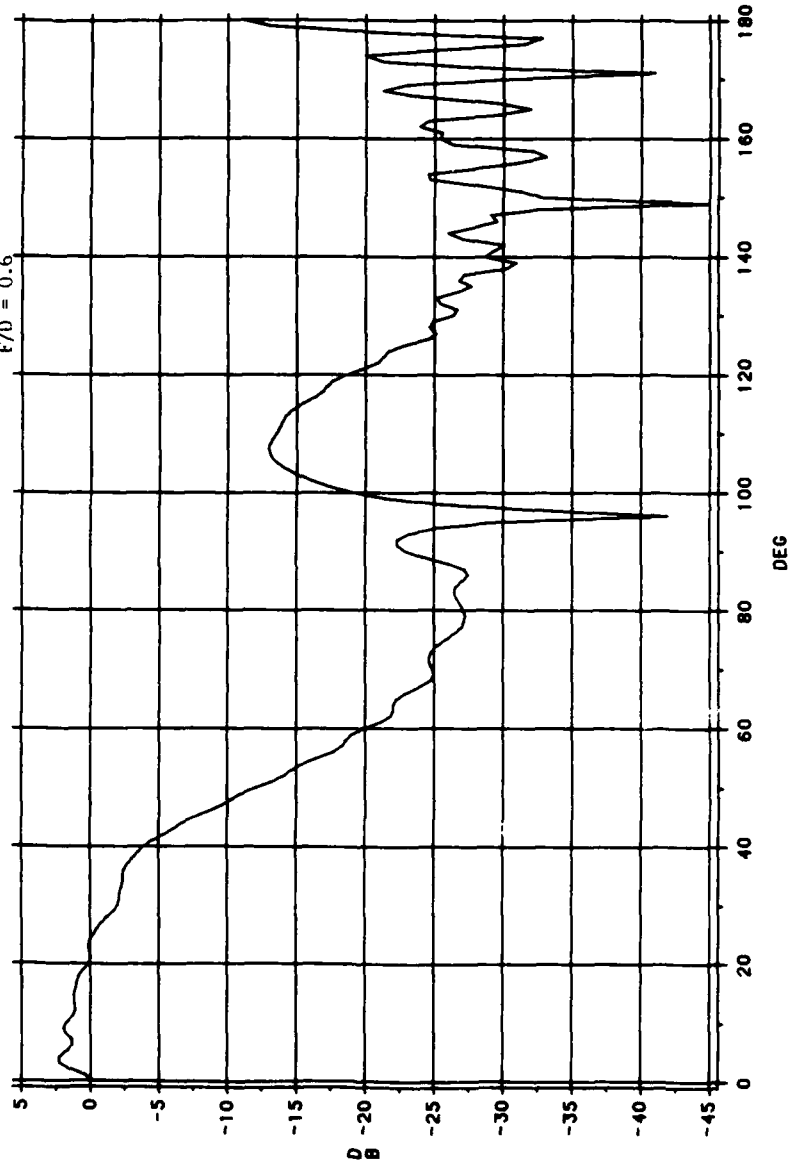
13JUN88,17:51:04

Figure 39. Primary Pattern for E-Plane for Design D

**TWIST CASSEGRAIN ANTENNA**  
PRIMARY PATTERN, H-PLANE

DIA. = 30.0 IN. FREQ = 9.2 GHZ

F/D = 0.6



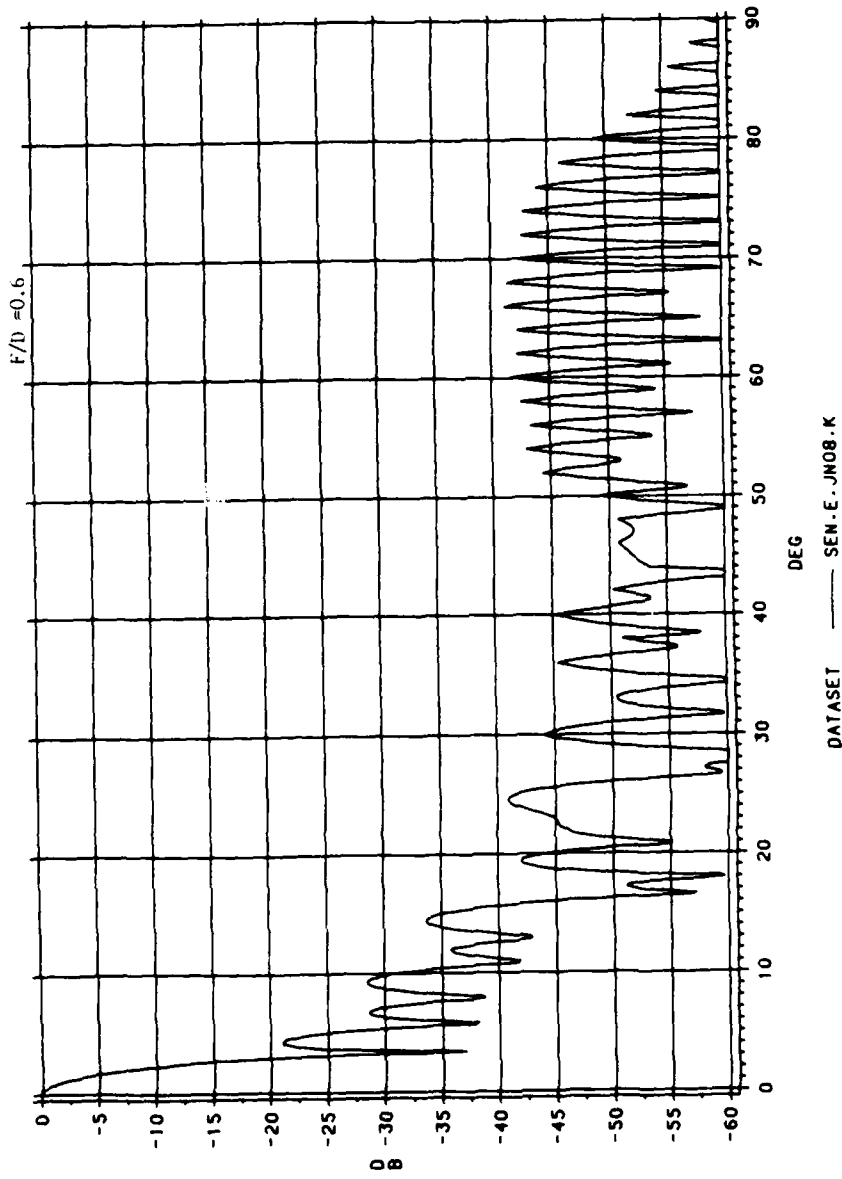
DATASET PRM.H.JN08.K

13JUN88:17:44:36

Figure 40. Primary Pattern for H-Plane for Design D

TWIST CASSEGRAIN ANTENNA  
SECONDARY PATTERN, E-PLANE

DIA. = 30.0 IN. FREQ = 9.2 GHZ

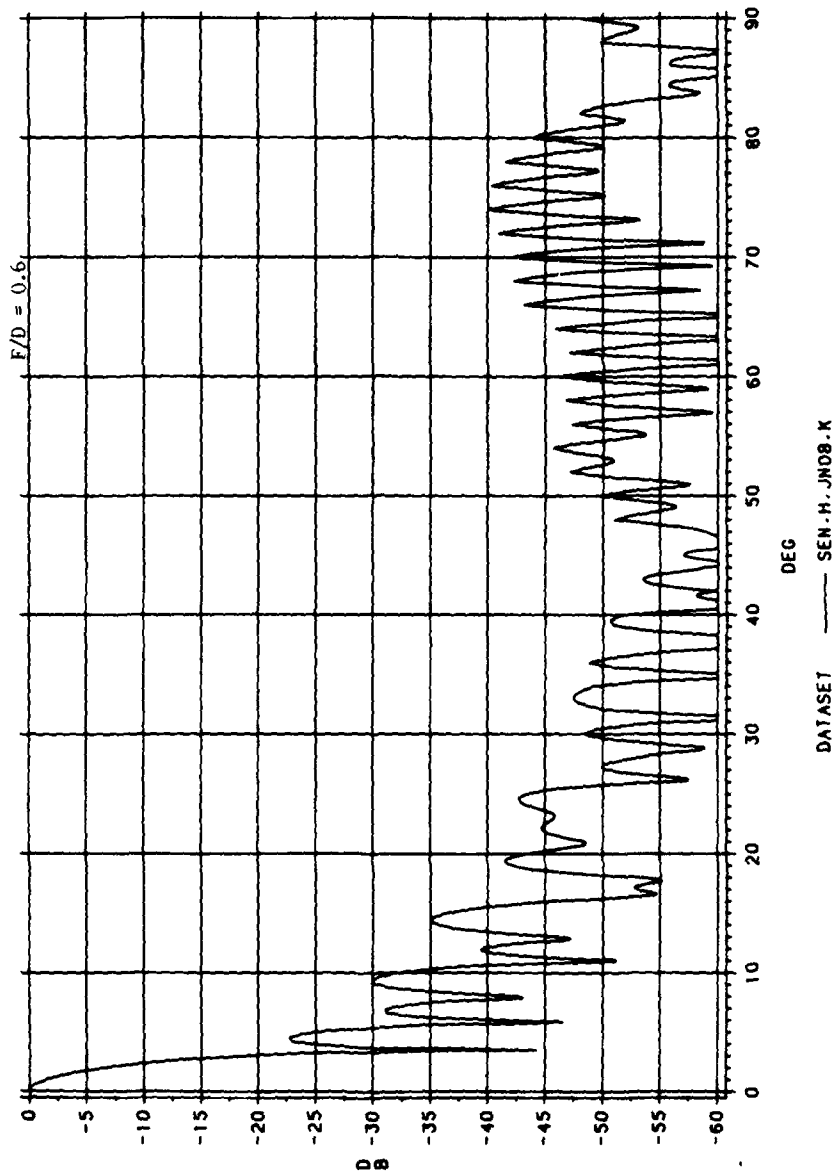


15JUN88 18:33:13

Figure 41. Secondary Pattern for E-Plane for Design D

TWIST CASSEGRAIN ANTENNA  
SECONDARY PATTERN: H-PLANE

DIA. = 30.0 IN. FREQ = 9.2 GHZ



15JUN88 18.15.56

Figure 42. Secondary Pattern for H-Plane for Design D

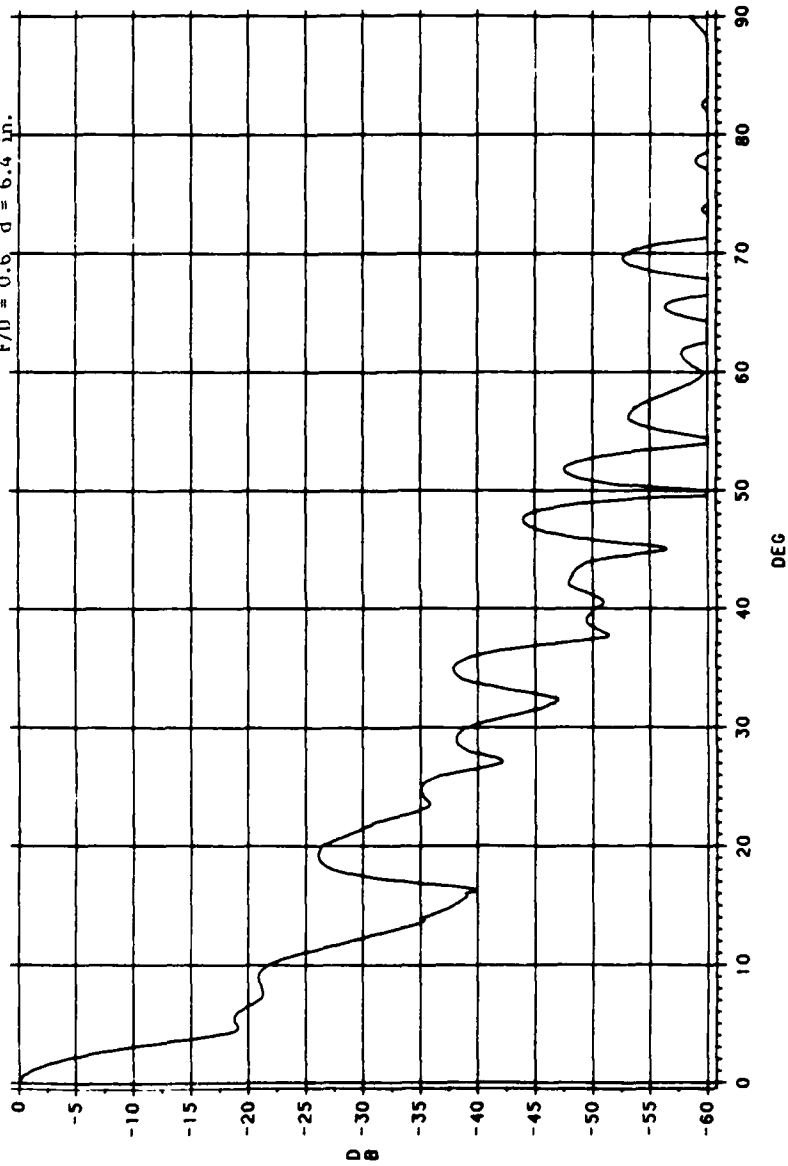
### Design E

In this design we use a 27 inch main reflector, maintain an F/D ratio of 0.6, but reduce the size of the subreflector to approximately  $5 \lambda$ . Since the subreflector size is now less than  $10 \lambda$  we would expect edge diffraction problems. This is indeed the case with the results obtained by simulation. The data for this simulation is in listing EG62131N. The E-Plane and H-Plane far field patterns are shown in Figures 43 and 44. The primary patterns are shown in Figures 45 and 46. Note the far-field patterns are totally unacceptable with the first sidelobe levels around -18 dB (only partial sidelobe forms here). Thus, this design is also ruled out.

**TWIST CASSEGRAIN ANTENNA**  
SECONDARY PATTERN, E-PLANE

DIA. = 27.0 IN. FREQ = 9.2 GHZ

F/D = 0.6 d = 6.4 in.

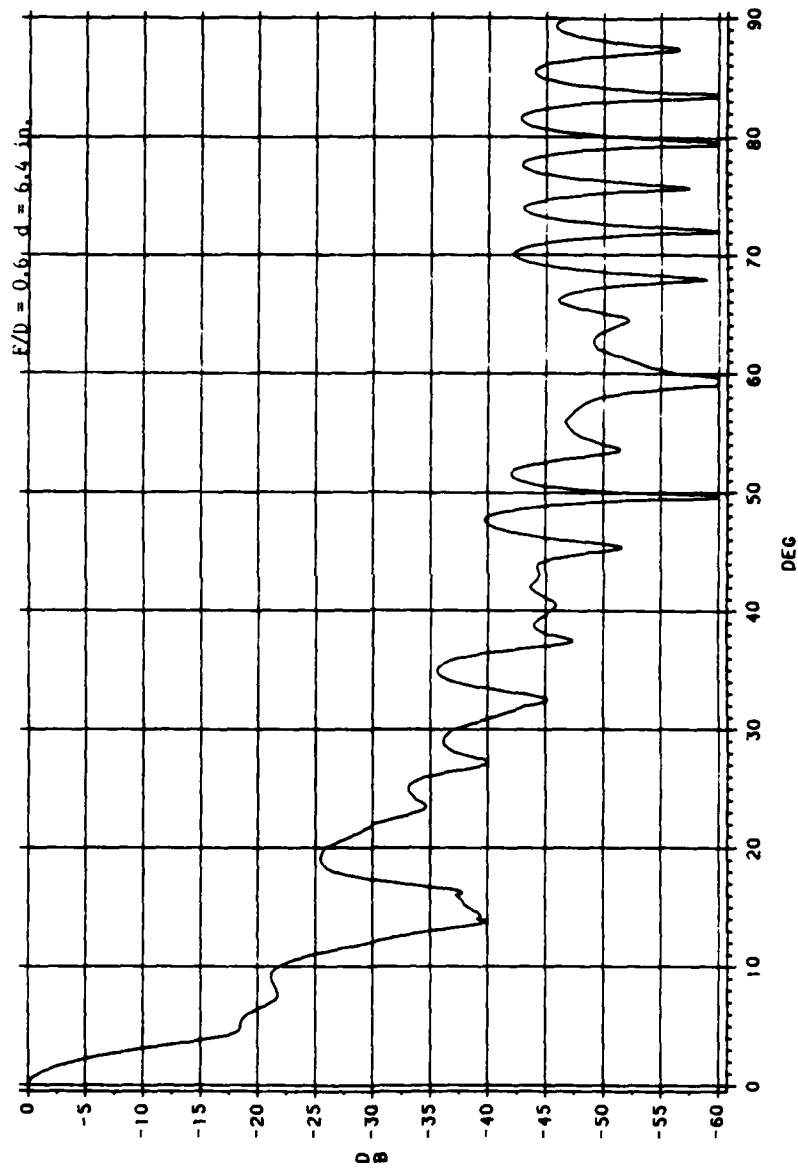


04AUG88 15:15:56

Figure 43. Secondary Pattern for E-Plane for Design E

TWIST CASSEGRAIN ANTENNA  
SECONDARY PATTERN, H-PLANE

DIA. = 27.0 IN. FREQ = 9.2 GHZ



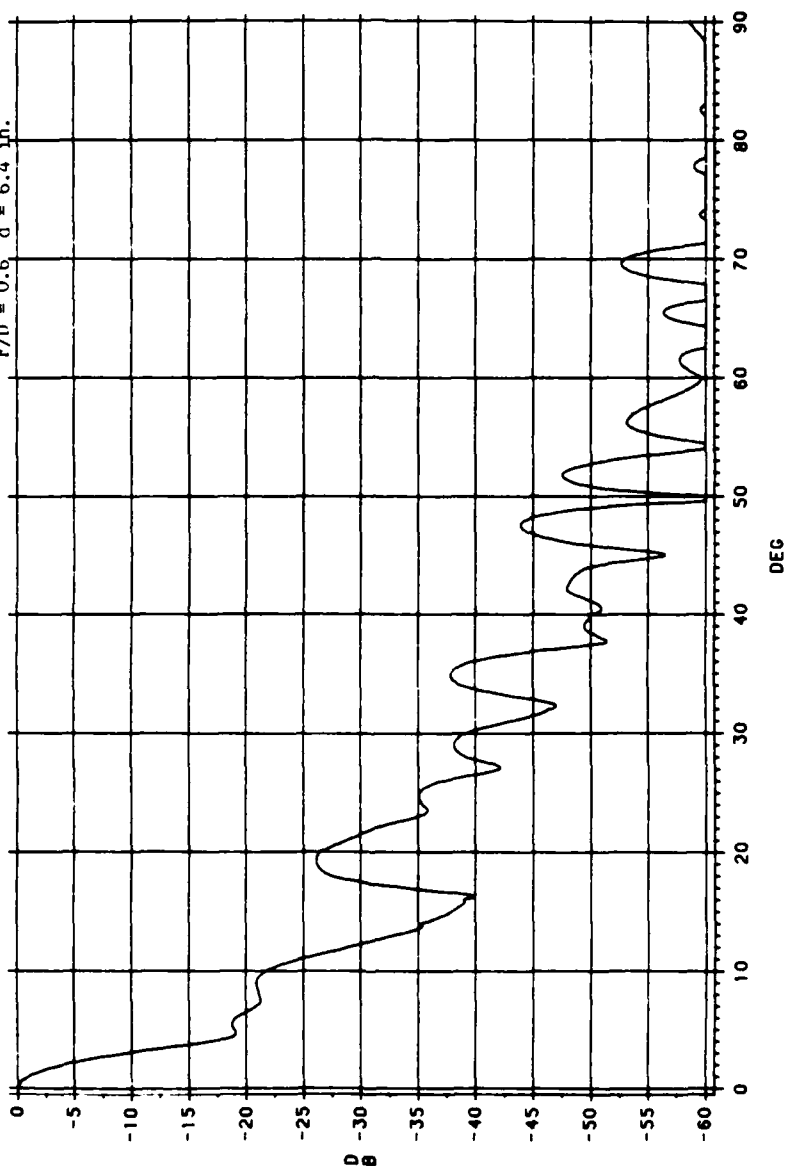
04AUG88:15:16:36

Figure 44. Secondary Pattern for H-Plane for Design E

**TWIST CASSEGRAIN ANTENNA**  
SECONDARY PATTERN, E-PLANE

DIA. = 27.0 IN. FREQ = 9.2 GHZ

F/D = 0.6 d = 6.4 in.



DATASET — SEN.E.JY19.N

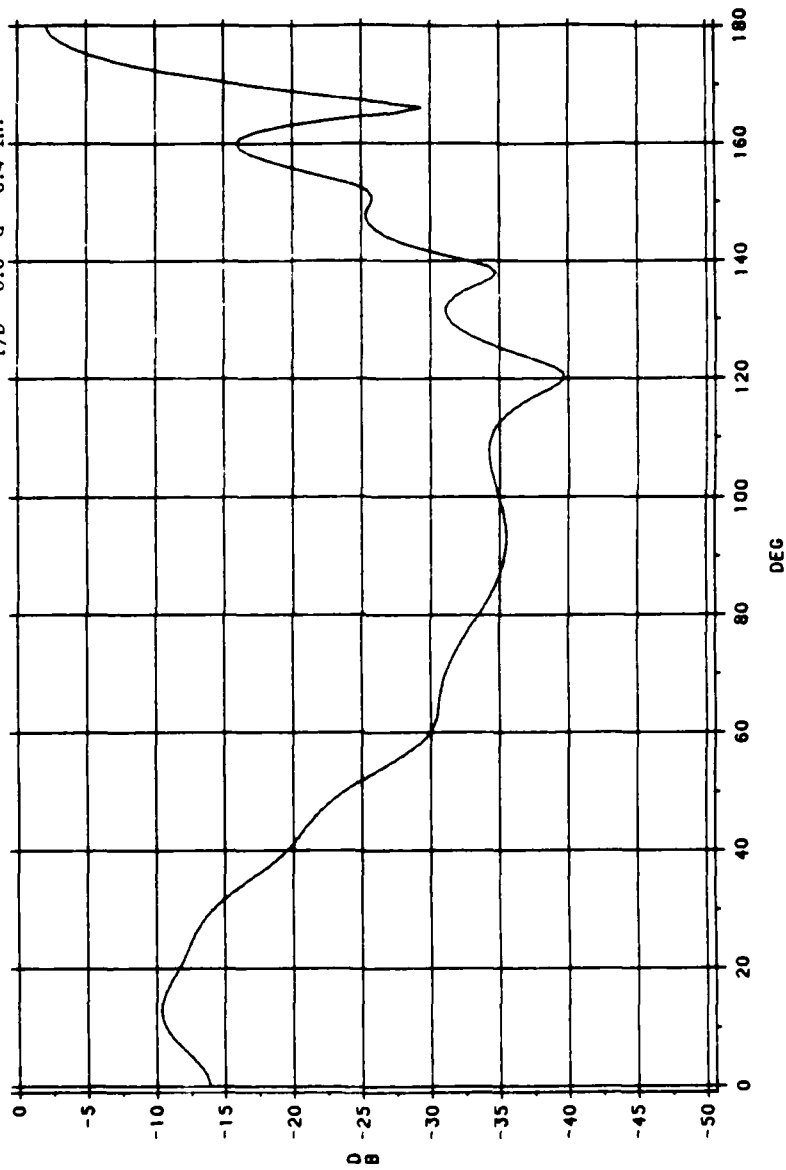
04AUG88,15:15:56

Figure 45. Primary Pattern for E-Plane for Design E

**TWIST CASSEGRAIN ANTENNA**  
PRIMARY PATTERN - H-PLANE

DIA. = 27.0 IN. FREQ = 9.2 GHZ

F/D = 0.6 d = 6.4 in.



04AUG88,15:15:29

Figure 46. Primary Pattern for H-Plane for Design E

## CHAPTER 5

### CONCLUSIONS AND RECOMMENDATIONS

Of all the reflector antennas derived from geometric optics, the optimized Swedish Twist-Cassegrain design seems to be most appropriate for airborne radar applications, especially for airborne intercept radars. The basic Swedish approach is desirable, however, it is not optimized for this application. The two channel monopulse feed creates multiple modes, which simply complicates the design. By use of a rectangular horn feed, we can create the  $TE_{10}$  mode without higher order modes appearing. A pyramidal horn structure can be used for a dual mode operation. Corrugated (pyramidal) horns simply add higher order modes which may need to be removed by a mode filter.

The Hughes Modified Vector Diffraction simulation provides an accurate approximation of the scattering of spherical waves by an arbitrary truncated surface of revolution, such as a paraboloid or a hyperboloid. This program currently is resident on an IBM 3038 computer. The simulation, is written in Fortran IV and is in excess of 10,000 lines of code.

The optimized Swedish design is derived by simulation of the far field (and near field) patterns. Seven cases were run (including two cases of the Swedish design) in order to get the most desirable patterns for both the E-plane and H-plane in the far field. Simulations were quite extensive taking an average of two hours per run to get results. These results were then plotted on a CAL COMP plotter model 1055 to actually obtain antenna patterns.

Design B, which uses the 28.346 inch main reflector and an F/D ratio of 0.5 provides the best far-field patterns of those designs simulated, except for the Swedish design. It has the lowest and most uniform sidelobes of those cases simulated. Though the original goal of -25 dB first sidelobes could not be met with any of these designs, the -22.3 to -22.5 dB first sidelobe levels are still respectable. Going to a wider paraboloid and hyperboloid combination improves gain significantly, however the far field patterns seem to degrade. The best compromise, then, is to choose the 28.346 design to get reasonable first sidelobes, yet still benefit from the increased antenna gain. This will yield a higher Effective Radiated Power than the basic Swedish Design and result in good overall target detection performance.

Finally, the writer recommends more work be accomplished in designing a coherent medium or high pulse repetition frequency airborne radar using a Twist-Cassegrain antenna design with low sidelobes in the neighborhood of -30 dB. This will be the subject for my doctoral dissertation at the University of Dayton in the near future.

APPENDIX A  
PROOFS OF FUNDAMENTAL PRINCIPLES AND APPROXIMATIONS

Blockage From A Subreflector

In Cassegrain antenna configurations the size and shape of the hyperboloidal subreflector is critical to the overall performance of the entire antenna system. It has been found that the size of the subreflector for minimum blockage in a simple Cassegrain arrangement (non-twist reflector), is:

$$d_{s, \min} = ([2 \lambda F] / k)^{1/2}. \quad (\text{A.1})$$

Here  $k$  is the ratio of the feed-aperture diameter to its effective blocking aperture diameter. Ordinarily  $k$  is slightly less than 1.0 (Hannon, 1961).

Now given Figure 47, shown on the following page, which portrays the geometry for aperture blockage, we can prove Hannon's relationship given above. The values  $d_s'$  and  $d_f$  are the diameter of the shadow cast on the paraboloid by the feed (equal to the diameter of the subreflector) and the aperture of the feed respectively. If the feed is adjusted so that the nulls of the main beam occur at the edges of the subreflector, then

$$2 \alpha_0 = 2 \lambda / d_f. \quad (\text{A.2})$$

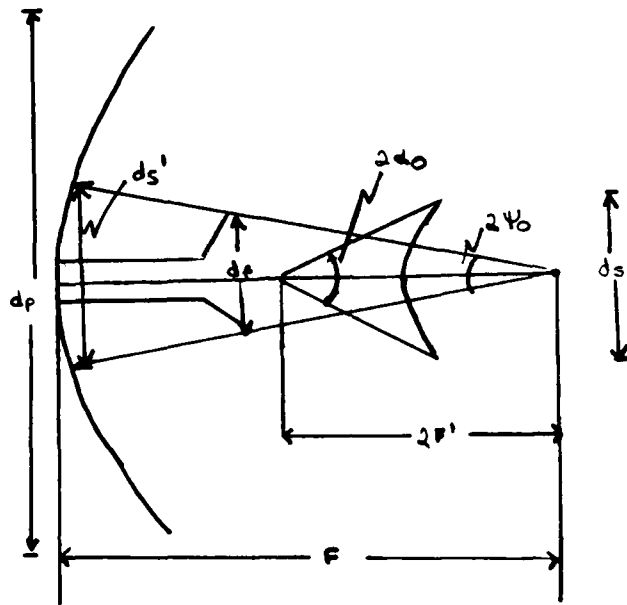


Figure 47. Geometry of Aperture Blockage

This is true since the beamwidth between nulls is given by (Wolff, 1988):

$$\Theta_n = 2 \lambda / a, \text{ at } z = 0, \quad (\text{A.3})$$

where  $a$  = length of aperture. This relationship is proved in the next section by integrating the electric field component  $E_\phi$ , and examining where the nulls of this pattern occur.

If the structure supporting the feed has significant dimensions, the blocking aperture diameter may be different from the radiating feed aperture diameter. Then equation A.2 becomes:

$$2 \alpha_0 = 2 \lambda / k d_f. \quad (\text{A.4})$$

Also, from the geometry of Figure 47, it can be seen that:

$$2 \Psi_0 = d_f / 2F' \quad (\text{A.5})$$

The portion of the paraboloid that is shadowed by the feed is then:

$$ds' = 2 \Psi_0 F = d_f F / 2 F'. \quad (\text{A.6})$$

Then, for minimum blocking, the ratio of the subreflector diameter to the feed diameter is:

$$d_s / d_f = F / 2 F'. \quad (\text{A.7})$$

The subreflector diameter is also given in Figure 47 as:

$$d_s = 4 \alpha_0 F'. \quad (\text{A.8})$$

Then equation A.4 can be rewritten as:

$$\alpha_0 = \lambda / k d_f. \quad (\text{A.4}')$$

Equation A.7 can also be rewritten in terms of  $F'$  as:

$$F' = F d_f / 2 d_s. \quad (\text{A.7'})$$

Now substituting A.4' and A.7' into A.8 we get the equation:

$$(d_s)^2 = 2 \lambda F / k \quad \text{or} \quad d_s = (2 \lambda F / k)^{1/2}. \quad (\text{A.9})$$

#### Proof of Beamwidth Between Nulls Formula

The writer will now examine a rectangular aperture of lengths  $a$  and  $b$  in the  $x$ - and  $y$ -directions respectively as shown in Figure 48. Let the electric field,  $E$ , be aligned with the  $y$ -axis and the magnetic field,  $H$ , be aligned with the  $z$ -axis to give a plane wave traveling in the  $x$ -direction. With uniform illumination, the  $E$ -field is constant over the entire rectangular aperture. Using the relation below and integrating over the entire aperture (Silver, 1949):

$$E_\theta = jE_0 e^{-jk r} (\sin \theta + \cos \phi) / 2 \lambda r \iint e^{jk r' \cos \psi} dy' dz'. \quad (\text{A.10})$$

$$\text{Let } r' \cos \psi = \mathbf{a}_r \cdot \mathbf{r}' = (a_x \sin \theta \cos \phi + a_y \sin \theta \sin \phi + a_z \cos \theta) \times (a_x y' + a_z z') \quad (\text{A.11})$$

$$\text{or} \quad r' \cos \psi = y' \sin \theta \sin \phi + z' \cos \theta. \quad (\text{A.12})$$

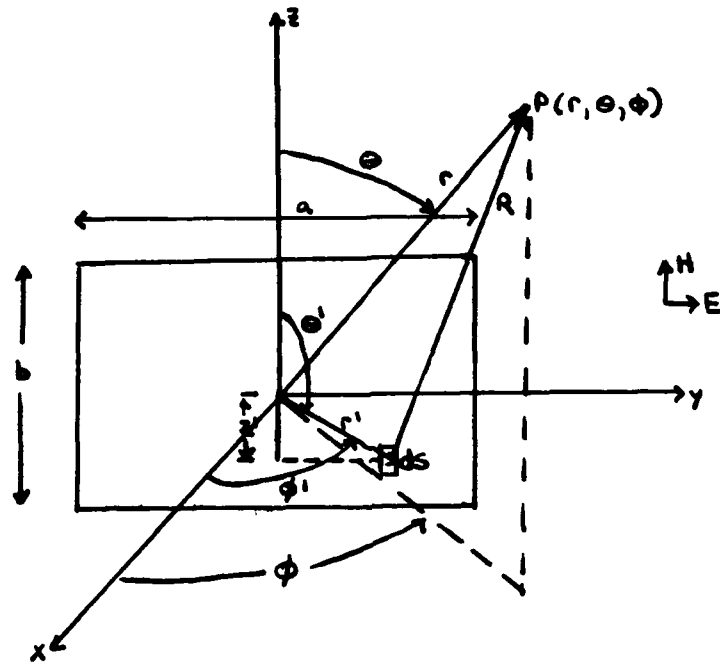


Figure 48. Geometry for Rectangular Aperture

Therefore Equation A.10 becomes:

$$E_{\phi} = jE_0 e^{-jk r (\sin\theta + \cos\phi)/2} \lambda r \int_{-b/2}^{b/2} \int_{-a/2}^{a/2} \exp[jk(y' \sin\theta \sin\phi + z' \cos\theta)] dy' dz' \quad (A.13)$$

Performing the integration gives:

$$E_{\phi} = jE_0 e^{-jk r (\sin\theta + \cos\phi)/2} \lambda r [(e^{jk y' \sin\theta \sin\phi} / jk \sin\theta \sin\phi) \Big|_{-a/2}^{a/2} (e^{jk z' \cos\theta} / jk \cos\theta) \Big|_{-b/2}^{b/2}] \quad (A.14)$$

and simplifying we get:

$$E_{\phi} = abE_0 e^{-jk r (\sin\theta + \cos\phi)/2} \lambda r [\sin(ka \sin\theta \sin\phi / 2) / (ka/2) (\sin\theta \sin\phi)] [\sin(kb \cos\theta / 2) / (kb/2) \cos\theta] \quad (A.15)$$

The field in the  $z = 0$  plane is:

$$E_{\phi}(r, \pi/2, \phi) = abE_0 e^{-jk r (1 + \cos\phi)/2} \lambda r [\sin u / u], \quad (A.16)$$

where  $u = (ka/2) \sin\phi$ . This function is plotted in Figure 49. The nulls in this pattern occur approximately at the points where:

$$\sin(ka \sin\theta_n / 2) = 0, \quad (A.17)$$

or

$$(\pi a / \lambda) \sin\theta_n = n \quad (A.18)$$

For relatively large apertures, the first nulls occur at

$\theta_1$ , where:

$$\theta = \lambda / a. \quad (A.19)$$

and the beamwidth between nulls is:

$$BW_n = 2 \lambda / a, \quad z = 0. \quad (A.20)$$

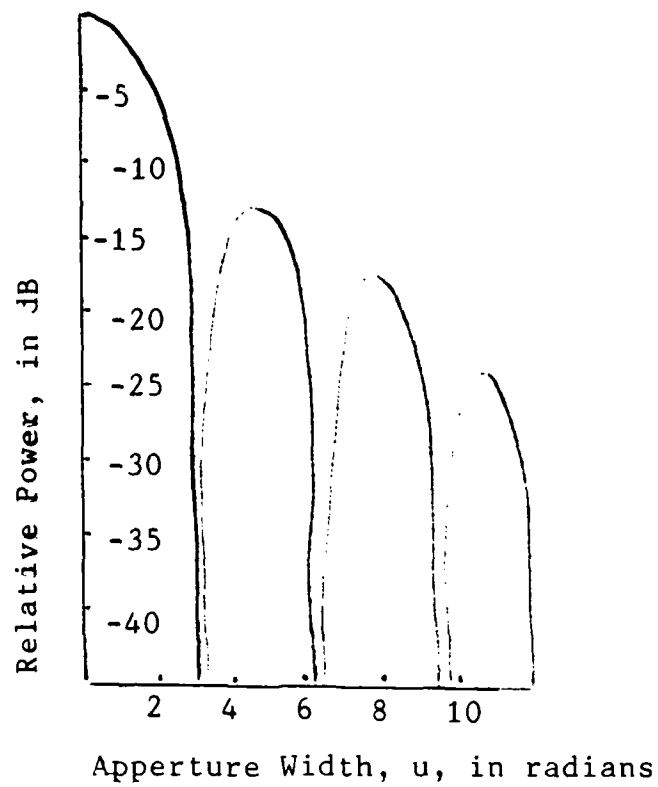


Figure 49. Pattern of Uniformly Illuminated Rectangular Aperture

APPENDIX B  
SUITABLE TRAVELING WAVE TUBES

<u>Manufacturer/ Number</u>	<u>Type</u>	<u>Frequency Range</u>	<u>Maximum Output Power</u>
Hughes/752H	Pulsed	8.4-9.4 GHz	150 KW
Thompson/TH3574	Pulsed	8.0-12.0 GHz	100 KW
Hughes/8753H	Pulsed	8.5-9.6 GHz	150 KW
Hughes/8716H	Pulsed	9.0-9.2 GHz	120 KW

Note: Data from manufacturer's specifications.

## APPENDIX C

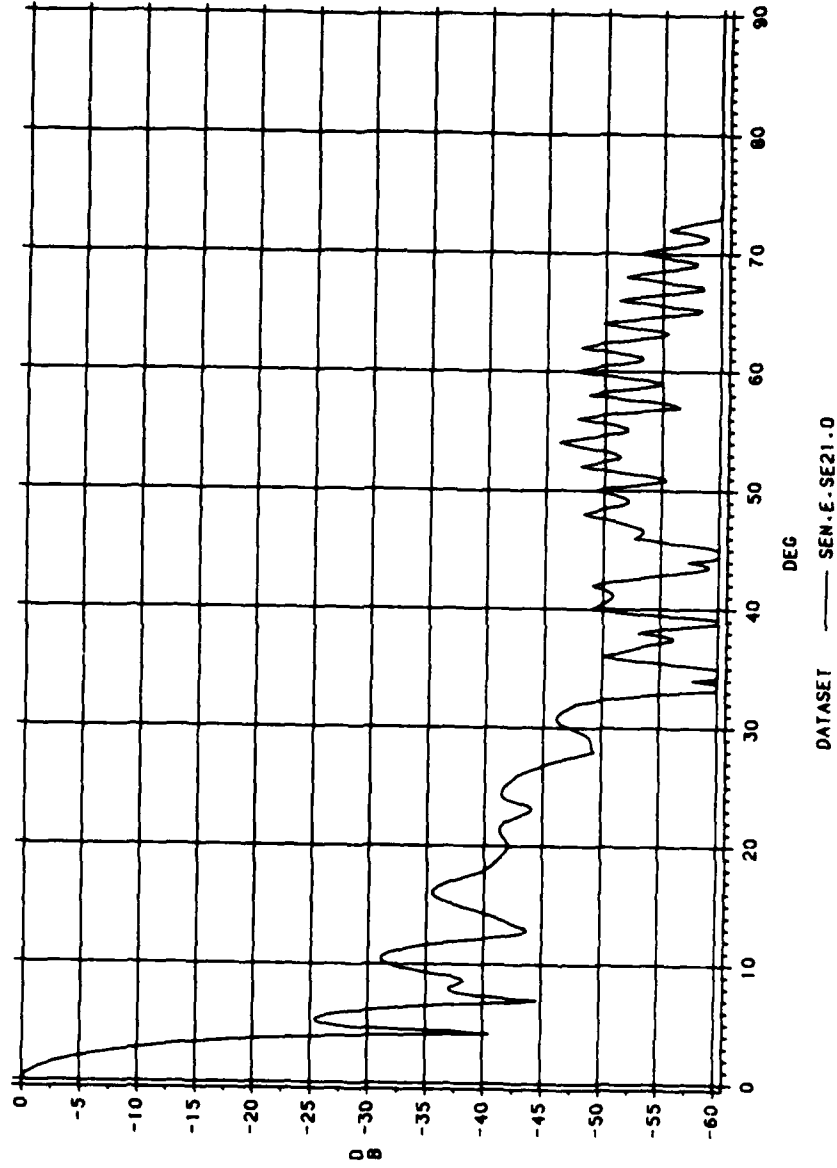
### SWEDISH ANTENNA DESIGN-SIMULATED PATTERNS

The far-field patterns for the basic Swedish antenna design (27 inch diameter paraboloid,  $F/D = 0.6$ ) are shown in Figures 50 and 51 respectively for the E-plane and H-plane at a simulation case run at 9.2 GHz. Figures 52 and 53 show the primary patterns for the E-plane and H-plane respectively.

For a simulation case of the Swedish design run at 9.3 GHz, Figures 54 and 55 depict the far-field patterns of the E-plane and H-plane respectively. Finally, Figures 56 and 57 depict the primary patterns of the E-plane and H-plane respectively.

**TWIST CASSEGRAIN ANTENNA**  
SECONDARY PATTERN, E-PLANE

DIA. = 27.0 IN. FREQ = 9.2 GHZ

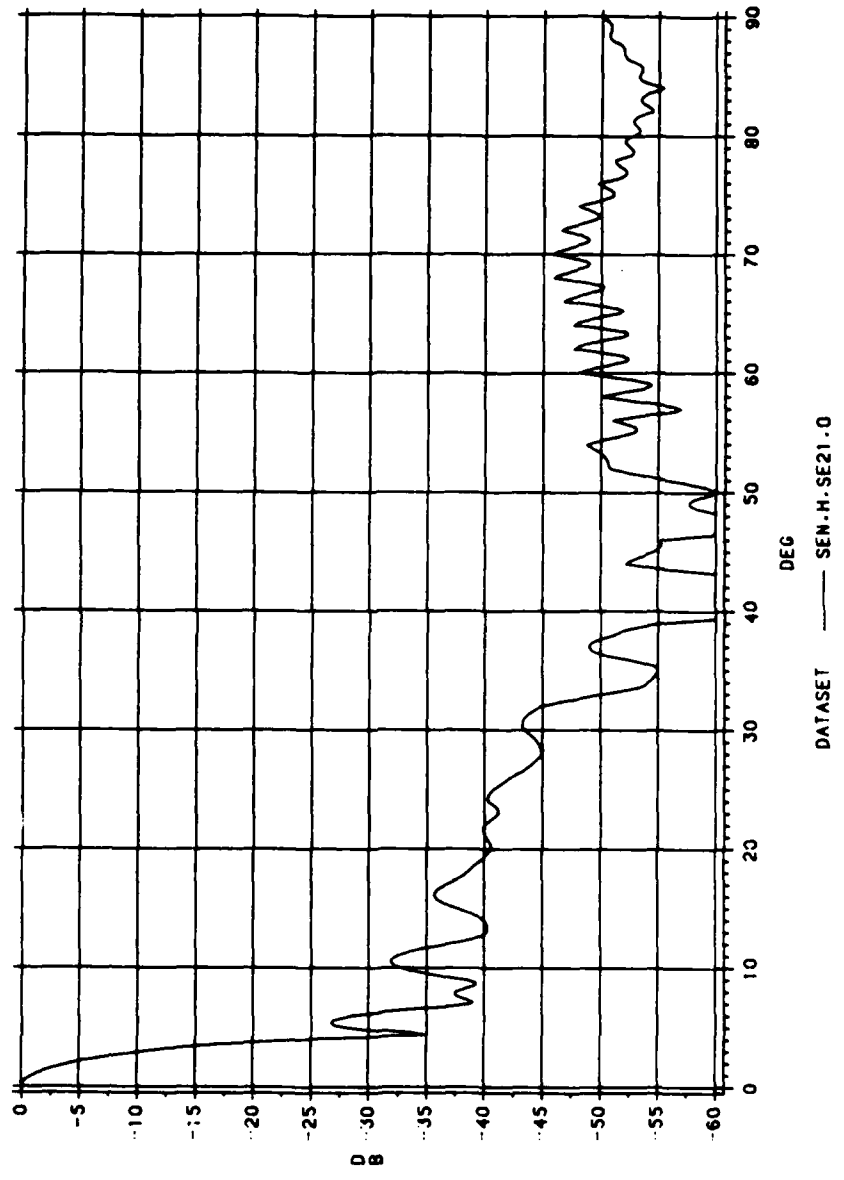


23SEP88.17.15.59

Figure 50. Secondary Pattern for E-Plane for Swedish Design at 9.2 GHz

TWIST CASSEGRAIN ANTENNA  
SECONDARY PATTERN, H-PLANE

DIA. " 27.0 IN. FREQ " 9.2 GHz

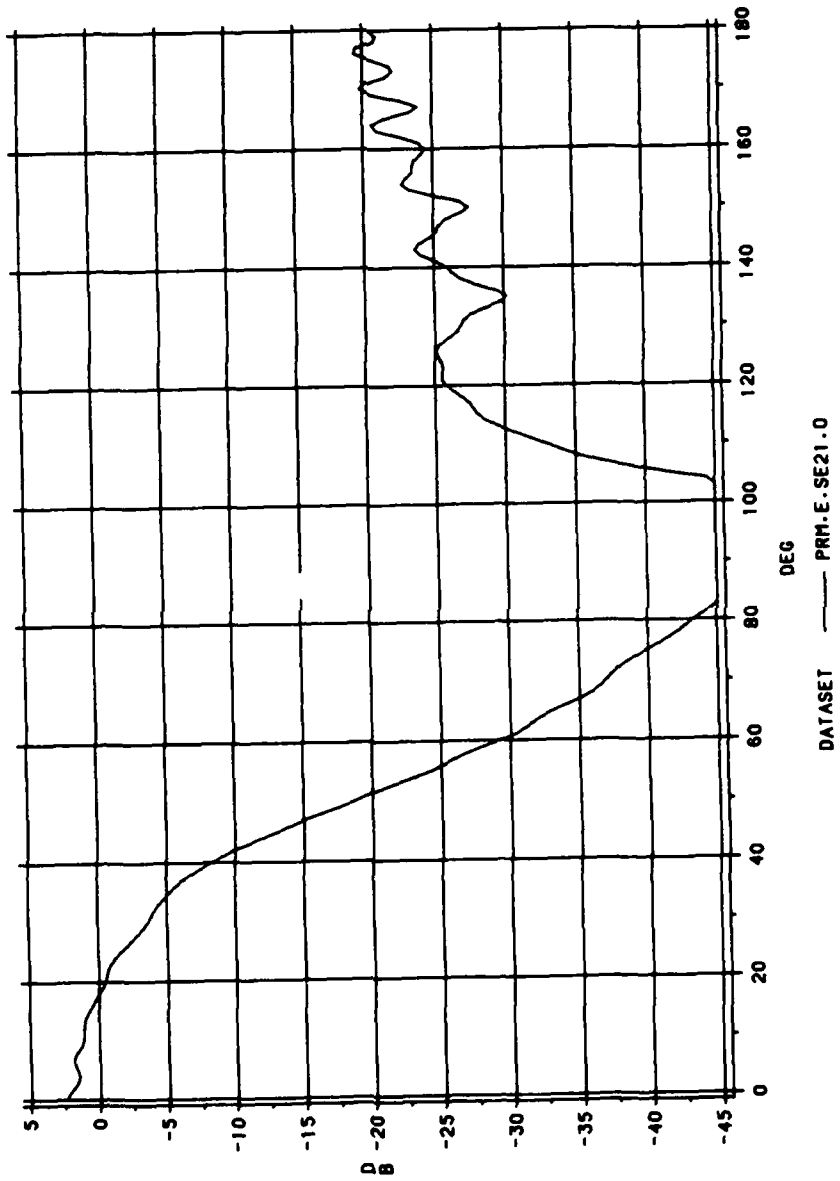


23SEP88 17:13:51

Figure 51. Secondary Pattern for H-Plane for Swedish Design at 9.2 GHz

**TWIST CASSEGRAIN ANTENNA**  
PRIMARY PATTERN, E-PLANE

DIA = 27.0 IN. FREQ = 9.2 GHZ



22SEP68:18:18.45

Figure 52. Primary Pattern for E-Plane for Swedish Design at 9.2 GHz

**TWIST CASSEGRAIN ANTENNA**  
PRIMARY PATTERN - H-PLANE

DIA = 27.0 IN. FREQ = 9.2 GHz

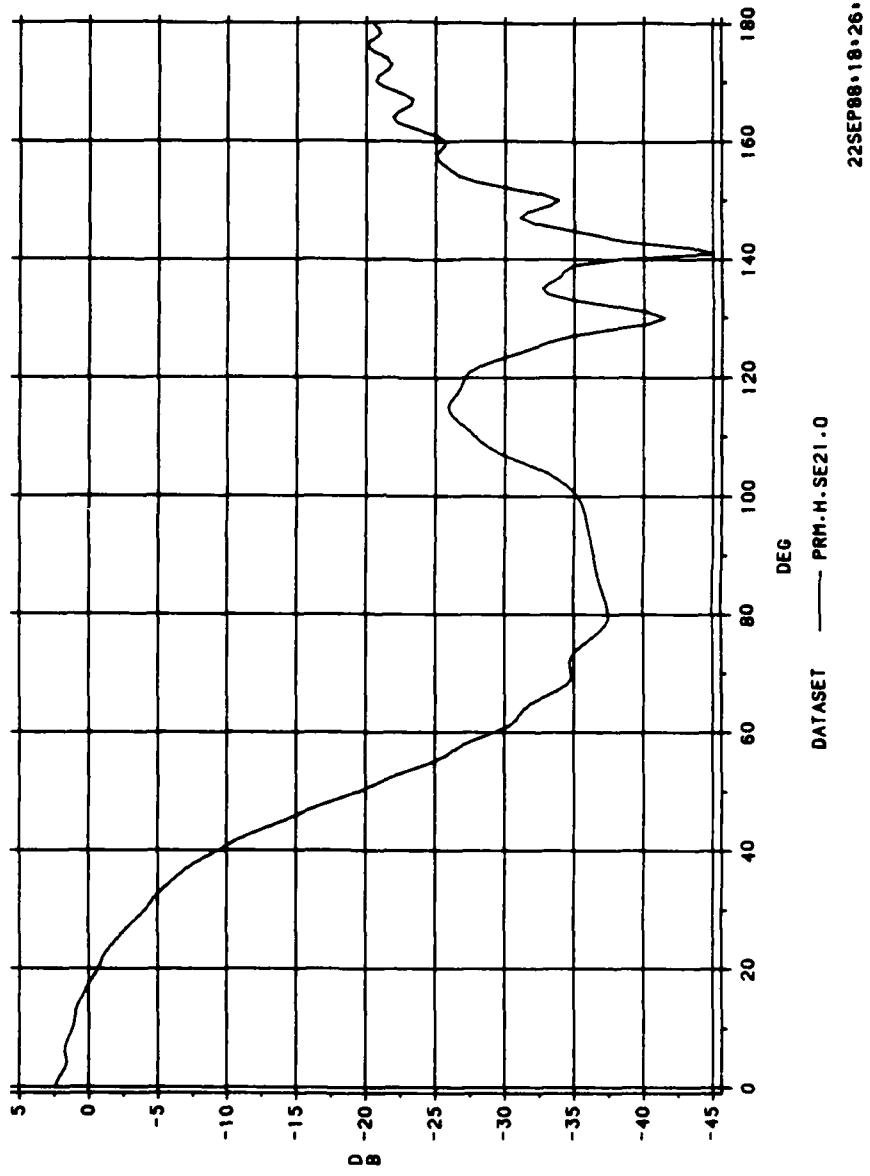
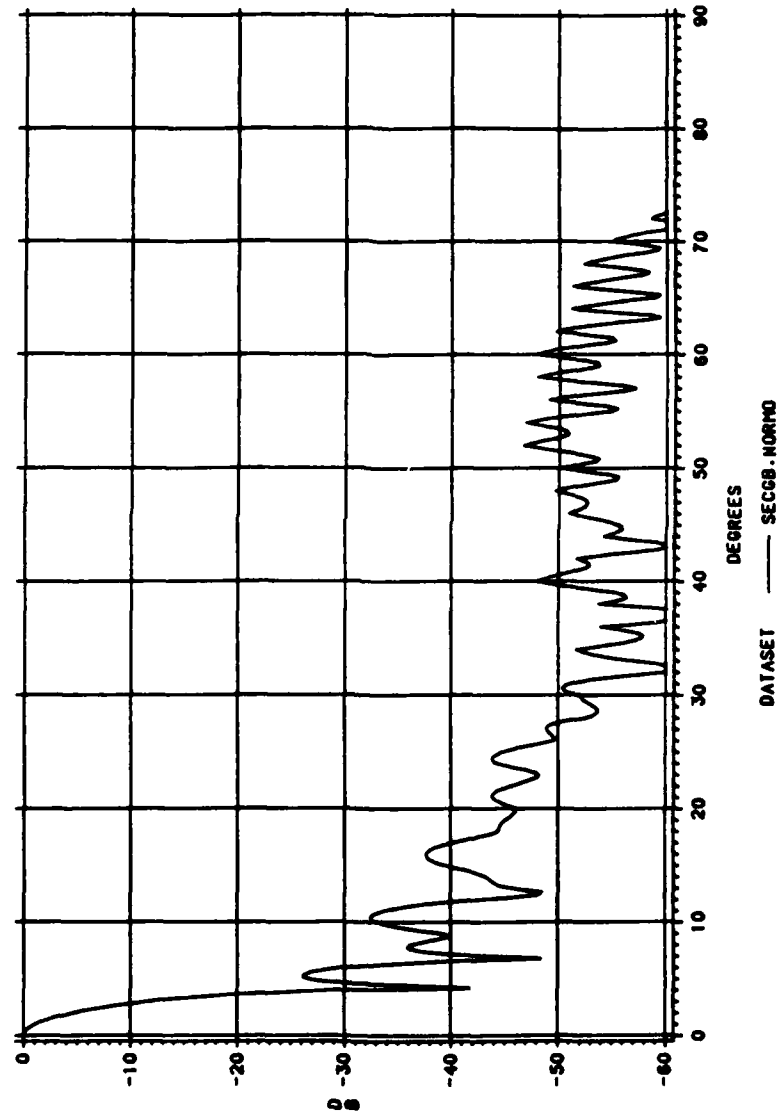


Figure 53. Primary Pattern for H-Plane for Swedish Design at 9.2 GHz

# TWIST CASSEGRAIN

F = 9.3 GHZ DIA = 27.0 IN.  
SECONDARY PATTERN PHI = 90 DEG.



23FEB88.15:51:58

Figure 54. Secondary Pattern for E-Plane for Swedish Design at 9.3 GHz

TWIST CASSEGRAIN  
ANTENNA

F = 9.3 GHz DIA = 27.0 IN.  
SECONDARY PATTERN PHI = 0 DEG

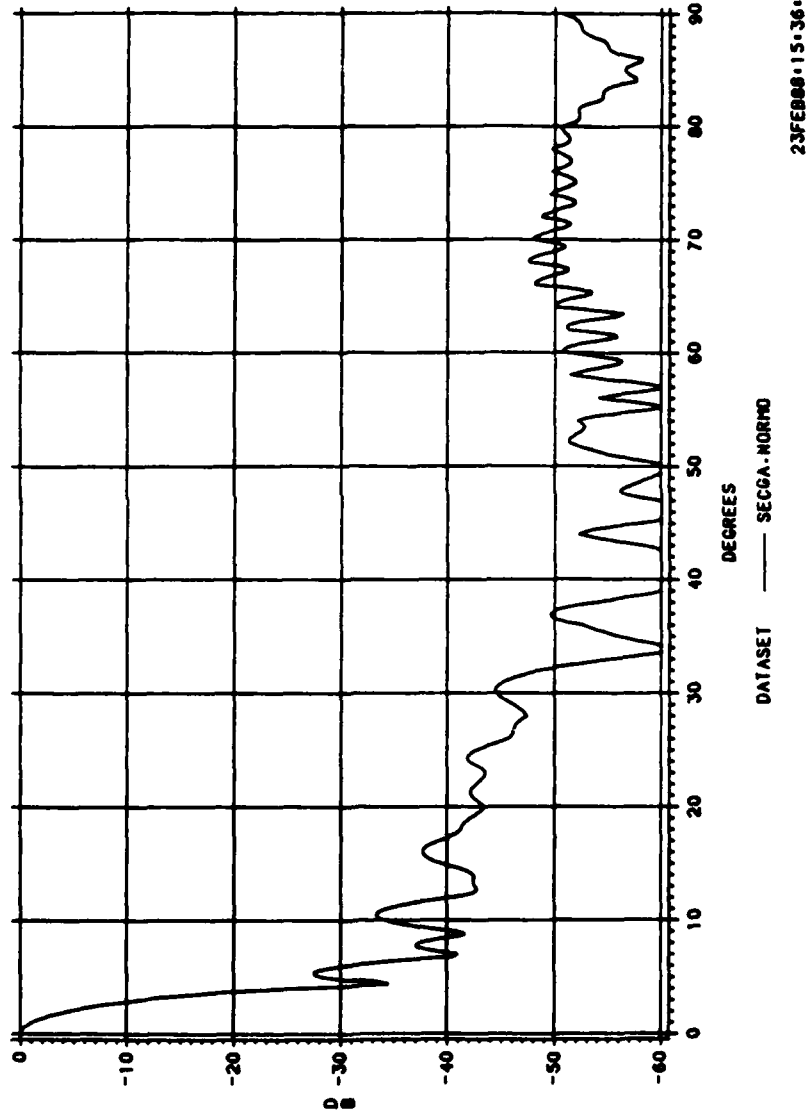


Figure 55. Secondary Pattern for H-Plane for Swedish Design at 9.3 GHz

# TWIST CASSEGRAIN ANTENNA

F = 9.3 GHz DIA = 27.0 IN.  
PRIMARY PATTERN: PHI = 90 DEG.

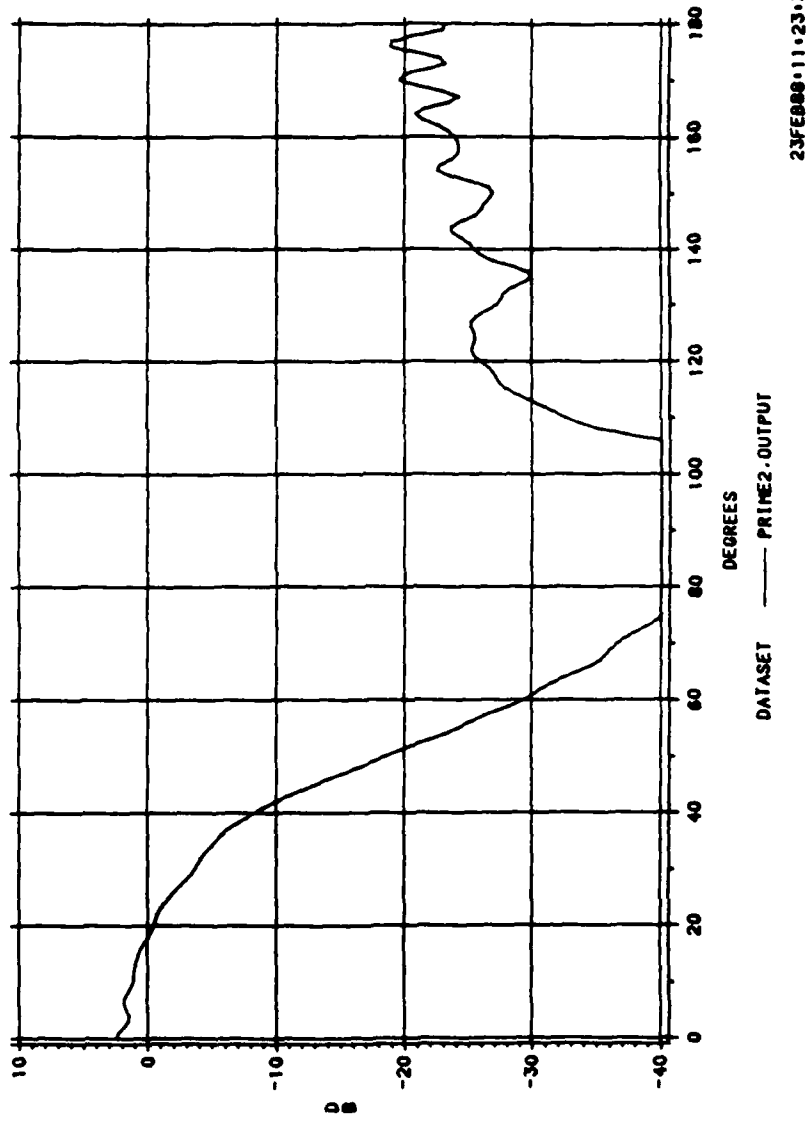


Figure 56. Primary Pattern for E-Plane for Swedish Design at 9.3 GHz

# TWIST CASSEGRAIN ANTENNA

F = 9.3 GHZ DIA = 27.0 IN.  
PRIMARY PATTERN: PHI = 0 DEG.

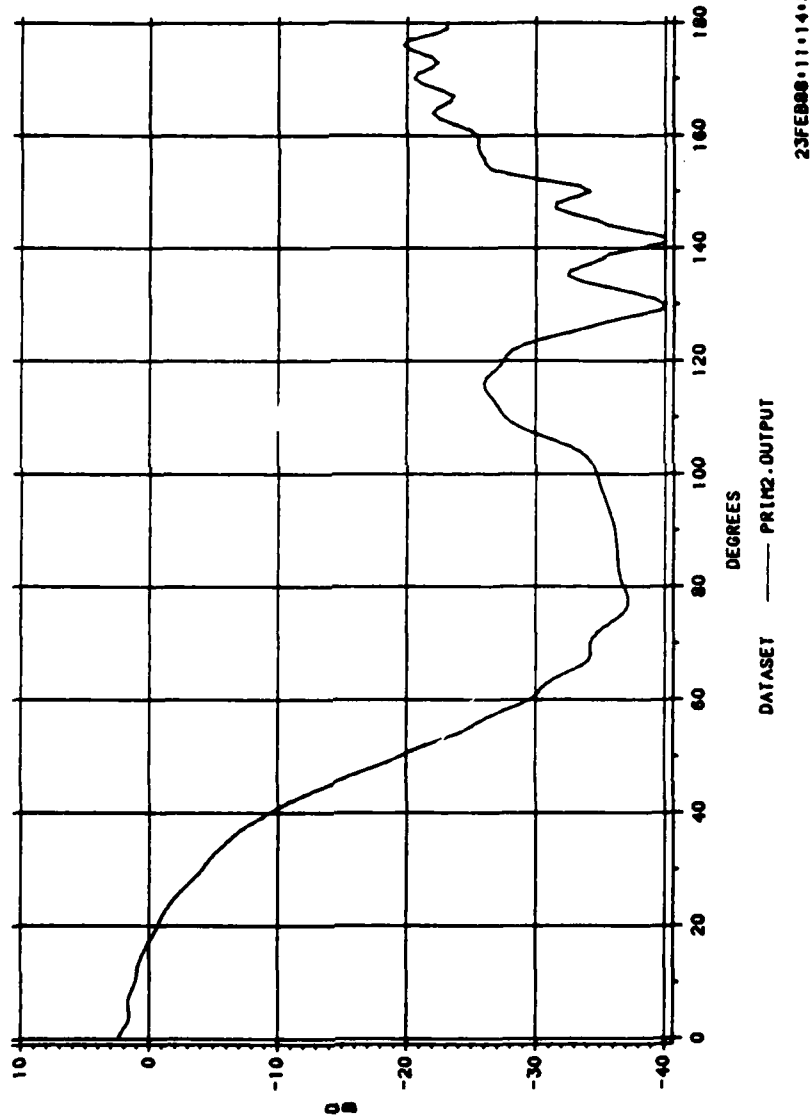


Figure 57. Primary Pattern for H-Plane for Swedish Design 9.3 GHz

APPENDIX D

VECTOR DIFFRACTION PROGRAM  
MODIFIED JENSEN PROGRAM  
THE RUSCH SCATTER EQUATIONS  
THIS IS THE MAIN PROGRAM TO CALCULATE THE INTERGRALS  
FOR SCATTERING FROM AN ARBITRARY REFLECTOR

INPUT DATA

CARD 1

TITLE

CARD 2

FK=FREQ(GHZ)

Y1=START OF OUTPUT(DEG)

DY=OUTPUT INCREMENT(DEG)

X1=START OF INTEGRATION(DEG) SUBREFLECTOR EDGE

X2=INTERMEDIATE DIVISION OF INTEGRATION(DEG)

X3=END OF INTEGRATION(NORMALLY 180 DEG)

P1=START OF AZIMUTH CUTS (DEG) H-PLANE = 0 DEG

CARD 3

DP=AZIMUTHAL ANGLE INCREMENT(DEG)

E=HYPERBOLOID ECCENTRICITY

E>1. USES CONVEX HYPERBOLOID SURFACE

+1. USES CONCAVE HYPERBOLOID SURFACE

A=HYPERBOLOID EQUATION CONSTANT

XL=LENGTH OF PLOTS (NOT USED AT THIS TIME)

FF - PARABOLOID FOCAL LENGTH

RF - PARABOLOID RADIUS

CCONE=0 THIS IS THE FINAL CASE

=1 ANOTHER CASE FOLLOWS THIS ONE

CARD 4

M1=1 NORMALLY COS(M\*PHI) DEPENDENCE LOWER LIMIT

M2=1 NORMALLY COS(M\*PHI) DEPENDENCE UPPER LIMIT

N1=NUMBER OF INTEGRATION POINTS X2>X>X1

N2=NUMBER OF INTEGRATION POINTS X3>X>X2

N1 AND N2 SHOULD BOTH BE EVEN NUMBERS

NY=NUMBER OF INCREMENTS DY IN POLAR ANGLE OUTPUT

NY MUST NOT EXCEED 180

NP=NUMBER OF INCREMENTS FOR AZIMUTH CUTS OUTPUT

IFN=NUMBER OF INPUT POINTS TO DEFINE SUBREFLECTOR

=0 PROGRAM CALCULATES SUBREFLECTOR

--1 USE VALUES OF PREVIOUS CASE

IAR=NUMBER OF POINTS TO DEFINE INCIDENT FIELDS  
=0 USE PREVIOUS CASE  
ISPOT=PRINTOUT OPTION FOR INTERMEDIATE ANSWERS  
=0 NORMALLY  
NPAR = 0 SUBREFLECTOR SCATTERING ONLY  
= 1 SUBREFLECTOR AND PARABOLOID SCATTERED FIELDS

CARD 5

Y1P=START OF PARABOLOID OUTPUT (DEG)  
DYP=PARABOLOID OUTPUT INCREMENT (DEG)  
PNY=NO. OF DYP INCREMENTS IN PARABOLOID POLAR ANGLE  
OUTPUT (MUST NOT EXCEED 180)  
P1P=START OF PARABOLOID AZIMUTH CUTS (DEG) H-PLANE=0 DEG  
DPP=PARABOLOID AZIMUTHAL ANGLE INCREMENT (DEG)  
PNP=NO. OF DPP INCREMENTS IN PARABOLOID AZIMUTH CUTS OUTPUT  
PN1=NO. OF PARABOLOID INTEGRATION POINTS X2>X>X1 (EVEN)

CARD 6

PN2=NO. OF PARABOLOID INTEGRATION POINTS X3>X>X2 (EVEN)  
X3P=180. MINUS ANGLE OF EQUIVALENT BLOCKAGE (DEG)  
=0 USES CALCULATED SUBREFLECTOR BLOCKAGE ANGLE  
FPT=FEED PATTERN TAPER AT EDGE OF SUBREFLECTOR  
(INPUT FPT AS MINUS DB)

CARD GROUP 1  
 DEFINES SUBREFLECTOR SURFACE,  $F(X)$ , IFN VALUES  
 IF IFN=0 OMIT  
 CARD GROUP 2  
 SUBREFLECTOR SLOPE,  $G(X)$ , IFN VALUES  
 OMIT FOR IFN=0  
 CARD GROUP 3  
 POLAR ANGLE FOR WHICH  $F(X)$  AND  $G(X)$  ARE DEFINED, IFN VALUES  
 OMIT FOR IFN =0  
 CARD GROUP 4           E-PLANE PATTERN  
   REAL PART OF E-THETA AT PHI=90 DEG  
   IMAG PART OF E-THETA AT PHI=90 DEG  
 CARD GROUP 5        CROSS POLARIZATION IN H-PLANE  
   REAL PART OF E-THETA AT PHI=0  
   IMAG PART OF E-THETA AT PHI=0  
 CARD GROUP 6        E-PLANE CROSS POLARIZATION  
   REAL PART OF E-PHI AT PHI=90 DEG  
   IMAG PART OF E-PHI AT PHI=90 DEG  
 CARD GROUP 7   H-PLANE PATTERN  
   REAL PART OF E-PHI AT PHI=0 DEG  
   IMAG PART OF E-PHI AT PHI=0 DEG

IAR VALUES FOR EACH COMPONENT OF FIELD

CARD GROUP 8  
 POLAR ANGLE IN RADIANS AT WHICH INCIDENT FIELDS ARE INPUT,  
 IAR VALUES

## REFERENCES

- Bakhrakh L.D. and Galimov, G.K. 1981. Reflector Scanning Antennas: Theory and Design Methods, (Moscow: "Nauka" Publisher).
- Bargeliotes, P. C. 1975. Hughes Interdepartmental Correspondence, August 20, 1975, No. 2265.30/563.
- Bodnar, D. G. 1984. "Radar Antennas", Principles of Modern Radar Short Course, Georgia Institute of Technology, November, 1984.
- Carter, D. 1955. "Wide-Angle Radiation in Pencil Beam Antennas" J. Applied Physics, No. 6, June 1955, pp. 645-652.
- Cutler, C. C. 1947. "Parabolic-Antenna Design for Microwaves," Proc. IRE, Vol 35, November, 1947, p. 1286.
- Dahlin, R. K. 1982. Technical Review of Design of Optimum Two-Mirror Antennas with the Oscillation of the Radiation Patterns, Arkady Assoc., Garden Grove, CA
- Dahlsjo, O. 1973. "A Low Side Lobe Cassegrain Antenna", IEE International Conference on Radar-Present and Future, 23-25 October 1973.
- Dahlsjo, O., Lungstrom, B., Magnusson, H. 1986. "Plastic and Composite Materials for Antennas-An Evolution Towards More Demanding Applications", Proceedings of the Military Microwaves '86 Conference, Brighton, England, June 24-26, 1986, pp. 237-242.
- Dijk, J., Jeuken, M., and Maanders, E. J. 1968. "Blocking and Diffraction in Cassegrain Antenna Systems", De Ingenieur, July 5, 1968, pp. 79-91.
- Galimov, G. K. 1969. Design of Optimum Two-Mirror Antennas with the Oscillation of the Radiation Patterns, Moscow.
- Hannon, Peter, W. 1955. "Design for a Twistreflector Having Wideangle Performance," Wheeler Laboratory Report No. 666.

- Hannon, Peter, W. 1961. "Microwave Antennas Derived from the Cassegrain Telescope," IRE Trans. on Antennas and Propagation, March 1961, pp. 140-153.
- Hannon, Peter, W. 1961. "Optimum Feeds for All Three Modes of a Monopulse Antenna," IEEE Trans. on Antennas and Propagation, September 1961, pp. 444-461.
- Hansen, R. C. 1959. "Low-Noise Antennas", Microwave Journal, June, 1959, pp. 19-24.
- Ingalls, A. G., 1953. "Amateur Telescope Making", Scientific American, Vol. 1, pp. 62-65, 215-218, 444-453.
- Jasik, Henry, 1961. Antenna Engineering Handbook, First Edition, (New York: McGraw Hill).
- Jensen, P. A. 1962. "Designing Cassegrain Antennas", Microwaves, December, 1962, pp. 12-19.
- Jensen, P. A. 1984. "Cassegrain Systems", Section 3.2 in The Handbook of Antenna Design, Vol. 1, (London: Peter Peregrinus Ltd.), pp. 162-184.
- Johnson, R. C. and Jasik, H. 1984. Antenna Engineering Handbook, (New York: McGraw-Hill Book Company).
- Johnson, R. C. and Jasik, H. 1987. Antenna Applications Reference Guide, (New York: McGraw-Hill Book Company).
- Josefsson, L. G. 1973. "A Broad-Band Twist Reflector", IEEE Trans. Ant. and Prop., July 1973, pp. 552-554.
- Josefsson, L. G. 1978. "Wire Polarizers for Microwave Antennas", Technical Report No. 81, Thesis of Chalmers Univ. of Technology, Goteborg, Sweden, March, 1978.
- Josefsson, L. G. 1978. "Wire Polarizers for Microwave Antennas", Ericsson Technics, No. 4, 1978.
- Josefsson, L. G. 1986. "Cassegrain Antennas with Broadband and Multiband Performance", Proc. IEEE Radar-86 Conference, Los Angeles, CA, pp. 115-119.
- Kraus, John, D. 1988. Antennas, Second Edition, (New York: McGraw Hill).

- Leonov, A. I. and Fomichev, K. I. 1986. Monopulse Radar, (Norwood, MA: Artech House).
- Lewis, B. L. and Shelton, J. P. 1980. "Mirror Scan Antenna Technology", Rec. IEEE International Radar Conference, April, 1980, pp. 279-283.
- Liao, Samuel, Y. 1985. Microwave Devices and Circuits (Englewood Cliffs, NJ: Prentice-Hall).
- MacFarlane, G. G. 1946. "Surface Impedance of an Infinite Parallel Wire Grid at Oblique Angles of Incidence", J. Inst. Elect. Engrs., pt. 3A, Vol 93, pp. 1523-1527.
- Mohony, J. D. 1981. "The Determination of the Fields Reflected From a Twist Reflector Following Illumination by a Plane Wave", Proceedings of the 2nd International Conference on Antennas and Propagation, York, England, April 13-16 1981, pp. 42-45.
- Orleansky, E., Samson, C., and Havkin, M. 1987. "A Broadband Meanderline Twistreflector for the Inverse Cassegrain Antenna", Microwave Journal, Vol. 30, No. 10, pp. 185-190.
- Rusch, W.V.T. and Potter, P.D 1970. Analysis of Reflector Antennas, (New York: Academic Press).
- Rusch, W.V.T., 1963. "Scattering From a Hyperboloidal Reflector in a Cassegrainian Feed System", IEEE Trans. on Antennas and Propagation, July, 1963, pp. 414-421.
- Rusch, W.V.T., 1963. "Scattering of a Spherical Wave by an Arbitrary Truncated Surface of Revolution", JPL Technical Report No. 32-434, May 27, 1963.
- Rusch, W.V.T, Jensen, P.A., et al. Hughes Vector Diffraction Program.
- Scorer, M., Graham, R., and Barnard, I. 1978. "The Analysis of an Elliptic Twist Reflecting Cassegrain Antenna Using GTD", Proceedings of the International Conference on Antennas and Propagation, London, November 28-30, 1978, pp. 208-212.
- Seaton, Arthur, F. 1988. Unpublished technical report at Hughes Aircraft Company, "Cassegrain Design".

- Seaton, Arthur, F. 1988. Unpublished technical data at Hughes Aircraft Company, "Cassegrain Reflector Loss Budgets".
- Silver, Samuel. 1949. Microwave Antenna Theory and Design, MIT Radiation Lab Series, Vol 12, (New York: McGraw Hill Book Co., 1949), pp. 447-448.
- Skolnik, Merrill. 1980. Introduction to Radar Systems, (New York: McGraw Hill Book Co.).
- Skolnik, Merrill. 1970. Radar Handbook, (New York: McGraw Hill Book Co.)
- Spooner, P. W. and Sage, D. S. 1985. "The Foxhunter Airborne Interceptor Radar", The GEC Journal of Research, Vol. 3, No. 2, pp. 114-123.
- Stimson, George, W. 1983. Introduction to Airborne Radar, (El Segundo, CA: Hughes Aircraft Co.).
- Stutzman, Warren L. and Thiele, Gary, A. 1981. Antenna Theory and Design, (New York: John Wiley & Sons).
- Tzannes, Nicolaos S. 1985. Communication and Radar Systems, (Englewood Cliffs, NJ: Prentice Hall).
- Williams, F. C. and Radant, M. E. 1983. "Airborne Radar and the Three PRFs", Microwave Journal, July, 1983, pp. 129-135.
- Williams, Frederick, 1984. Modern Air to Air Radar Systems, George Washington University Short Class 1034.
- Wolff Edward A. 1988. Antenna Analysis (Norwood, MA: Artech House).
- Young, Leo, Robinson, Lloyd, A. and Hacking, Colin, A. 1973. "Meander-Line Polarizer", IEEE Trans. on Antennas and Propagation, May, 1973, pp.376-378.